Functionalization of Si(111) surfaces and the formation of mixed monolayers for the covalent attachment of molecular catalysts in photoelectrochemical devices
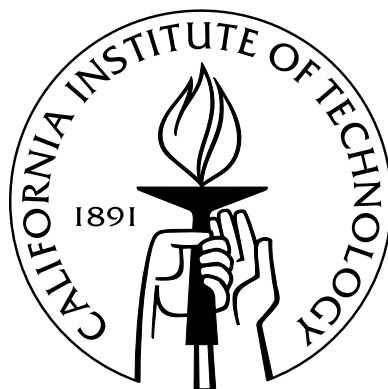
Thesis by

Judith Rebecca Cabelli Lattimer

In Partial Fulfillment of the Requirements

for the Degree of

Doctor of Philosophy

California Institute of Technology

Pasadena, California

2014

(Defended April 21, 2014)

This work is dedicated to the memory of my beloved Saba, Victor Cabelli, who shared with me his love for science, his love for family, and his birthday.

Acknowledgments

My research advisor, Harry Gray, is one of the most outgoing and enthusiastic people I have ever met. His overwhelming love of science and affection for his students made his group a truly wonderful place to be a graduate student, and I can't thank him enough for welcoming me into his group. Thanks also to Bruce Brunschwig, who really directed my research project and was always available to discuss my latest results, or lack thereof. Working together in the MMRC I learned so much about instrumentation and the importance of plumbing. While I was formally a member of Gray Nation, my research project grew out of work done in Nate Lewis's group, and I would like to thank Nate for allowing me to be an unofficial member of the Lewis group. I learned so much from Nate and his students, and I am so grateful for that opportunity. Thanks also to Mitchio Okamura and Theo Agapie for all the feedback and advice they provided at my committee meetings and exams. The entire Caltech chemistry faculty makes this school and division a truly welcoming place to be a graduate student, and I could not have asked for a better committee.

I could not have joined a better research group than the Gray group. The depth and breadth of knowledge exhibited by everyone in the group meant that there was always someone who could provide insight on whatever problem had come up. Surface science is hard, and I'm grateful to the many Gray and Lewis groupers with whom I tackled this problem over the years. Leslie O'Leary showed me the ropes when it came to silicon surface chemistry, got me started on my project, showed me how to do electrochemistry and how to use all the surface science instruments, and has been an endless source of help for my entire graduate career. Thank you. My collaboration with James Blakemore over the past few years on the bipy work has been invaluable and I am so glad that we had this opportunity to work together. My thanks also to Mike Rose, with whom I did much of the early work on the cross-coupling project. Special thanks to Wesley Sattler and Maddie Radlauer (of the Agapie group) for providing me with chemicals I did not have the expertise to synthesize myself.

Abstract

The functionalization of silicon surfaces with molecular catalysts for proton reduction is an important part of the development of a solar-powered, water-splitting device for solar fuel formation. The covalent attachment of these catalysts to silicon without damaging the underlying electronic properties of silicon that make it a good photocathode has proven difficult. We report the formation of mixed monolayer-functionalized surfaces that incorporate both methyl and vinylferrocenyl or vinylbipyridyl (vbpy) moieties. The silicon was functionalized using reaction conditions analogous to those of hydrosilylation, but instead of a H-terminated Si surface, a chlorine-terminated Si precursor surface was used to produce the linked vinyl-modified functional group. The functionalized surfaces were characterized by time-resolved photoconductivity decay, X-ray photoelectron spectroscopy (XPS), electrochemical, and photoelectrochemical measurements. The functionalized Si surfaces were well passivated, exhibited high surface coverage and few remaining reactive Si atop sites, had a very low surface recombination velocity, and displayed little initial surface oxidation. The surfaces were stable toward atmospheric and electrochemical oxidation. The surface coverage of ferrocene or bipyridine was controllably varied from 0 up to 30% of a monolayer without loss of the underlying electronic properties of the silicon. Interfacial charge transfer to the attached ferrocene group was relatively rapid, and a photovoltage of 0.4 V was generated upon illumination of functionalized n-type silicon surfaces in CH_3CN. The immobilized bipyridine ligands bound transition metal ions, and thus enabled the assembly of metal complexes on the silicon surface. XPS studies demonstrated that $[Cp^*Rh(vbpy)Cl]Cl$, $[Cp^*Ir(vbpy)Cl]Cl$, and $Ru(acac)_2vbpy$ were assembled on the surface. For the surface prepared with iridium, x-ray absorption spectroscopy at the Ir L_{III} edge showed an edge energy and post-edge features virtually identical to a powder sample of $[Cp^*Ir(bipy)Cl]Cl$ (bipy is 2,2´-bipyridyl). Electrochemical studies on these surfaces confirmed that the assembled complexes were electrochemically active.

Contents

List of Figures

List of Schemes

xv

List of Tables

2.1   Surface coverage in monolayers of carbon and bromine on various silicon surfaces functionalized with varying amounts of methyl and allyl groups 20

3.1   Properties of modified silicon surfaces 52

3.2   Properties of vFc-modified Cl-terminated Si surfaces using UV-light induced reaction 63

3.3   Properties of n-type silicon electrodes modified by mixed methyl/vinylferrocenyl monolayers 66

4.1   Surface coverage of selected elements on mixed vbpy/methyl surfaces 76

Chapter 1

Background and Motivation

1.1   Solar Energy

The development of solar energy as a commercially viable and scalable energy source is a major focus of academic and industrial research. The limitations of current fossil fuel technologies— in terms of the availability, cost, environmental impact, and geopolitical uncertainty involved in maintaining the levels of fuel production and use currently in place—have become more apparent, making the case for developing solar technologies. While there are certainly other renewable energy sources available (e.g., wind, water, and biofuels), none has the scale and ubiquity of solar energy. The challenge of solar energy lies in converting it into forms of energy that can be used directly or stored for use during periods of time when sunlight is not available.

There are several methods for converting sunlight into more usable forms of energy. Two of the most widespread of these methods are photosynthesis, used by plantlife globally, and photovoltaics, used in most commercially available solar energy systems. Photosynthesis uses sunlight to do energetically-uphill chemical reactions via complex biological molecules, creating high-energy chemical bonds. Thus solar energy is converted into chemical energy and stored in stable molecules. Photovoltaics, on the other hand, use semiconductors to create electron–hole pairs upon the excitation of those materials with light, creating electricity from the generated voltage. This electricity can then be used to power devices directly. Other methods of generating storable energy from sunlight, such as solar-thermal and solar battery technologies,[1] have also been demonstrated, but were not the focus of this work and will not be discussed here.

While photosynthesis managed to exclusively support virtually all life on earth for billions

of years, it is an extremely inefficient process. Alone, photosynthesis cannot support current energy needs in real time. Instead we rely on fossil fuels, the byproduct of billions of years of photosynthesis. Therefore, we would like to combine the science behind both photosynthesis and photovoltaics to carry out artificial photosynthesis, wherein solar energy is converted to chemical energy by using semiconductors to facilitate energetically-uphill chemical reactions.

Most of the work discussed herein was supported by the NSF-funded Solar Fuel Center for Chemical Innovation (CCI Solar).[2] This center was designed to fund the research and development of a device for the direct conversion of sunlight into chemical energy by splitting water into hydrogen and oxygen. Hydrogen was chosen as the chemical fuel to be generated for several reasons. For one, combustion of hydrogen in a fuel cell releases only water, which makes it a clean energy source without carbon emissions. There is a growing interest in utilizing clean energy sources to minimize the environmental impact of fossil fuel consumption. For instance, California has mandated the reduction of statewide greenhouse gas emissions to 1990 levels by 2020 and requires that 33 % of electricity be generated using renewable resources through the Clean Energy Future initiative. Water-splitting is also a relatively simple chemical reaction, which makes it attractive as a starting point for the development of a new technology. Hydrogen-formation in particular is a well-studied reaction involving the simplest of all processes: the reduction of two protons with two electrons.[3] Having a relatively well-understood reaction as the basis for a research effort with so many new components could help to minimize the inevitable problems to be encountered. Ideally, the methods and devices developed by this project will be applied to the formation of more complex fuels from sunlight as well.

The original concept for the device to be developed by the CCI Solar program was of a tandem-cell consisting of a photocathode and a photoanode separated by a membrane. The membrane was optically transparent, both proton- and electron-conducting, and separated the hydrogen and oxygen generated *in situ* by catalysts appended to the photocathode and photoanode, respectively. These catalysts were attached to the semiconductor surfaces to facilitate efficient charge transfer of the photogenerated charge carriers from the cathode or anode to the catalyst for fuel formation. A schematic of the proposed device, affectionately referred to as "the Liz" after the student who created the graphic, is shown in Figure 1.1.[4] The semiconducting photocathode and photoanode are shown as rods for axial light absorption and radial charge collection. The rods provided the necessary depth of substrate for high light-

2H₂O

4e⁻

O₂ + 4H⁺

H⁺

H⁺

Photoanode with
O₂-evolving catalyst

H⁺   H⁺

H⁺

Semi-permeable
membrane

4e⁻   4H⁺

2H₂

Photocathode with
H₂-evolving catalyst
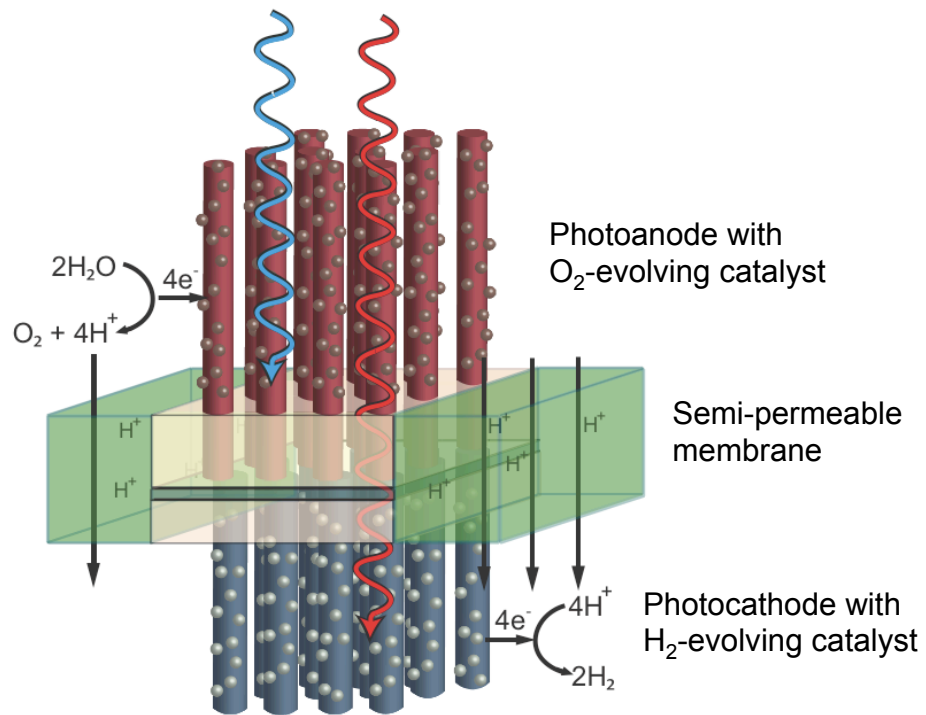
FIGURE 1.1: A schematic of the solar water-splitting device proposed by the CCI Solar project, adapted from a graphic by E. Santori.[4]

absorption and charge-carrier generation. Radial charge collection minimized the necessary carrier diffusion length and lead to increased charge collection by the catalysts. In addition, the increased surface area of this design over a planar equivalent allowed for up to ten times the catalyst loading in the device. The focus of the present work is on the interface between the hydrogen-evolution catalyst and the photocathode, which in this case is assumed to be p-type silicon.

1.2 Semiconductor Photoelectrochemistry

Silicon is a semiconductor, which means that it is neither conductive nor insulating, but somewhere in between. The atomic orbitals of the silicon atoms combine in the crystal, forming bands of energy levels rather than discrete orbitals.[5] In a semiconductor, there is an energy gap between the filled valence band of the crystal and the empty conduction band above it. The size of this band gap is what determines the energetics of the semiconductor. In silicon, the band gap is $1.1\,\text{eV}$, which corresponds to light with a wavelength of $1100\,\text{nm}$.[6] This is in the infrared region of the light spectrum, which means that silicon can absorb infrared, visible, and higher energy light. This makes it ideal for use in a solar energy conversion device, which should cover as much of the solar spectrum as possible. When a photon with enough energy hits the semiconductor, it can be absorbed, thus exciting an electron from the valence band into the conduction band and leaving a hole in its place. If these excited electrons can be collected before they recombine with the holes in the valence band, then their excess energy can be harnessed as chemical or electrical energy. Electrons that have been excited into the silicon conduction band have $1.1\,\text{eV}$ of excess energy, which is enough to drive the reduction of protons in water into hydrogen. This is shown schematically in Figure 1.2 as a comparison of the energy levels of several different materials that have been considered for use as a photocathode. As can be seen in the figure, the silicon band gap straddles the H^+/H_2 redox potential, which means that electrons in the conduction band will have enough energy to reduce protons to hydrogen.[7]

The Fermi level of a semiconductor is defined as the electrochemical potential of an electron in the material, or the energy at which the probability of finding an electron is $1/2$.[5] In an pure, undoped semiconductor at $0\,\text{K}$, where the valence band is completely filled and the conduction band is completely empty, the Fermi level would be halfway between
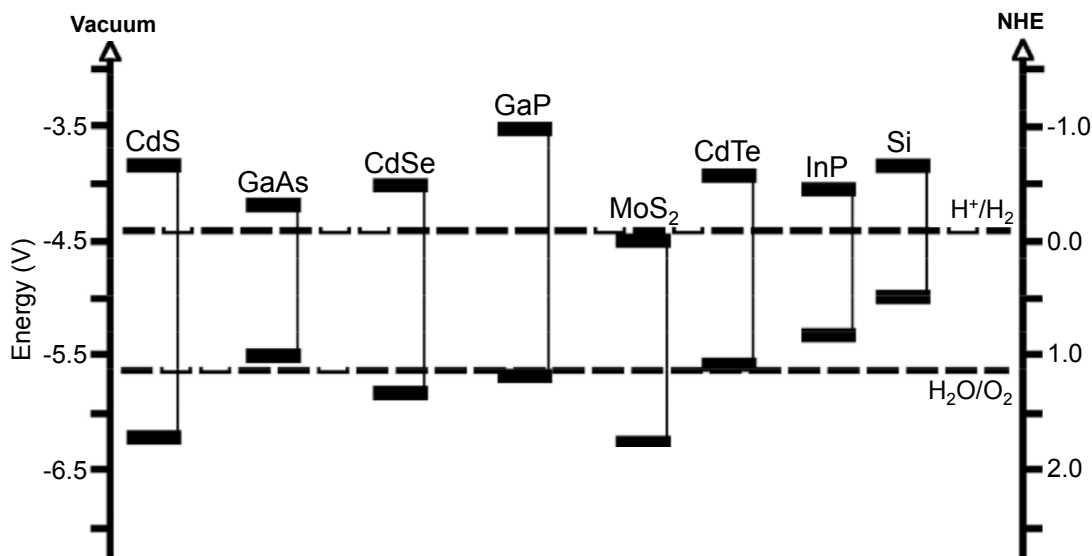
FIGURE 1.2: Band edge positions of several non-oxide semiconductors in contact with an aqueous electrolyte at pH 1. Adapted from Grimes et al.[7]

the two bands. The Fermi level can be adjusted by doping the semiconductor to form n- or p-type materials. In a p-type semiconductor, for example the silicon we propose for the solar energy device, there is an excess of holes in the valence band, pushing the Fermi level down towards the valence band edge. These extra holes are formed by doping the semiconductor with an element with fewer valence electrons than silicon, like boron. Alternatively, n-type silicon is formed by doping with an element with extra valence electrons, like phosphorus, which pushes the Fermi level up towards the conduction band edge. The Fermi level of the semiconductor will determine the energy of the electrons and holes formed upon illumination, which will be critical when analyzing the semiconductor-liquid junction in the solar device.

In the CCI Solar Project's vision of the device, there is a semiconductor-liquid junction between the silicon-based photocathode and the aqueous solvent containing protons for reduction to hydrogen. This junction creates an electric field in the semiconductor, enabling charge separation of the photogenerated electrons and holes. This field pushes the electrons toward the semiconductor surface, allowing them to be collected and used to reduce protons in the solution. A schematic of the semiconductor-liquid junction is shown in Figure 1.3. The electric field is formed by the migration of electrons from the solution into the semiconductor (or holes from the semiconductor into the solution, depending on your point of view) in order to equilibrate the electric potentials of the semiconductor and the solution. The higher
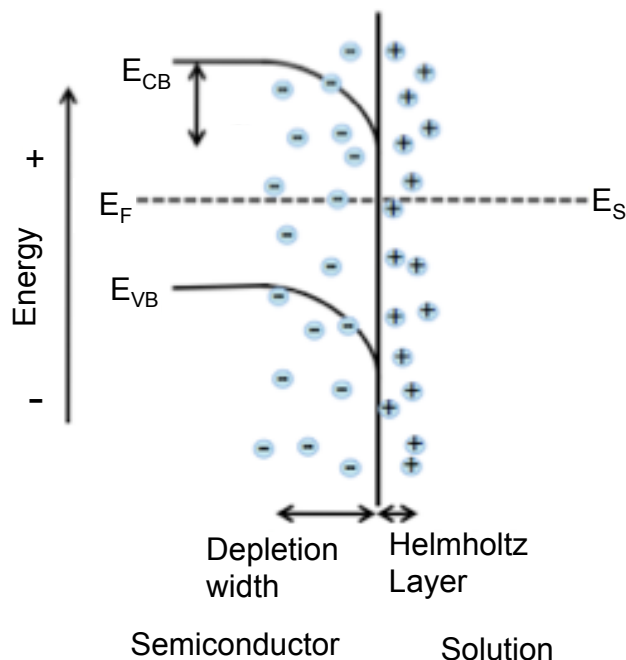
FIGURE 1.3: p-Type semiconductor-liquid junction. E_{CB} and E_{VB} indicate the energy of the conduction and valence bands, respectively. E_F indicates the Fermi level of the semiconductor and E_S indicates the redox potential of the solution, which have equilibrated by charge transfer. The excess of electrons in the depletion width creates an electric field in the semiconductor, causing bending of the conduction and valence bands.

relative concentration of charge carriers in the solution dictates that the solution potential will remain nearly unchanged after the charge transfer, with a build-up of positive charges at the interface, called the Helmholtz layer. Conversely, the relatively low density of charge carriers in the semiconductor leads to a region of diffuse negative charge, called the depletion region. The negative charge build-up in the depletion region gives rise to the electric field, which causes the band bending that drives the electrons towards the surface, as illustrated by the curved lines in the figure. Thus, when the semiconductor is illuminated, electron-hole pairs are generated and then separated by the electric field. If the electrons reach the surface without recombining with holes, they can be used to reduce the protons in solution to hydrogen. The electric field also moves the holes toward the semiconductor bulk, where they can be captured and converted to electrical energy at an electrode, or transferred through the membrane to the photoanode and used to oxidize water.[5]

For our purposes then, this semiconductor-liquid junction will determine the efficiency of charge-carrier collection at the surface. We would like to maximize the number of electrons that reach the surface and are transferred to a catalyst for hydrogen-formation. Silicon

surface functionalization can be used to improve the quality of this junction by extending the charge-carrier lifetime, controlling the energetics of the electrons at the surface, and facilitating the transfer of those electrons to a catalyst. Our efforts to modify silicon surfaces to enable solar fuel generation is the subject of this thesis.

1.3 Silicon Surface Modification

Several methods have been developed to functionalize Si surfaces, primarily by exploiting the reactivity of a H-terminated Si surface.[8–10] The H-terminated Si(111) surface is atomically flat, which makes it an excellent surface for studying the fundamental chemical properties and reactivity of silicon. This surface is electronically passivated, implying that it has low charge-carrier recombination rates at the surface. Surface recombination of charge carriers is a problem for any device in which the collection of charges at the surface is important, such as a solar cell. Low surface recombination results in longer charge-carrier lifetimes, making the charges available for collection by catalysts or redox centers at the surface. Conversely, high surface recombination means that charge-carriers that do get to the surface are trapped there and rapidly recombine with holes, making them unavailable for further reactions.

The electronic passivation of the H-terminated surface is fleeting, however, as surface oxidation under aqueous conditions occurs within minutes, resulting in a decrease in charge-carrier lifetime.[11] This can be seen when measuring the surface recombination velocity (SRV) of a freshly prepared H-terminated Si(111) surface. The SRV, which is calculated from the charge-carrier lifetime (measured using microwave conductance spectroscopy; details in Appendix B.3), is an indirect measure of the surface defect density. Fresh H-terminated silicon has an SRV of $<10\,\mathrm{cm\,s^{-1}}$, corresponding to a charge-carrier lifetime of $>1\,\mathrm{ms}$.[12] However, after several hours in air, the SRV increases dramatically, to $>1000\,\mathrm{cm\,s^{-1}}$, corresponding to a charge-carrier lifetime of $<10\,\mathrm{\mu s}$.[13]

Various methods of surface functionalization have been employed to passivate silicon under aqueous and ambient conditions, including thermal[14]-, radical[15,16]-, ultraviolet[17,18]- and white light[19,20]- initiated hydrosilylation processes, as well as metal-catalyzed routes.[21] Although synthetically versatile, hydrosilylation leaves a significant fraction of unfunctionalized sites on the Si surface due to the steric bulk of the functional groups. The unfunctionalized Si sites, which typically consist of residual Si−H bonds, are easily oxidized and therefore

result in non-ideally terminated surfaces that exhibit undesirable chemical, electrochemical, and electrical properties.

Complete termination of Si(111) atop sites by carbon bonds is therefore desirable, and can be achieved by use of a two-step halogenation/alkylation procedure.[11,22–25] In this method, H-terminated Si surfaces are first halogenated and then reacted with an alkyl-Grignard or alkyl-Li reagent to yield an alkylated Si surface. Methyl Grignard can be used via this process to functionalize the surface with methyl groups, which are the only saturated alkyl groups small enough to be capable of terminating essentially 100% of the atop sites on an unreconstructed Si(111) surface.[26,27] Hydrosilylation, on the other hand, cannot be used to methylate a silicon surface. This complete termination of the silicon atop sites can be seen in an STM image of a methyl-terminated silicon surface, shown in Figure 1.4.[28] Methyl-terminated Si surfaces are well passivated against oxidation in air,[29] and exhibit low SRVs even after weeks of exposure to ambient atmospheric conditions.[30] In addition, $CH_3-Si(111)$ surfaces have a low density of mid-gap states, as revealed by scanning tunneling spectroscopy,[26] and exhibit resistance to oxidation in electrochemical and photoelectrochemical cell applications.[29,30]

While methyl-terminated silicon has some excellent photoelectrochemical properties, it is not ideal for use in a water-splitting solar device. Silicon is a poor catalyst for proton reduction and will require an efficient hydrogen-evolution catalyst to do the actual proton-reduction reaction on the surface. This catalyst would ideally be tethered to the surface to minimize catalyst loading in the device and maximize electron-transfer kinetics to the catalyst from the silicon. In addition, the methyl group on the silicon surface results in a negative shift in the interfacial dipole. For p-type silicon, this increases the ohmic behavior of $CH_3-Si(111)$ relative to $H-Si(111)$, resulting in lower photovoltages being measured on the methyl-terminated surface than on the H-terminated surface.[31] For these reasons, a methyl-terminated silicon surface, while exhibiting many of the desirable properties for a photocathode, will require some additional functionality before it can be incorporated into a water-splitting device.

Further functionalization, to introduce desirable dipoles and/or molecular catalysts, is limited on $CH_3-Si(111)$ surfaces, owing to the lack of controllable reactivity of the terminal methyl groups. Therefore, other means are necessary to attach catalytic groups to the surface. The halogenation/alkylation procedure can be used to attach other functional
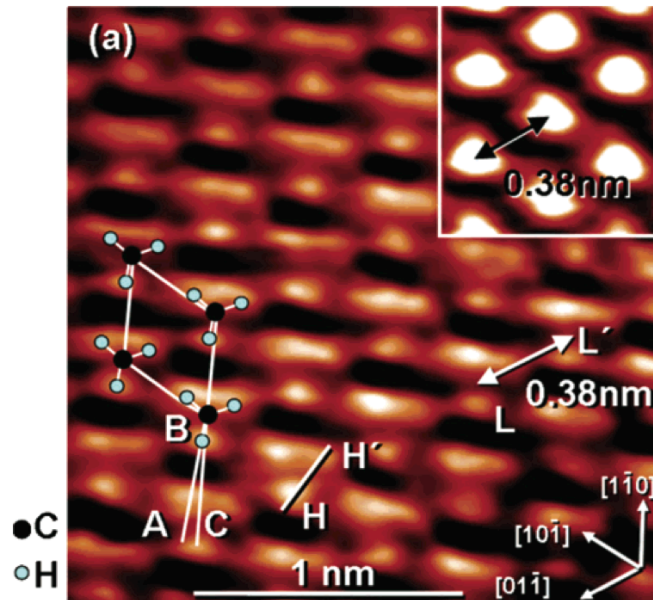
FIGURE 1.4: STM image of methyl-terminated Si(111) (4.7 K, sample bias $V_s = -2.5$ V, constant current of 0.050 nA). The color range (dark = low; bright = high) is 0.05 nm. The low-index planes of this crystal are indicated in the lower right by directional arrows. The drawn parallelogram represents the surface unit cell. Superimposed onto the image are four $-CH_3$ group drawings illustrating their position and relative orientation. The distance between $-CH_3$ groups (L–L$'$) is 0.38 cm. (Inset) STM image (77 K) of the same surface. Image size: 1 nm $\times$ 1 nm. Adapted from Yu et al.[28]

groups directly to the surface, but these groups are generally larger than methyl groups. Even a two-carbon ethyl chain is too large to allow for complete termination of the surface by the chemically inert Si−C bonds, leaving unreacted sites on the surface.[13] Synthetic strategies to produce mixed monolayers have therefore been developed to simultaneously impart stability and functionality to Si(111) surfaces by forming monolayers composed of both functional and methyl groups.[32,33] The mixed monolayers produced by these methods possess the resistance to oxidation typically observed for methyl-terminated silicon, and incorporate desired functional species that are covalently bound to surface silicon atoms.

In this work, we will discuss the formation of several new classes of mixed monolayers on silicon surface and their uses for solar-fuel forming devices. In Chapter 2, we expanded on the work done using mixed methyl/allyl monolayers as the starting point for secondary functionalization. We developed and characterized a new class of mixed methyl/butenyl monolayers on which we performed cross-coupling reactions using the Grubbs' catalyst. The surfaces formed by this method were electroactive and had excellent photoelectronic properties. In Chapter 3, we developed a new method for forming mixed monolayers on silicon by combining different modes of reactivity. We showed that the mixed methyl/vinylferrocenyl monolayers formed using this new method had high electroactive surface coverage, low SRVs, and resistance to oxidation in air. In addition, these surfaces displayed rapid charge transfer to the surface-attached redox couple and generated photovoltages of 400 mV. In Chapter 4, we expanded the scope the reaction developed in Chapter 3 to form a new class of mixed methyl/bipyridyl monolayers that were used as the starting point for the development of surface-attached hydrogen-evolution catalysts for solar fuel formation. We showed that these complexes could be assembled on the surface by a variety of spectroscopic techniques, and that the resultant structures were electroactive and catalytic under acidic conditions. In Chapter 5, possible mechanisms for the new reaction developed in Chapters 3 and 4 were discussed. Portions of the preceding chapter have been adapted with permission from Lattimer et al.[34] Copyright 2013 American Chemical Society.

Chapter 2

Cross Metathesis Reactions on Silicon Surfaces using the Grubbs' Catalyst, 2nd Generation

2.1 Introduction

Carbon-carbon bond formation can be an important tool for the covalent attachment of functional groups to silicon surfaces. Cross-metathesis of two terminal olefins is a well-established method for the formation of new $C-C$ bonds.[35,36] Terminal olefins can be prepared on silicon surfaces by reacting vinyl or allyl Grignard reagents with chlorine or bromine terminated silicon surfaces. These surfaces have been prepared and characterized by Plass et al.[37] and O'Leary et al.[32] Some work has indicated that surface-terminal olefins are reactive with terminal olefins, via a cross-metathesis reaction using the Grubbs' catalyst.[38,39] The Grubbs' catalyst, 1st generation (G1), is more formally known as Bis(tricyclohexylphosphine)benzylidine ruthenium(IV) dichloride (Figure 2.1-**G1**). Initial experiments used this catalyst as a cross-coupling agent to react the allyl-terminated Si(111) surface with 4-fluorostyrene, a terminal aryl olefin. The fluorine acts as a spectroscopic tag to measure the efficacy of the reaction.[37] Methyl-terminated Si(111) was used as a control surface to ensure that non-specific binding did not occur. This work suggested that G1 could be used as a cross-coupling agent to covalently attach fluorostyrene selectively to allyl-terminated silicon surfaces.
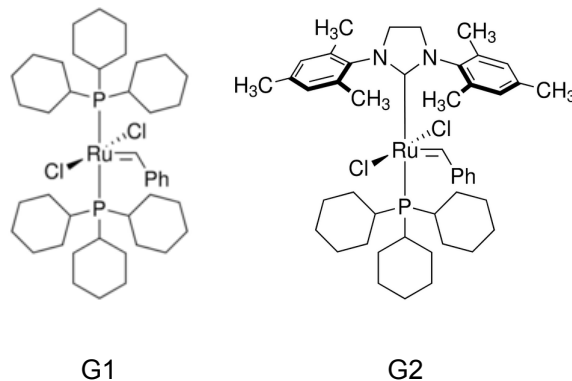
FIGURE 2.1: Grubbs catalyst, 1st generation (**G1**) and Grubbs catalyst, 2nd generation (**G2**).
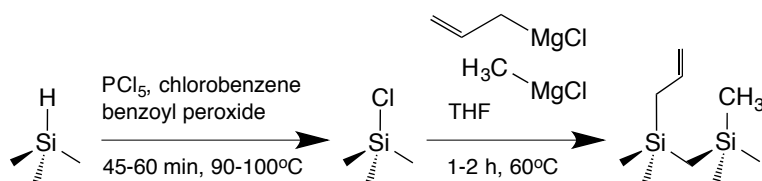
SCHEME 2.1: Formation of mixed methyl/allyl monolayers on Si(111) surfaces starting from the H-terminated surface.

2.2 Mixed Methyl/Allyl Surfaces and Reactions

The results presented by Plass et al.[37] provided the impetus for this research project, which was to attach redox active molecules and hydrogen-evolution catalysts to silicon surfaces using the cross-metathesis reaction. We began by forming methyl and mixed methyl/allyl surfaces on silicon, as done previously by O'Leary.[32] The experimental details can be found in Appendix A.2. A reaction scheme for the formation of the mixed monolayers is shown in Scheme 2.1. A similar reaction was used to form methyl- and allyl-terminated surfaces, using the halogenation/alkylation procedure developed in the Lewis group.[22] These surfaces were characterized using X-ray photoelectron spectroscopy (XPS) and transmission fourier-transform infrared (FTIR) spectroscopy. The instrumentation information, as well as sample preparation for each technique, can be found in Appendix B.1 and B.2.

XPS of a representative mixed methyl/allyl monolayer can be found in Figure 2.2. The survey spectrum (Figure 2.2a) showed the silicon 2p and 2s signals at 100 and 150 eV, respectively, the C 1s signal at 285 eV, and the O 1s signal at 532 eV. While oxygen was not intentionally incorporated onto the surface, there was always a small oxygen signal present
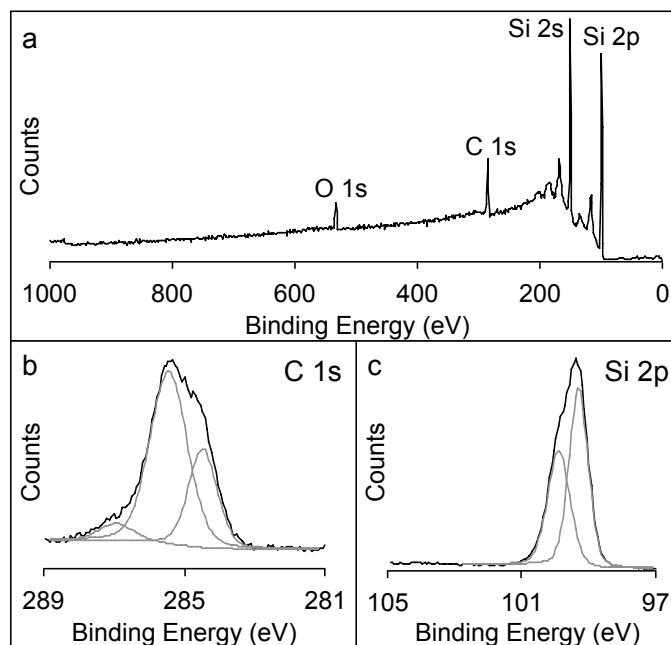
FIGURE 2.2: XPS of a mixed methyl/allyl surface. a) Survey spectrum, with the Si 2p, Si 2s, C 1s, and O 1s peaks labeled. b) High-resolution C 1s peak, showing the three components of the signal. The lowest energy peak, at $284\,\mathrm{eV}$, was from the carbon directly bound to silicon. The peak at $285\,\mathrm{eV}$ was from the allylic carbons as well as adventitiously adsorbed hydrocarbons. The highest energy peak at $287\,\mathrm{eV}$ was from adventitiously adsorbed CO and CO_2. c) High-resolution Si 2p peak, with the doublet shown. There was no peak at $103\,\mathrm{eV}$, indicating that the surface was not oxidized during the formation of this mixed monolayer.

due to adventitiously adsorbed water and CO_2 from the air onto the surface. High-resolution spectra of the C 1s and Si 2p peaks are found in Figure 2.2b and c, respectively. The Si 2p signal consisted of a doublet of peaks at 99 and $100\,\mathrm{eV}$, with an area ratio of 2:1. When the silicon surface was oxidized, a Si–O peak appeared between 102 and $104\,\mathrm{eV}$.[40] The high-resolution Si 2p XPS signal (Figure 2.2c) showed that there was little to no surface oxidation present on these mixed monolayers. The C 1s XPS signal (Figure 2.2b) consisted of three peaks, at 284, 285, and 287 eV. These corresponded to carbon directly bound to silicon at $284\,\mathrm{eV}$,[13,29] carbon bound to carbon or hydrogen at $285\,\mathrm{eV}$, and carbon bound to more electronegative elements like oxygen at $287\,\mathrm{eV}$. The peak at $287\,\mathrm{eV}$ was ascribed to adventitiously adsorbed species like CO and CO_2, while the peak at $285\,\mathrm{eV}$ resulted from a combination of the allyl carbons on the surface and adventitiously adsorbed species like CH_4 and higher-order hydrocarbons. These species were present in small quantities even under ultra high vacuum conditions from the atmosphere of the lab or from residual pump oil in the instrument.

14
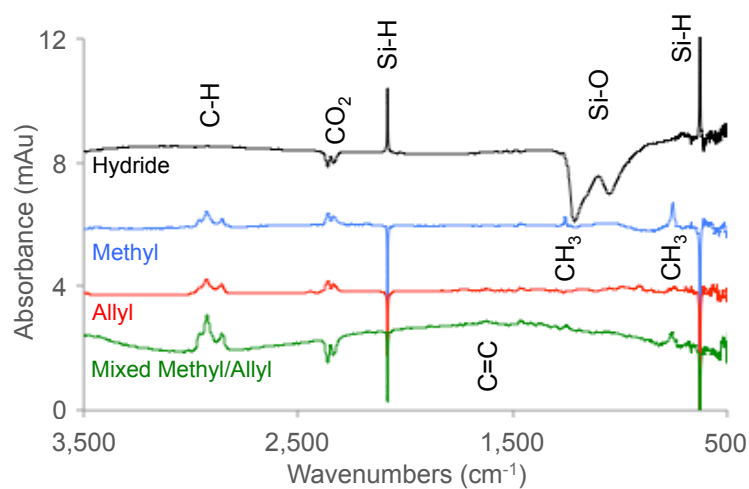
FIGURE 2.3: FTIR spectra of a series of functionalized silicon surfaces. In black is the hydride-terminated surface. There were Si−H peaks at 2083 and 627 cm^{-1}. The silicon oxide spectrum was used as the background for this spectrum, and so the negative peaks at 1000–1200 cm^{-1} were from the Si−O stretches in the background spectrum. In blue is the methyl-terminated surface with a hydride background. There were CH$_3$ stretches at 1257 and 757 cm^{-1}. In red is the allyl-terminated surface with a hydride background. There was a small peak around 1600 cm^{-1} from the C=C double bond of the allyl group, and no stretches in the methyl regions. In green is the mixed methyl/allyl surface with a hydride background. There were stretches at 1257, 757, and 1600 cm^{-1} from the methyl and allyl groups. None of the functionalized surfaces showed significant absorbance between 1000–1200 cm^{-1}, indicating that the surfaces were not oxidized.

These surfaces were further characterized by transmission Fourier-transform infrared spectroscopy (FTIR), shown in Figure 2.3. First, the surface was cleaned with piranha ($1:2$ v/v $10.1\,\mathrm{M}$ hydrogen peroxide (H_2O_2, aq) : $18\,\mathrm{M}$ sulfuric acid (H_2SO_4)), resulting in a thin silicon oxide layer on the silicon wafer. An FTIR spectrum of this surface was collected and used as the background for subsequent spectra. Next, the surface was etched with HF and NH_4F, resulting in atomically flat H-terminated silicon. An FTIR spectrum of this surface with the oxide surface as a background is shown in Figure 2.3. The characteristic Si−H stretches at 2083 and $627\,\mathrm{cm}^{-1}$ were clearly visible, as are the negative Si−O peaks at 1224 and $1058\,\mathrm{cm}^{-1}$.[41] This demonstrates that the surface had lost all Si−O bonds, which were replaced by Si−H bonds. After functionalization of the Si−H surface to form a methyl-terminated surface, a mixed methyl/allyl surface, or an allyl-terminated surface, more FTIR spectra were collected, as shown in Figure 2.3. The hydride-terminated surface was used for background subtraction in these spectra.

The experimental details for the preparation of these surfaces can be found in Appendices A.1, A.2, and A.3. There were peaks from the methyl groups at 1257 and $757\,\mathrm{cm}^{-1}$,[41] and a small peak from the terminal olefin of the allyl group at $\sim 1600\,\mathrm{cm}^{-1}$.[37] In addition, a negative peak at $2083\,\mathrm{cm}^{-1}$ can be seen in the spectra with a hydride background, indicating that the Si−H bonds have been replaced by Si−C bonds. There was no significant absorption around 1000–$1200\,\mathrm{cm}^{-1}$, indicating that the surface had not been oxidized during the formation of these monolayers, verifying our Si 2p XPS observations.

A series of surfaces with varying allyl:methyl ratios was formed by varying the amount of methyl and allyl Grignard in each $1\,\mathrm{M}$ solution. A series of such surfaces was analyzed using FTIR spectroscopy, and the results are shown in Figure 2.4. While the methyl peaks at 1257 and $757\,\mathrm{cm}^{-1}$ were fairly well defined, the allylic peak at $\sim 1600\,\mathrm{cm}^{-1}$ was much harder to see.

2.2.1 Cross-Coupling Reactions

These mixed methyl/allyl surfaces were then used as the substrate for the cross-coupling reaction seen by Plass et al.[37] using the Grubbs' catalyst, 2nd generation. This newer catalyst was used rather than G1 by recommendation from Leslie O'Leary because the 2nd generation catalyst had shown increased activity under solution conditions. The Grubbs' catalyst, 2nd generation (G2, Figure 2.1-**G2**) is also known as Benzylidene[1,3-bis(2,4,6-trimethylphenyl)-2-
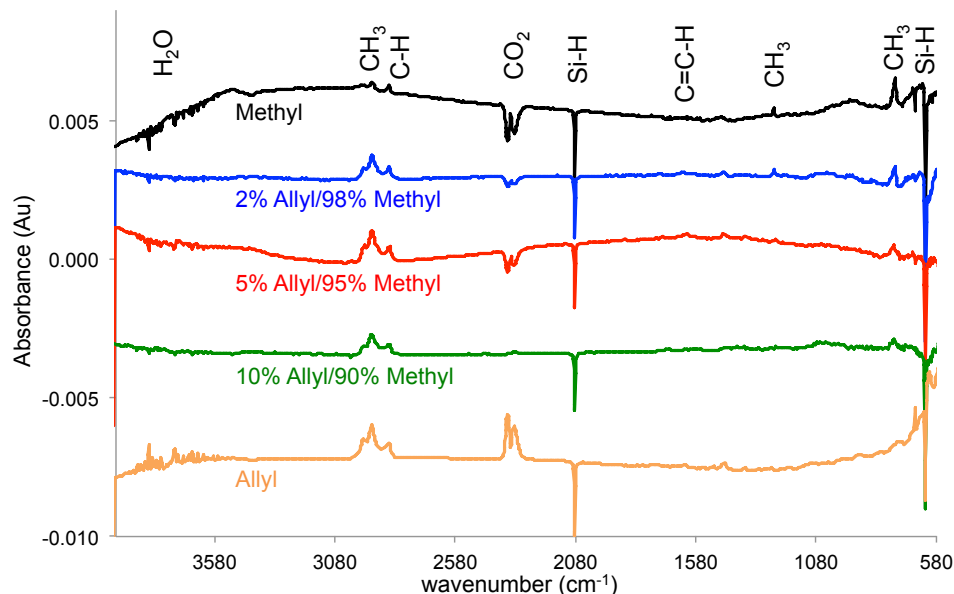
FIGURE 2.4: Surface transmission FTIR spectra of a series of mixed methyl/allyl functionalized silicon surfaces. Each spectra is labeled by the formulation of the 1 M Grignard solution used to functionalize the surface. The surfaces containing methyl groups had peaks at 1257 and 757 cm^{-1}, while the surfaces with allyl groups had small absorbances around 1600 cm^{-1}.

imidazolidinylidene]dichloro(tricyclohexylphosphine)ruthenium. The reaction was performed in an Ar-filled glove box, and was done by placing the functionalized silicon wafer in a solution of 1 M catalyst in dichloromethane (CH_2Cl_2) at 50 °C overnight. The wafer was then rinsed with CH_2Cl_2 and placed under 4-fluorostyrene at 50 °C for 12–24 additional hours. After the reaction, the wafer was rinsed with CH_2Cl_2, and cleaned by sequential sonication in CH_2Cl_2, CH3OH, and water before analysis by XPS. However, none of the many surfaces exposed to these conditions displayed any fluorine signal in XPS.

After observing these disappointing results, we tried to replicate the results seen by Plass et al.[37] using allyl surfaces for the cross-coupling reaction, and methyl-terminated silicon as the control surface. In addition, the control reaction without using the Grubbs' catalyst was done. The results are shown in Figure 2.5. From the F 1s XPS signals on these four surfaces, it was clear that the cross-coupling reaction did not proceed as expected. Surface coverages of fluorostyrene on these surfaces were quantified based on the F 1s and Si 2p XPS signals, as described in Appendix B.1.1. On the methyl surface exposed to G2 and 4-fluorostyrene (4-FS), the surface coverage of 4-FS on the surface was 0.04 ± 0.05 monolayers. For the methyl surface exposed only to 4-FS, the surface coverage was 0.03 ± 0.05. These values
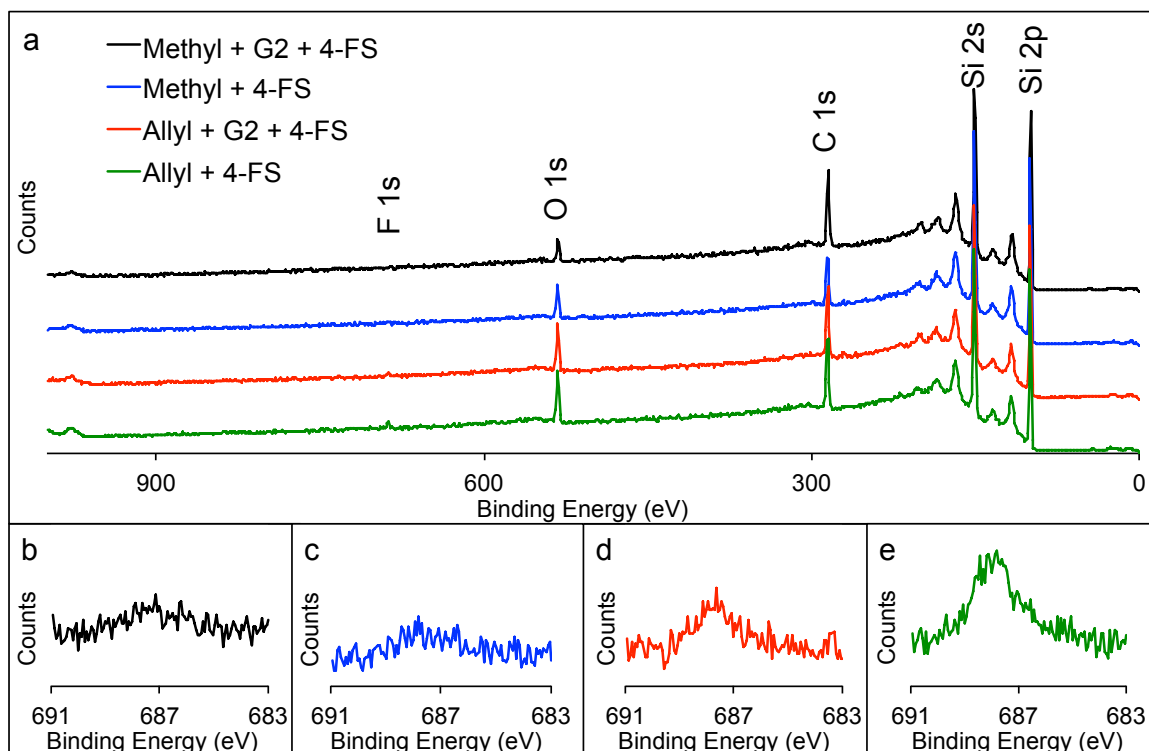
FIGURE 2.5: XPS of methyl- and allyl-terminated silicon surfaces reacted with the Grubbs' catalyst (G2) and 4-fluorostyrene (4-FS). Top: Survey spectra of the 4 surfaces with various treatments, with the relevant XPS signals labeled. Bottom: High-resolution F 1s XP spectra of each surface. All spectra are shown on the same scale for easy comparison of the relative fluorine coverage on each surface. b) Methyl + G2 + 4-FS, surface coverage of 0.04 ± 0.05 monolayers of 4-FS. c) Methyl + 4-FS, surface coverage of 0.03 ± 0.05 monolayers of 4-FS. d) Allyl + G2 + 4-FS, surface coverage of 0.10 ± 0.05 monolayers of 4-FS. e) Allyl + 4-FS, surface coverage of 0.11 ± 0.05 monolayers of 4-FS.

are within experimental error of zero, suggesting that the methyl surface did not react with either G2 or 4-FS, as expected. The allyl surface exposed to G2 and 4-FS had 0.10 ± 0.05 monolayers of 4-FS, and the allyl surface exposed only to 4-FS had 0.11 ± 0.05 monolayers of 4-FS. These values are well within experimental error of one another, indicating that the catalyst did not have a significant affect on reaction of the 4-FS with the surface. The most fluorine was actually observed on the surface that was never exposed to the Grubbs' catalyst, suggesting that nonspecific adsorption of the fluorostyrene to the surfaces could be responsible for the fluorine signals previously seen under similar reaction conditions.

2.2.2 Bromination Reactions

At this point, we determined that endeavoring to reproduce the results from Plass et al.[37] was not a constructive use of time, and instead began to explore other methods to characterize the mixed methyl/allyl surfaces. Bromination of the allyic groups on the surface could help to differentiate between the allyl and methyl groups, and thus better enable the quantification of the various components of the mixed monolayers. Knowledge of how much of each species is actually on the mixed monolayer surfaces could help explain why the cross coupling reactions do not appear to proceed as expected.

Silicon-attached terminal alkenes have been brominated previously using Br_2.[42] Alkene bromination has been demonstrated to occur using a dilute solution of Br_2 in methanol,[43] and so we used this method for the bromination of the mixed methyl/alkyl monolayers. Bromination of a series of surfaces was done by immersing the prepared surface in a 5 % solution of Br_2 in anhydrous methanol in a N_2-purged flush box; this is a glove box with a constant flow of N_2 to maintain an inert atmosphere, or an O_2 and H_2O-free environment. This was done to minimize oxidation of the surface and to control the bromination reaction. The experimental details of the bromination reaction can be found in Appendix A.4. Hydrogen-terminated silicon was used as a control surface look at silicon-bromine reactivity, and to study the Br 3d peak at 70 eV in XPS to see how bromine bonded to silicon would appear. While reaction between the Br_2 and methyl groups was expected to be minimal, reaction of unfunctionalized silicon sites in the mixed monolayer with Br_2 was likely. Distinguishing between the bromine bound to silicon (Br−Si) and bromine bound to carbon (Br−C) signals via XPS was thus critical to these experiments.

Figure 2.6 shows the high-resolution Br 3d XPS signals from a series of silicon surfaces reacted with 5 % Br_2 in methanol (v/v) for 5 min, with normalized counts for ease of comparison. There were clearly two sets of doublets within the peaks, most likely corresponding to Br−Si (blue) and Br−C (red), though residual Br_2 from the reaction cannot be ruled out completely, despite the low probability of any remaining on the surfaces after the rigorous sonication and rinsing to which the surfaces were all exposed during the cleaning procedure, as well as the ultra high vacuum atmosphere of the XPS chamber. The brominated Si−H surface is shown in Figure 2.6a, and the dominant peaks in this Br 3d spectrum were at 69 and 70 eV, in the 3:2 ratio expected for a d-type XPS signal. Thus we assigned the
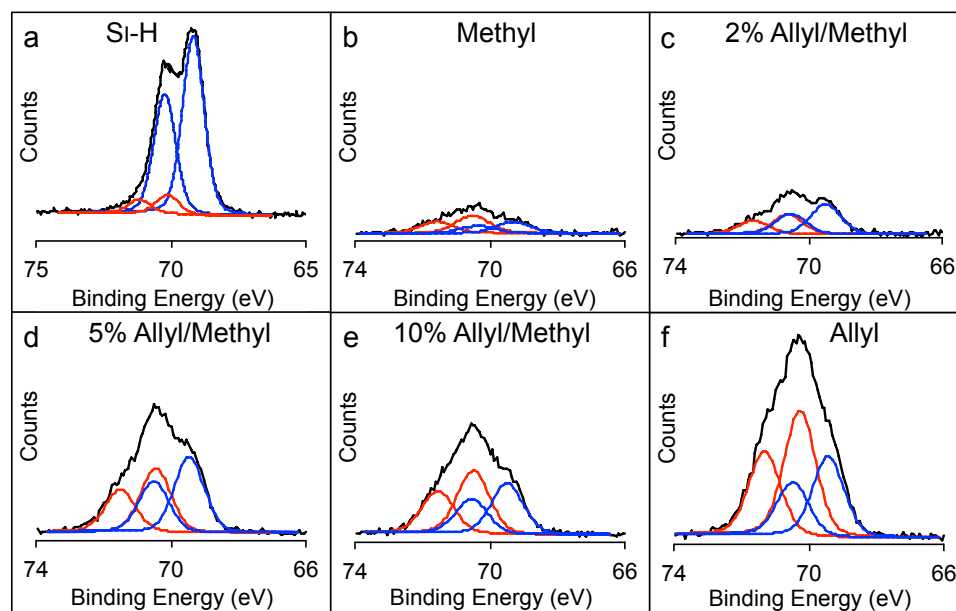
FIGURE 2.6: High-resolution Br 3d XPS of a series of silicon surfaces exposed to Br_2 in methanol for 5 min. The counts in all panels are normalized for ease of comparison, with the doublet corresponding to Br−Si in blue and the doublet corresponding to Br−C in red. a) H-terminated silicon had a large doublet at 69 and 70 eV, indicating that the surface was highly susceptible to attack by Br_2 to form Si−Br. b) Methyl-terminated silicon showed very little reaction with the Br_2, as expected. c,d,e) Mixed monolayers formed with 2, 5, and 10 % allyl Grignard in 1 M Grignard reaction solutions, with the remainder made up by methyl Grignard. Increasing allyl concentration lead to increased surface coverage of bromine bound to both silicon and carbon. f) Allyl-terminated silicon had two doublets, at 69/70 eV from Br−Si, and 70/71 eV from Br−C due to bromination of the allylic group.

doublet at 69/70 eV to be the one arising from bromine bound to the silicon surface, or Br−Si. The methyl-terminated surface exposed to Br_2 (Figure 2.6b) shows very little Br 3d signal, as expected, corresponding to 0.01 ± 0.01 monolayers. Details of the monolayer coverage calculations can be found in Appendix B.1.1.

Mixed methyl/allyl surfaces formed by varying the relative ratios of methyl and allyl Grignard in the reaction solution were prepared and then reacted with Br_2 in methanol, with the results shown in Figure 2.6c-e. These surfaces showed increasing amounts of bromination as the allyl Grignard concentration in the reaction solution was increased. This suggested that by increasing the allyl Grignard concentration of the reaction solution, more allyl groups were incorporated into the mixed monolayer, as had been shown previously by O'Leary et al.[32] The increased allyl concentration on the surface then lead to higher levels of bromination of those surfaces. However, both the Br−Si and Br−C components of the Br 3d peak seemed

	C−Si[a]	C−Si[b]	Br−C[b]	Br−Si[b]
Methyl	1.00	0.97	0.02	0.01
2 % Allyl	0.90	0.94	0.04	0.06
5 % Allyl	0.82	0.66	0.11	0.14
10 % Allyl	0.73	0.65	0.13	0.11
100 % Allyl	0.70	0.64	0.25	0.16

[a]Surface as prepared.

[b]Surface after reaction with Br_2 in methanol.

TABLE 2.1: Surface coverage in monolayers of carbon and bromine on various silicon surfaces functionalized with varying amounts of methyl and allyl groups. The error in all reported numbers is ±0.1. C−Si was calculated using the C 1s peak at 284 eV corresponding to surface-bound carbon. Br−C was calculated using the Br 3d doublet at 70 and 71 eV, corresponding to the bromine bound to carbon. Br−Si was calculated using the Br 3d doublet at 69 and 70 eV, corresponding to the bromine bound to the silicon surface.

to be increasing, suggesting that the silicon surface had become more susceptible to attack by the Br_2 than in the case for the methyl-terminated surface, probably because the larger allyl group prevented 100 % termination of the silicon atop sites,[13] leading to larger numbers of unfunctionalized sites as the allyl incorporation into the mixed monolayer was increased. This was supported by the apparent decrease in surface coverage of carbon bound to silicon on the surface after the bromination reaction. Table 2.1 contains the surface coverage of selected elements for all samples shown in Figure 2.6.

Finally, an allyl-terminated surface was prepared and reacted with Br_2 in methanol, shown in Figure 2.6f. This surface had the largest Br−C and Br−Si peaks, as expected. However, this surface had only ∼25 % surface coverage of Br−C, which was much lower than the total amount of allyl-group coverage measured using the C 1s XPS signal. This suggested that the reaction was incomplete or that the sterics of the allyl-terminated surface did not allow for all the allyl groups to react with the Br_2. However, the large amount of Br−Si seen on this and the mixed surfaces suggested that increasing the reaction time could result in damage to the mixed monolayer by reaction of the Br_2 with the silicon surface.

We tested the stability of the surfaces to Br_2 over time by exposing methyl-, allyl-, and mixed monolayer-terminated surfaces to the Br_2 in methanol solution for 0–60 min. The methyl surface was quite stable to bromination, with effectively no loss of the C−Si peak and very low (0.01 ± 0.01 monolayers) bromination of the surface after 60 min in a 5 % Br_2 in methanol (v/v) solution. Thus we concluded that the silicon-methyl bond was not particularly reactive with Br_2. The allyl surface showed immediate reactivity with Br_2, and after 60 min

did not change significantly. The C−Si and Br−C coverages were nearly identical, and hovered around 0.5 ± 0.1 monolayers from 2–60 min exposure to Br_2 in methanol, indicating that the allyl group reacted quickly. The Br-Si coverage also remained fairly constant, around 0.20 ± 0.05 monolayers, indicating that both the unreacted silicon atop sites and some Si−C bonds reacted with Br_2. However, this reaction appeared self-limiting, which was indicative of the stability of the allyl surface. On a mixed monolayer made from a 2 % allyl and 98 % methyl Grignard solution (2 % allyl surface), the reaction also proceeded rapidly, with little change to the surface from 2–60 min of exposure to Br_2 in methanol. The C−Si coverage dropped from 0.9 ± 0.1 to 0.7 ± 0.1 monolayers over the hour, with a concomitant increase in Br−Si to 0.10 ± 0.05 monolayers. The Br−C coverage also stayed fairly constant around 0.08 ± 0.10 monolayers. This suggested that allyl coverage was quite low, but previous studies using 2 % allyl surfaces indicated that allyl coverage is closer to 0.4 monolayers.[32]

From these results, it appeared that there was an olefin on the surface that was available to react, at least with Br_2. However, the allylic concentration on the 2 % allyl surface may have been much lower than initial estimates. Based on these results, the absence of reactivity of the allyl surface with G2 could have been a steric problem. To test this hypothesis, we studied how longer-chain olefins reacted on the surface.

2.3   Mixed Butenyl/Methyl Surfaces

The 4-carbon chain terminal olefin, or butenyl Grignard, was used to form mixed monolayers with methyl Grignard. This reagent was chosen because it had an additional carbene group extending the olefin from the surface, and was also commercially available. Mixed butenyl/methyl surfaces were formed by mixing the Grignard reagents in various ratios in solution to form a 1 M Grignard solution and allowing the chlorine-terminated silicon wafers to react for 1–2 h at 65 °C. The experimental details can be found in Appendix A.5. These mixed monolayers were characterized using XPS, FTIR, and microwave conductance spectroscopy to measure surface recombination velocity (SRV). The experimental details for these techniques can be found in Appendices B.1, B.2, and B.3.

XPS was used to determine the total carbon surface coverage on these surfaces. Figure 2.7 shows the C−Si coverage of a series of mixed monolayers formed by varying the ratio of butenyl and methyl Grignards in the reaction mixure. These surfaces were functionalized in
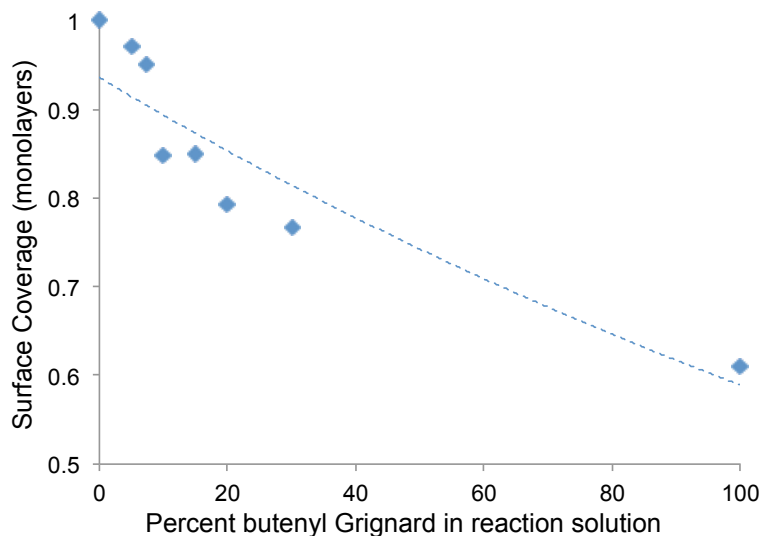
FIGURE 2.7: Plot of total surface coverage as measured using the C−Si peak from the C 1s XPS data collected on a series of mixed monolayers on silicon formed by varying the ratio of methyl to butenyl Grignard in solution. Dashed line shown as guide for the eye. Total surface coverage decreased nonlinearly from 1.0 ± 0.1 monolayers to 0.6 ± 0.1 monolayers as the butenyl Grignard concentration in solution increased from 0 to 100 %.

solutions with butenyl Grignard concentrations ranging from 0–100 % in solution, hereafter referred to as X %ButMM, where X is the percentage of butenyl Grignard in the reaction solution. The remainder of the solution comprised methyl Grignard, for a final concentration of 1 M Grignard in THF. The high-resolution C 1s XPS was composed of both the methyl and butenyl groups of the mixed monolayers and therefore the quantification of the relative amounts of each component could not be determined by XPS. The surface oxidation could be measured using the high-resolution Si 2p XPS regions of each surface, and the absence of any surface oxide peak at 103 eV was used to ensure high quality surfaces for subsequent reactivity.

FTIR spectra of a series of mixed monolayers containing various amounts of methyl and butenyl Grignard in the reaction solution were analyzed to look for the terminal olefin peak at $\sim 1600\,\mathrm{cm}^{-1}$, as well as the methyl peaks at 1257 and $757\,\mathrm{cm}^{-1}$. These spectra are shown in Figure 2.8. All four surfaces had distinct signals at 1257 and $757\,\mathrm{cm}^{-1}$, indicating that all four surfaces had methyl groups on the surface, as expected. While there was some indication of the C=C stretch in the spectrum of the 15 %ButMM surface, it was small and difficult to distinguish. There was very little surface oxidation based on the absence of a significant absorbance around 1000 to $1200\,\mathrm{cm}^{-1}$ on all the surfaces. This agreed well with the XPS
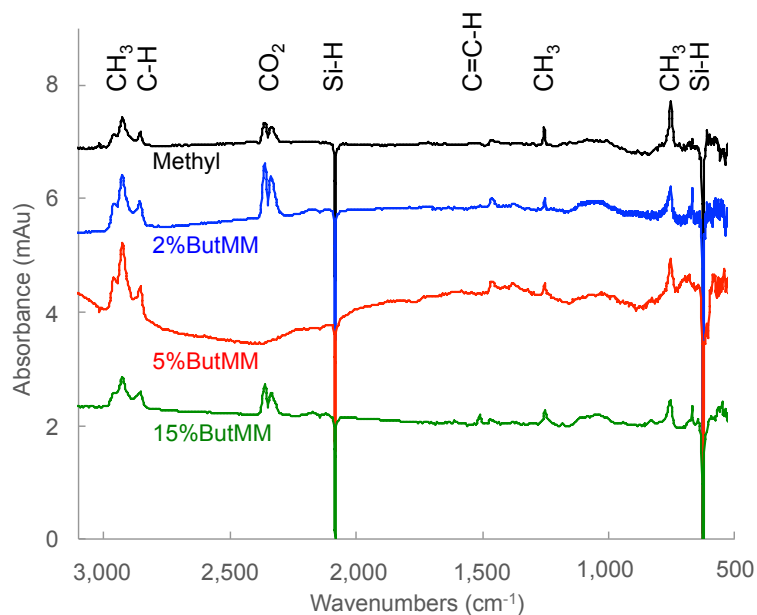
FIGURE 2.8: FTIR spectra of a series of silicon wafers with surfaces functionalized by mixed methyl/butenyl monolayers of various composition. The surfaces were each functionalized in a 1 M Grignard solution made with 0–15 % butenyl Grignard in solution, with the remainder made up of methyl Grignard. The IR stretches of interest are labeled with the relevant chemical groups.

data from these surfaces, which did not show any surface oxide in the Si 2p regions.

SRV measurements were carried out on mixed methyl/butenyl monolayers formed on intrinsically doped silicon wafers. These results are shown in Figure 2.9. The SRVs measured on all the mixed monolayers were below $100\,\mathrm{cm\,s^{-1}}$, which is generally considered to be the cutoff for a silicon surface with reasonable photoelectronic properties. The 100 %ButMM surface had a much higher SRV ($850\,\mathrm{cm\,s^{-1}}$), indicating rapid recombination of charge carriers at the surface. This was consistent with the XPS data, which showed high surface coverage (>0.75 monolayers) for all the mixed monolayer surfaces, but fairly low coverage (0.6 monolayers) for the 100 %ButMM surface (Figure 2.7). The lower coverage on this surface indicated that there were unreacted surface sites, which were prone to oxidation in air and could facilitate charge carrier recombination.

2.3.1 Sequential Reactions

Because of the difficulty in calculating the relative coverage of butenyl and methyl groups on the mixed surfaces, we changed the reaction sequence. Rather than controlling surface
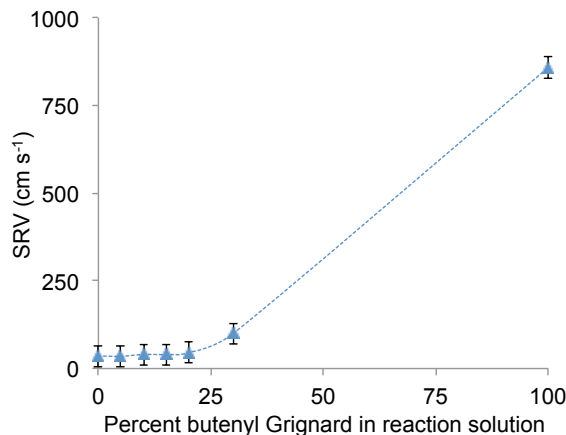
FIGURE 2.9: Plot of the surface recombination velocity (SRV) measured on intrinsic silicon surfaces modified by mixed methyl/butenyl monolayers of various compositions. The ratio of butenyl to methyl on the surface was varied by changing the relative ratios of butenyl Grignard to methyl Grignard in the reaction solution.

SCHEME 2.2: Formation of mixed methyl/butenyl monolayers on Si(111) surfaces sequentially, starting from the H-terminated surface.

coverage by varying the butenyl : methyl ratio in solution, we first reacted the surface with butenyl Grignard alone for a set period of time, followed by reaction with methyl Grignard to fill in the unreacted atop sites, resulting in a mixed methyl/butenyl monolayer. This reaction sequence is shown in Scheme 2.2. The experimental details for the formation of these surfaces are in Appendix A.5.

The coverage of butenyl groups on the surface could be controlled by varying the time that the silicon wafer was placed in the butenyl Grignard solution. These partially functionalized surfaces could then be placed in methyl Grignard to fill in the remaining unreacted surface sites. Figure 2.10 shows the surface coverage of the partial butenyl surfaces and mixed butenyl/methyl surfaces vs. time in the butenyl Grignard solution, as measured using the C−Si peak in the C 1s XPS. The surface coverage of the partial butenyl surfaces increased with reaction time, as expected, from 0.25 ± 0.50 to 0.55 ± 0.05 monolayers. The mixed butenyl/methyl surfaces showed increased coverage when compared to the partial butenyl surfaces, from the addition of methyl groups to the surface. The total surface coverage
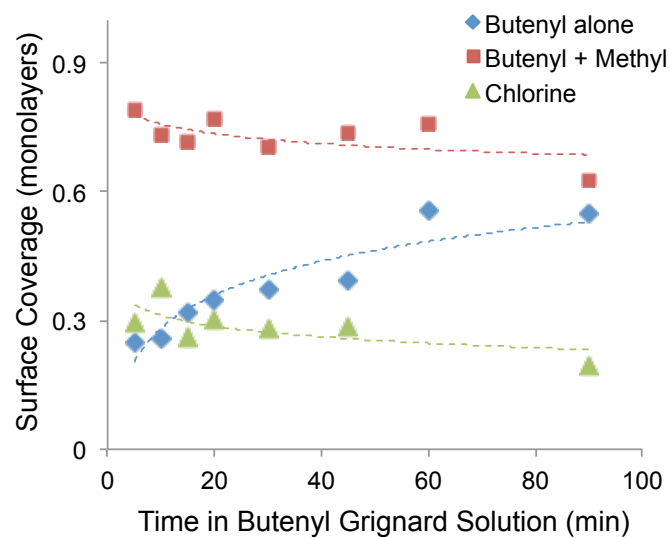
FIGURE 2.10: Plot of surface coverage of a series of functionalized silicon surfaces prepared by varying the reaction time in butenyl Grignard solution. Butenyl alone (blue diamonds) were only exposed to butenyl Grignard, and the remaining chlorine on the surfaces is shown in green (triangles). The mixed methyl/butenyl surfaces (red squares) were first exposed to the butenyl Grignard solution for the time shown, and then placed in methyl Grignard solution for 1 h to fill in the unreacted sites. The mixed surfaces did not show any remaining chlorine by XPS. Surface coverage increased with reaction time for the butenyl alone surfaces and decreased with reaction time for the mixed butenyl/methyl surfaces, converging around 0.6 monolayers. The surface coverage of chlorine on the butenyl alone surfaces remained fairly constant at around 0.3 monolayers.

decreased with reaction time in butenyl Grignard, however, from 0.80 ± 0.05 to 0.60 ± 0.05 monolayers. This suggested that with high enough butenyl coverage, there were some surface sites that could not be functionalized by the methyl group, probably for steric reasons. The remaining chlorine on the partial butenyl surfaces, as measured using the Cl 2s XPS signal, is also shown in Figure 2.10. The surface coverage of chlorine remained fairly constant around 0.30 ± 0.05 monolayers, though it did decrease slightly with reaction time in butenyl Grignard solution. The total coverage of butenyl and chlorine on the partial butenyl surfaces did not add up to 1.0 monolayers, however. This suggested that the chlorine coverage measured by XPS may have been be influenced by some outside factor which could artificially decrease the amount of chlorine remaining on the surface, possibly during the cleaning process. The surfaces were all sonicated in CH_3OH prior to analysis by XPS, which could have replaced some of the chlorine groups on the surface, or the chlorine sites could have reacted with water or oxygen in the air. After methylation of the partial butenyl surfaces, there was no measureable Cl 2s signal by XPS, indicating that the methyl Grignard had reacted with the remaining chlorinated surface sites.

Representative high-resolution XPS of the Si 2p, C 1s, and Cl 2s peaks of a partial butenyl and a mixed methyl/butenyl surface are shown in Figure 2.11. These surfaces were both reacted with 1.0 M butenyl Grignard at 65 °C for 20 min. The mixed methyl/butenyl surface was then reacted with 1.0 M methyl Grignard at 65 °C for 2 h. The Si 2p region of both surfaces did not have a silicon oxide peak at 103 eV, indicating that the surfaces were not oxidized during functionalization. The C 1s region of both surfaces were composed of three peaks, at 284, 285.5, and 287 eV. The C-Si component at 284 eV was larger for the mixed methyl/butenyl surface than for the partial butenyl surface, corresponding to 0.78 ± 0.05 and 0.35 ± 0.05 monolayers, respectively. This increase in surface coverage suggested that the methyl Grignard reacted with the chlorine groups remaining on the partial butenyl surface, resulting in a surface that was composed of both butenyl and methyl groups. The partial butenyl surface showed a large chlorine signal in the Cl 2s region, at 270 eV, corresponding to 0.30 ± 0.05 monolayers. The Cl 2s region of the mixed methyl/butenyl surface did not show any chlorine remaining on the surface, which supported the idea that the methyl Grignard could react with the remaining chlorine groups on the partial butenyl surface, forming a mixed monolayer.

The SRVs measured on partial butenyl and mixed methyl/butenyl surfaces are shown in

Butenyl 20 min
Butenyl 20 min + methyl
a
Cl 2s
b
C 1s
c
Si 2p
d
Cl 2s
e
C 1s
f
Si 2p
Counts
274
270
266
289
285
281
105
101
97
Binding Energy (eV)
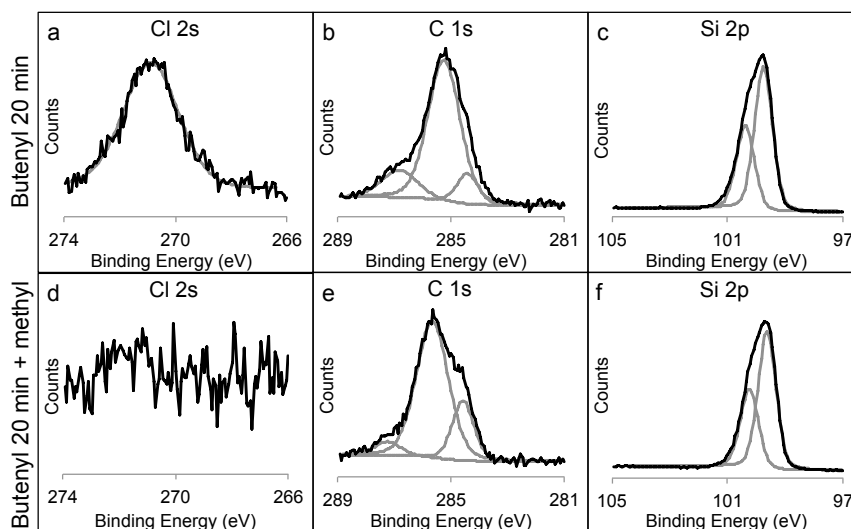
FIGURE 2.11: High-resolution XPS of the Si 2p, C 1s, and Cl 2s peaks for both a partial butenyl (top) and a mixed methyl/butenyl (bottom) modified silicon surface. These surfaces were both reacted with butenyl Grignard for 20 min, followed by reaction with methyl Grignard on the mixed methyl/butenyl surface. a,d) The Cl 2s region of the partial butenyl surface showed a large signal at 270 eV from chlorine remaining on the surface, while the mixed methyl/butenyl surface did not have any chlorine signal. b,e) The C 1s region of both surfaces was composed of three peaks at 284, 285.5, and 287 eV. The C-Si peak at 284 eV was larger on the mixed methyl/butenyl surface than on the partial butenyl surface, as expected. c,f) The Si 2p region of both surfaces showed no silicon oxide signal at 103 eV, indicating that these surfaces were not oxidized during functionalization.
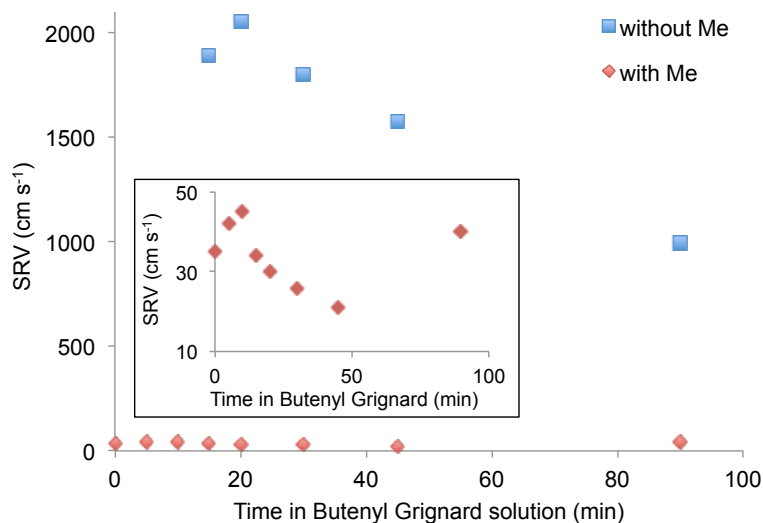
FIGURE 2.12: Plot of the SRV vs. time in butenyl Grignard solution measured on a series of functionalized silicon surfaces. Shown in blue (squares) are the surfaces that were only exposed to butenyl Grignard. In red (diamonds) are the surfaces that were first reacted with butenyl Grignard solution for the given amount of time, and then placed in methyl Grignard for 2 h. The inset shows the SRVs of the mixed methyl/butenyl surfaces on an expanded scale for clarity.

Figure 2.12. The surfaces formed by varying the time in butenyl Grignard all had large SRVs, of $>1000 \, \mathrm{cm \, s^{-1}}$, indicating fast charge carrier recombination at the surface, and therefore poor photoelectronic properties. However, the same treatment with butenyl Grignard followed by reaction with methyl Grignard resulted in SRVs of $<50 \, \mathrm{cm \, s^{-1}}$. These long charge-carrier lifetimes indicated that charge-carrier recombination at the surface was slow, suggesting that these surfaces had excellent photoelectronic properties. All of this data indicated that methylation of the partial butenyl surfaces formed a mixed monolayer of butenyl and methyl groups on the surface, resulting in surfaces that had high total surface coverage as well as high coverage of the functional moiety (namely butenyl). These mixed monolayers did not show any surface oxidation by XPS or FTIR and displayed low SRVs, indicating that they had good photoelectronic properties.

2.4 Cross-coupling Reactions of Butenyl/Methyl Surfaces

Based on the above data, we have developed a method for forming mixed butenyl/methyl monolayers on silicon with high coverage of butenyl groups and good photoelectronic properties. Cross-coupling of functional groups onto the surface using the Grubbs' 2nd generation
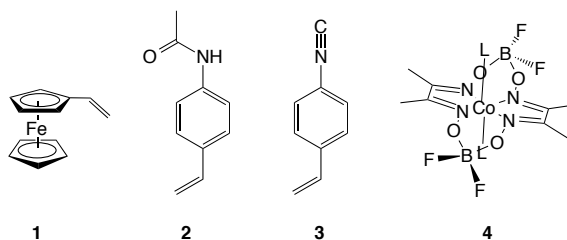
FIGURE 2.13: The three molecules investigated for cross-coupling efficacy using the Grubbs' 2nd generation catalyst on mixed methyl/butenyl surfaces, and the final proton-reduction catalyst to be assembled on the surface. **1**: Vinylferrocene (vFc), **2**: 4-vinylphenyl acetamide (4-VPA), **3**: 4-vinylphenyl isocyanide (4-VPI), and **4**: Co(dimethylglyoximeBF$_2$)$_2$(L)$_2$ complex (Codmg) to be used as a proton reduction catalyst on the surface.

catalyst (G2) was the next step. There were several possible routes for attaching catalysts to the surface using cross-coupling reactions. One possibility was the direct attachment of an entire catalytic complex or redox active group via the terminal olefin on one of its ligands. This route was tested by using vinylferrocene (vFc, Figure 2.13-**1**) as a model one-electron redox couple. Another possible route was to cross-couple the ligand to the surface first, followed by metallation of that ligand with the remainder of the catalytic or redox-active group to form the active species on the surface. This was done using 4-vinylphenyl isocyanide (4-VPI, Figure 2.13-**3**) as an axial ligand for the Co(dmg)$_2$(L)$_2$ complex (Codmg, Figure 2.13-**4**). This complex has been shown to be catalytic for proton reduction in acetonitrile.[44,45] As a test substrate, 4-vinylphenyl acetamide (4-VPA, Figure 2.13-**2**) is an analogue for 4-VPI with a strong IR signal that should be visible by surface FTIR. This molecule will undergo the same cross-coupling reaction as 4-VPI, but this FTIR tag can be used to characterize the surfaces to investigate the efficacy of the reaction. Experimental details for the cross-coupling reaction can be found in Appendix A.6

2.4.1 4-VinylPhenyl Acetamide

4-Vinylphenyl acetamide, which was synthesized by M. Rose, had an IR stretch at $1661\,\mathrm{cm}^{-1}$ that should be easily distinguished in the FTIR spectrum of a functionalized silicon surface. The IR spectrum of this molecule is shown in Figure 2.14 (collected by M. Rose). This species was cross-coupled onto mixed butenyl/methyl surfaces using G2, as shown in Scheme 2.3. All reactions took place under a N$_2$ atmosphere. First, the mixed butenyl/methyl surface was placed into a solution of 1.0 M G2 in CH$_2$Cl$_2$ for 6–10 h at 50 °C. The wafer was then rinsed
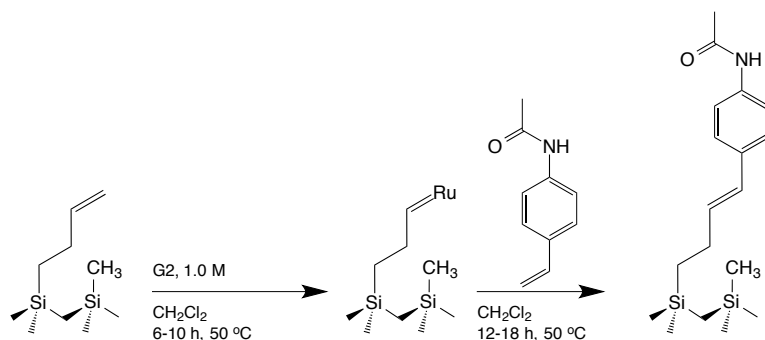
SCHEME 2.3: Reaction scheme for the 2-step cross-coupling of 4-VPA onto a mixed methyl/butenyl surface using the Grubbs' 2nd generation catalyst.
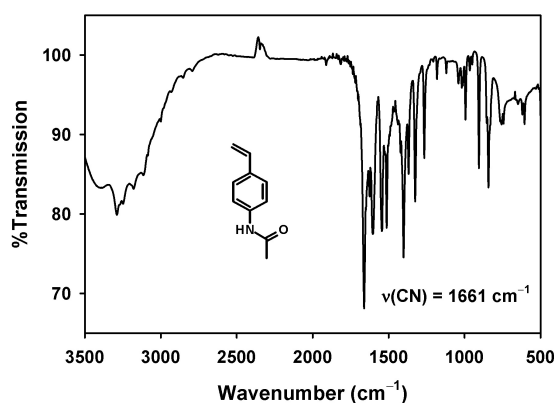
FIGURE 2.14: Transmission infrared spectrum of 4-vinylphenyl acetamide (4-VPA), collected by M. Rose. There was a strong C−N stretch in this molecule at $1661\,\mathrm{cm}^{-1}$.

with CH_2Cl_2 and placed in $1.0\,M$ 4-VPA in CH_2Cl_2 for 12–18 h at 50 °C. After reaction, the wafer was rinsed with CH_2Cl_2 and sonicated sequentially in CH_2Cl_2, methanol, and water to clean the surface and remove unreacted starting material. Experimental details for the cross-coupling reaction can be found in Appendix A.6.

The surfaces were analyzed by FTIR and XPS. Figure 2.15 shows the FTIR spectra collected on a mixed butenyl/methyl surface, a mixed butenyl/methyl surface reacted with G2 and 4-VPA, and a mixed butenyl/methyl surface reacted with only 4-VPA to control for non-specific adsorption. The butenyl/methyl surface had a small signal around $1600\,\mathrm{cm}^{-1}$, possibly from the butenyl olefin, and there was no signal around $1661\,\mathrm{cm}^{-1}$, as expected for a surface that was not exposed to 4-VPA. The butenyl/methyl + G2 + 4-VPA surface had a strong series of signals between 1500 to $1700\,\mathrm{cm}^{-1}$, including a significant absorbance at $1661\,\mathrm{cm}^{-1}$. The butenyl/methyl + 4-VPA had the same series of signals between 1500
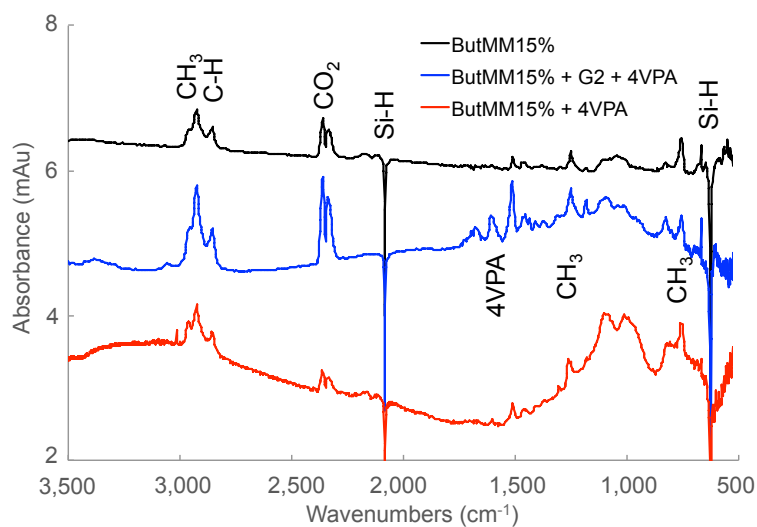
FIGURE 2.15: FTIR spectra of a series of mixed butenyl/methyl silicon surfaces modified by reaction with 4-VPA. In black is a mixed butenyl/methyl surface as prepared, showing the characteristic methyl stretches at 1257 and $757\,\mathrm{cm}^{-1}$. This surface had a small signal around $1600\,\mathrm{cm}^{-1}$ from the butenyl olefin, and little surface oxidation around $1000\,\mathrm{cm}^{-1}$. In blue is the same surface after reaction with the Grubbs' 2nd generation catalyst (G2) and 4-VPA. The methyl stretches remained unchanged, and large signals between 1500 and $1700\,\mathrm{cm}^{-1}$ appeared, consistent with the 4-VPA stretch at $1661\,\mathrm{cm}^{-1}$. In red is the mixed butenyl/methyl surface after reaction with only 4-VPA. There were some small signals around 1500 to $1700\,\mathrm{cm}^{-1}$, indicating a small amount of non-specific reactivity with the mixed monolayer surface. This surface also showed significant surface oxidation between 1000 and $1200\,\mathrm{cm}^{-1}$. Other relevant IR signals are labeled.
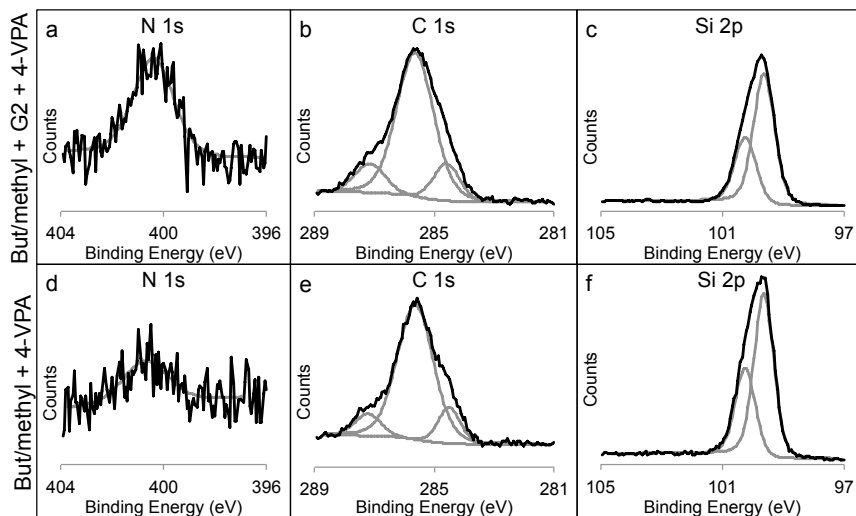
FIGURE 2.16: High-resolution XPS of the mixed butenyl/methyl + G2 + 4-VPA and the mixed butenyl/methyl + 4-VPA surfaces. a,d) The N 1s XPS region of the respective surfaces. The surface exposed to G2 + 4-VPA had significantly more nitrogen from the acetamide group than the surface only exposed to 4-VPA (0.20 ± 0.05 vs. 0.06 ± 0.05 monolayers). b,e) The C 1s XPS region of the respective surfaces. These surfaces both showed a large C-Si component at 284 eV, from the surface-attached species. c,f) The Si 2p XPS region of the respective surfaces. These signals were very similar, with little surface oxidation visible at 103 eV, indicating that the reaction conditions do not damage the surfaces.

to $1700 \, \text{cm}^{-1}$, but with much lower intensity than on the surface that was exposed to both G2 and 4-VPA. These signals were likely due to non-specific adsorption of 4-VPA onto the mixed butenyl/methyl surface, or from reactivity of the olefin with the few remaining unfunctionalized silicon atop sites on the mixed surface. However, the strong signal seen on the butenyl/methyl + G2 + 4-VPA surface indicated that the cross-coupling reaction was successful. In addition, there was little surface oxidation of the mixed butenyl/methyl and butenyl/methyl + G2 + 4-VPA surfaces, based on the absence of IR signals around $1000 \, \text{cm}^{-1}$. The butenyl/methyl + 4-VPA surface, on the other hand, had significant absorption between 1000 to $1200 \, \text{cm}^{-1}$ where the $Si{-}O$ stretches can be found, indicating that there was surface oxidation in this case. All three surfaces had the expected signals at 757 and $1257 \, \text{cm}^{-1}$ from the methyl groups on the surface.

High-resolution XPS of the butenyl/methyl + G2 + 4-VPA and butenyl/methyl + 4-VPA surfaces are shown in Figure 2.16. Surface oxidation remained low, based on the lack of a silicon oxide peak at 102 eV in the Si 2p spectra, indicating that the reaction conditions did not damage the surface. The C 1s regions of both surfaces looked very

similar, with a peak at 284 eV from the silicon-bound carbons. The butenyl/methyl + G2 + 4-VPA surface had a N 1s peak at 401 eV corresponding to 0.20 ± 0.05 monolayers of 4-VPA on the surface. Details of surface coverage calculations using XPS can be found in Appendix B.1.1. The butenyl/methyl + 4-VPA surface also had a small N 1s peak at 401 eV corresponding to 0.06 ± 0.05 monolayers of 4-VPA on the surface. This number was almost within experimental error, suggesting that nonspecific adsorption or reaction of the 4-VPA with the mixed butenyl/methyl surface was limited. This was consistent with the FTIR data, which showed a larger 4-VPA signal on the surface exposed to both G2 and 4-VPA than on the surface exposed to 4-VPA only. This indicated that the cross-coupling reaction with G2 was successful on the mixed butenyl/methyl surface under these conditions, with little non-specific reaction of the 4-VPA with the surface.

2.4.2   4-VinylPhenyl Isocyanide

The attachment of 4-VPA to the surface via cross-coupling with G2 was apparently successful. 4-VPI, which can act as a ligand to the Codmg complex shown in Figure 2.13-4, is an analogue of 4-VPA and should react with the mixed butenyl/methyl surface in a similar manner. This molecule does not have an easily distinguished IR signal, but the nitrogen of the isocyanide group can be used as an XPS tag to characterize the reaction product. Cross-coupling of 4-VPI to the surface was done similarly to the 4-VPA, in a two-step process starting from the mixed butenyl/methyl surface. Experimental details for this reaction can be found in Appendix A.6. High-resolution XPS of a mixed methyl/butenyl surface modified with 4-VPI is shown in Figure 2.17a-c. The N 1s signal of the butenyl/methyl + G2 + 4-VPI surface had a peak corresponding to 0.15 ± 0.05 monolayers, indicating that the cross-coupling reaction was successful on this surface. The Si 2p region had no peak at 103 eV, indicating that the surface was not oxidized during the functionalization and cross-coupling reactions. The C 1s region retained the peak at 284 eV from the carbon directly bound to silicon from the methyl and butenyl groups.

Metallation of the surface with the Codmg complex was performed by soaking the butenyl/methyl + G2 + 4-VPI modified surface in a solution of 10 mg Codmg in 8 mL CH_3CN for 2.5 h at RT. The experimental details for metallation with Codmg can be found in Appendix A.7. The XPS of the metallated surface is shown in Figure 2.17d-f. A F 1s peak at 688 eV appeared from the BF_2 groups in the Codmg complex, corresponding to
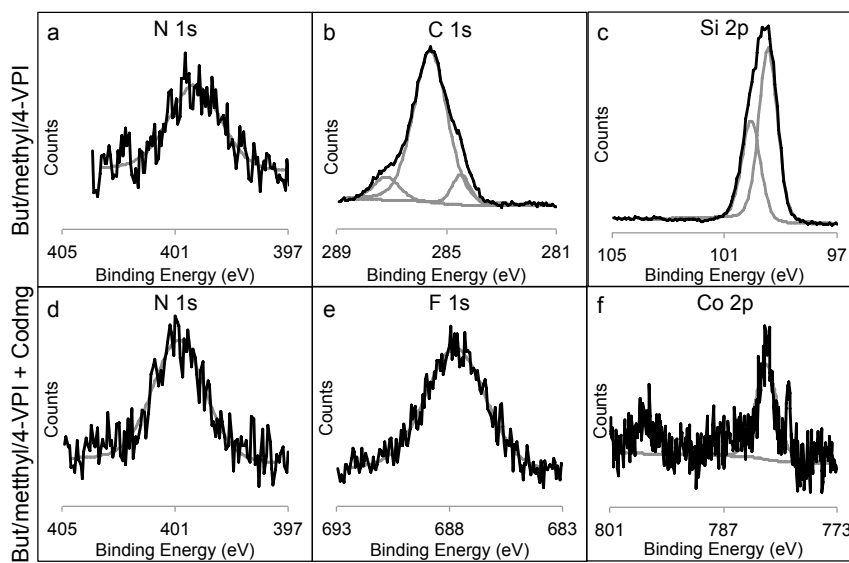
FIGURE 2.17: High-resolution XPS of mixed butenyl/methyl surfaces modified by cross-coupling with 4-VPI and metallated with Codmg. a, b, c) The N 1s, C 1s, and Si 2p high-resolution XPS, respectively, of the mixed butenyl/methyl + G2 + 4-VPI surface. a) The N 1s peak at 400 eV from the isocyanide group indicated that the cross-coupling reaction with 4-VPI was successful. This peak corresponded to 0.15 ± 0.05 monolayers of 4-VPI on the surface. b) The C 1s peak had a large C−Si component at 284 eV, corresponding to 0.75 ± 0.05 monolayers, indicative of high surface coverage. c) The Si 2p region showed little oxidation of the silicon surface based on the absence of a Si−O peak at 103 eV. d, e, f) The N 1s, F 1s, and Co 2p high-resolution XPS, respectively, of the butenyl/methyl + G2 + 4-VPI surface after metallation with the Codmg complex. d) The N peak shifted to slightly higher energy, at 401 eV, consistent with ligation by Co. This peak also increased in intensity, to 0.20 ± 0.05 monolayers of nitrogen. e) The F 1s region had a peak at 688 eV from the BF_2 groups of the Codmg complex. f) The Co 2p region had a doublet of peaks at 782 and 797 eV from the Codmg complex, indicating that the complex is intact on the surface.

0.20 ± 0.05 monolayers. The Co 2p doublet at 782 and 797 eV, corresponding to 0.03 ± 0.01 monolayers, was also present on the surface from the Codmg complex. These peak positions were consistent with previous XPS studies on similar Codmg complexes, suggesting that the Co center was intact and was in the chemical environment of the Codmg complex.[46] The N 1s peak at 401 eV corresponded to 0.20 ± 0.05 monolayers, a small increase from the 4-VPI modified surface. This increase in N signal was from the dimethylglyoxime ligands on the Codmg complex. There should be 4 F atoms per Co, and 5 N atoms per Co, so the relative coverages were within experimental error (0.05 monolayers F, 0.04 monolayers N, 0.03 monolayers Co). All of this data together suggested that the Codmg complex was intact on the surface.

2.4.3 Vinylferrocene

Cross-coupling of a presynthesized metal complex that can serve as a one-electron redox couple onto the surface was done by using G2 to couple vinylferrocene (vFc) to a mixed methyl/butenyl surface. This was done in a similar manner to the reactions used to cross-couple 4-VPA and 4-VPI onto mixed butenyl/methyl surfaces. The experimental details can be found in Appendix A.6. XPS of the butenyl/methyl + G2 + vFc surface is shown in Figure 2.18. The Si 2p peak had no indication of surface oxidation, based on the absence of a Si−O peak at 103 eV. The C 1s peak showed a C−Si peak at 284 eV of 0.7 ± 0.1 monolayers, indicating that surface coverage remained high. The Fe 2p peak showed a set of two doublets, one at 708 and 721 eV, corresponding to the Fe(II) signal from the ferrocene group, and another at 712 and 725 eV, corresponding to Fe(III).[47] The Fe(III) signal was presumably from ferrocenium, formed by oxidation of the ferrocene on the surface, or from ferrocene that had decomposed to another Fe(III) species. The total Fe on the surface corresponded to 0.15 ± 0.05 monolayers.

To investigate how the cross-coupling reaction affected the photoelectronic properties of the silicon, we prepared some control samples for SRV. Figure 2.19 shows the SRVs measured on a mixed butenyl/methyl surface, a mixed butenyl/methyl surface reacted with G2 for 6–10 h at 50 °C, and a mixed butenyl/methyl surface reacted with G2 followed by reaction with vFc for 12–18 h at 50 °C. The mixed butenyl/methyl surface started out with an SRV just over $100\,\mathrm{cm\,s^{-1}}$, but over the course of a few days the SRV decreased to $\sim 50\,\mathrm{cm\,s^{-1}}$. The SRV then remained steady around $50\,\mathrm{cm\,s^{-1}}$ for several months in air. The mixed butenyl/methyl
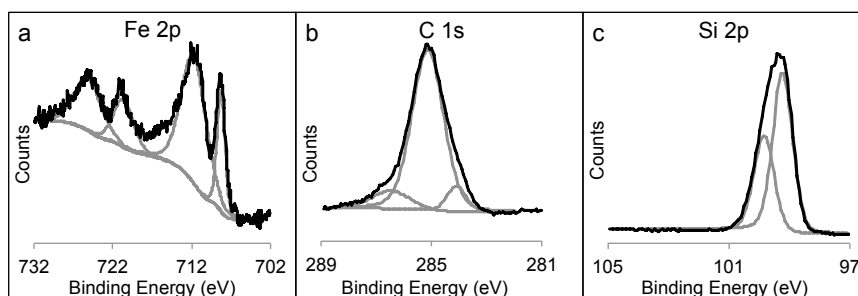
FIGURE 2.18: High-resolution XPS of the mixed butenyl/methyl surface with vinylferrocene (vFc) cross-coupled to the surface using the Grubbs' 2nd generation catalyst. a) The Fe 2p signal, corresponding to 0.15 ± 0.05 monolayers, indicated that the cross-coupling reaction was successful. b) The C 1s signal had a C−Si peak at $284\,\mathrm{eV}$ corresponding to 0.7 ± 0.1 monolayers, indicating high surface coverage. c) The Si 2p peak showed little to no surface oxidation at $103\,\mathrm{eV}$.

surface reacted with G2 had an SRV that remained steady at $40 \pm 5\,\mathrm{cm\,s^{-1}}$ over the course of several months. The mixed butenyl/methyl surface reacted with G2 followed by reaction with vFc had an SRV of $55 \pm 10\,\mathrm{cm\,s^{-1}}$ over several months. These surfaces all maintained SRVs of around $50\,\mathrm{cm\,s^{-1}}$ for months while sitting in air. Silicon surfaces with SRVs of $<100\,\mathrm{cm\,s^{-1}}$ were generally considered to have reasonable photoelectronic properties. This indicated that the photoelectronic properties of these surfaces were not adversely affected by the cross-coupling reaction.

Electrochemistry on the mixed butenyl/methyl surfaces with cross-coupled vFc were performed in an Ar-purged glove box. The experimental details of the electrochemistry setup can be found in Appendix B.4. Figure 2.20 shows that there was a reversible electrochemical signal at $0.1\,\mathrm{V}$ vs. $\mathrm{Ag/AgNO_3}$ in $\mathrm{CH_3CN}$ with $0.10\,\mathrm{M}$ tetraethylammonium perchlorate ($(\mathrm{NEt_4})\mathrm{ClO_4}$) as the supporting electrolyte from the surface-attached $\mathrm{Fc/Fc^+}$ couple. This was consistent with previous studies on surface-attached ferrocene on silicon surfaces under similar experimental conditions.[48] Figure 2.20 shows the peak current density vs. the scan rate and vs. the square root of the scan rate. The peak current had a linear dependence on scan rate, indicating that the redox couple was surface-bound.[49] The peak current was clearly non-linear with the square root of the scan rate, which indicated that this was not a diffusional process. Integration of the anodic and cathodic current vs. time gave the total charge transferred to the redox couple, which was used as a measure of the electroactive material on the surface. Details of this surface coverage calculation can be found in Appendix B.4.1. The total coverage measured electrochemically was 0.03 ± 0.01 monolayers of ferrocene. This
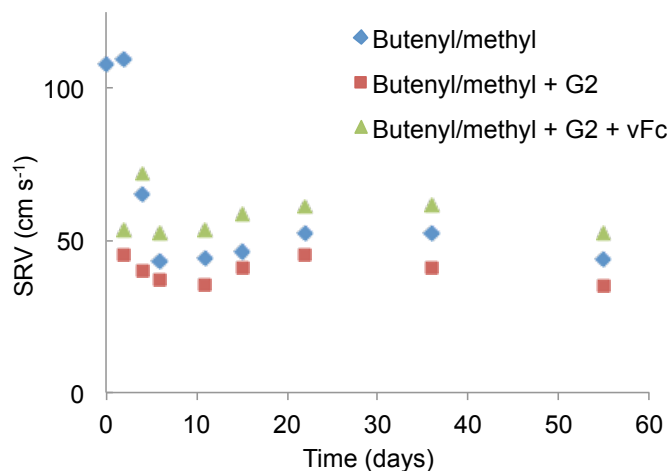
FIGURE 2.19: Surface recombination velocity (SRV) measured on a series of mixed butenyl/methyl surfaces after cross-coupling reactions over 60 days in air. In blue (diamonds), a mixed butenyl/methyl surface. In red (squares), a mixed butenyl/methyl surface reacted with the Grubbs' 2nd generation catalyst (G2). In green (triangles), a mixed butenyl/methyl surface reacted with G2 followed by reaction with vinylferrocene (vFc). All three surfaces had SRVs of $\sim 50\,\mathrm{cm\,s^{-1}}$ over the course of several months, indicating that these surfaces had long charge-carrier lifetimes, and therefore excellent photoelectrochemical properties.

was significantly lower than the XPS measurement indicated, but it was possible that the oxidized ferrocenium seen in the Fe 2p spectrum was not electroactive on this surface. In that case, the surface coverage of Fe(II) seen by XPS was similar to the electroactive vFc coverage measured here.

XPS of the surface collected after the electrochemical cycling is shown in Figure 2.21. The Si 2p region had no Si−O peak at 103 eV. This indicated that the surface was stable under electrochemical conditions and had not oxidized. The C 1s region had a C−Si peak at 284 eV, indicating that there were still carbonaceous surface-attached species. The Fe 2p region showed increased Fe(III) and decreased Fe(II) components as compared with the XPS collected prior to redox cycling. The total Fe coverage on the surface after the electrochemistry was 0.10 ± 0.05 monolayers, which indicated that some of the Fe was lost from the surface. However, the electrochemically active Fe(II) component from the ferrocene was still present after the electrochemical cycling and cleaning procedure. There was also a new N 1s peak at 400 eV following electrochemical cycling. This could be due to residual solvent, CH_3CN, remaining on the surface, or it could be from possible contamination by the electrolyte, $(NEt_4)ClO_4$.
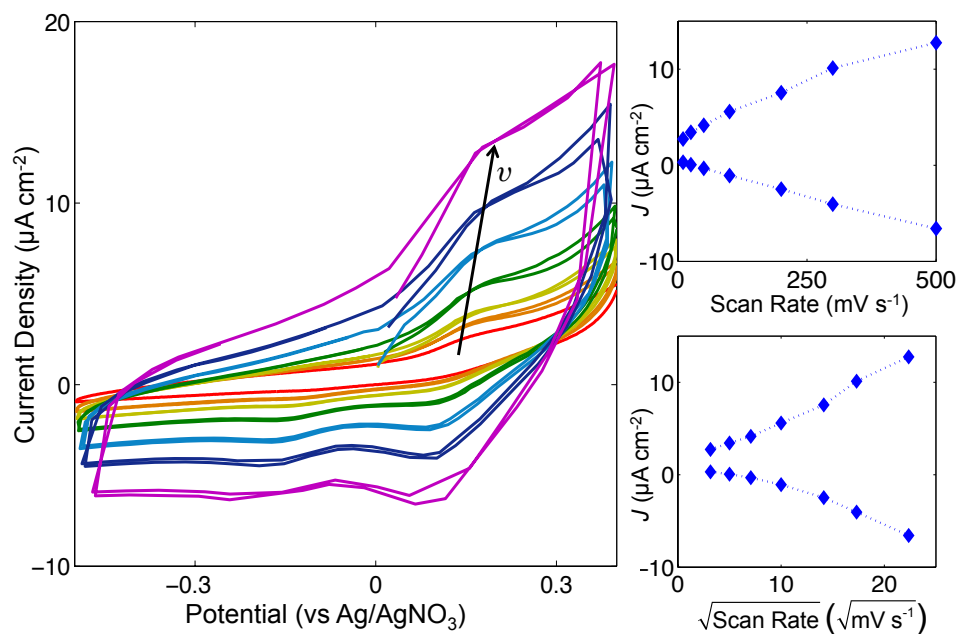
FIGURE 2.20: Cyclic voltammetry of a mixed butenyl/methyl monolayer on silicon with vinylferrocene cross-coupled on using the Grubbs' 2nd generation catalyst. Left: There was a reversible redox couple at $0.1\,\mathrm{V}$ vs. $\mathrm{Ag/AgNO_3}$. Increasing scan rate (v) from 10 to $500\,\mathrm{mV\,s^{-1}}$ is indicated by the black arrow. Top right: The peak current density (J) was linear with the scan rate, as predicted for a surface-attached redox couple. Bottom right: The peak current density (J) was not linear with the square root of the scan rate, indicating that this was not a diffusional process.
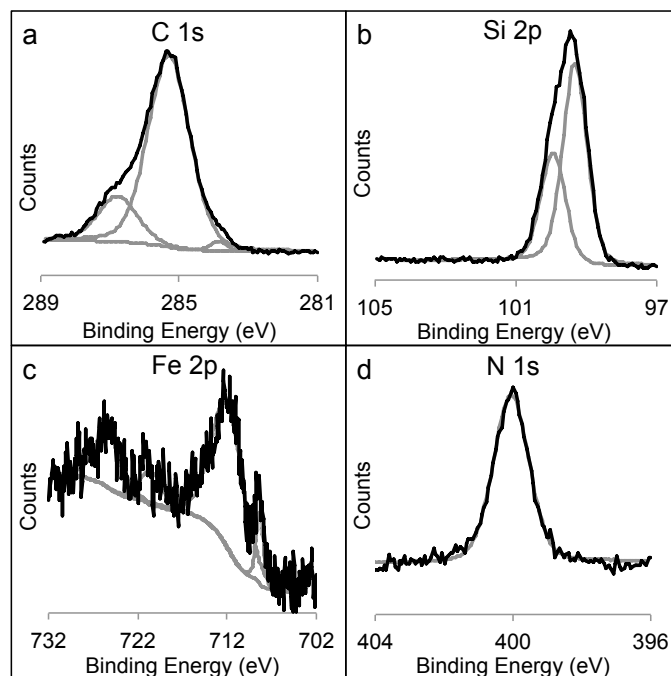
FIGURE 2.21: High-resolution XPS of the butenyl/methyl surface with cross-coupled vinyl-ferrocene following electrochemical cycling. a) The C 1s peak still had a C−Si component at 284 eV, indicating that there were still surface-attached species. b) The Si 2p peak did not show any indication of surface oxidation, based on the absence of a Si−O peak at 103 eV. c) The Fe 2p region showed increased Fe(III) components, suggesting that the ferrocene on the surface had become more oxidized as a result of the electrochemistry experiments. There were still Fe(II) components remaining on the surface as well. d) There was a new peak in the N 1s region at 400 eV, possibly from the solvent or the electrolyte used in the electrochemical experiments.

2.5   Conclusion

These results showed that it was possible to cross-couple ferrocene to the mixed butenyl/methyl surface using the Grubbs' 2nd generation catalyst and form electrochemically active surfaces with a surface-attached redox couple. We developed and characterized a new class of mixed methyl/butenyl monolayers with controllable surface coverage of each species. We used the Grubbs' catalyst to form electroactive monolayers by cross-coupling vinylferrocene onto the mixed methyl/butenyl surfaces. We showed that these mixed monolayers had excellent photoelectronic properties, based on the low SRVs measured on mixed methyl/butenyl surfaces before and after the cross-coupling reaction. This indicated that these electroactive surfaces have the necessary properties for use in a solar-fuel forming device. However, many attempts at this reaction with a variety of surfaces with varying amounts of butenyl never resulted in greater than 0.05 monolayers of electrochemically active ferrocene on the surface. This could be due to inherent steric constraints of the cross-coupling reaction, or it could be that the reaction was simply inefficient. Our thorough investigations of this reaction have established that this method of attachment for redox-active species resulted in low coverage, and was therefore unlikely to be useful for photoelectrochemical devices.

Chapter 3

Formation and Characterization of Mixed Vinylferrocenyl/Methyl Monolayers on Si(111) Surfaces

3.1 Introduction

Hydrosilylation of terminal olefins onto H-terminated silicon surfaces is a well-established technique for the covalent attachment of functional moieties to the silicon.[20,50] These hydrosilylated surfaces can have relatively high coverage of functional groups, in some cases approaching 60 % of the silicon atop sites, as for thermally-immobilized vinylferrocene on a Si(111) surface.[47] However, as discussed earlier, surfaces functionalized by hydrosilylation have limited surface coverage of the silicon atop sites because the steric bulk of the functional groups will not fit on every Si atop site. The remaining unfunctionalized sites are generally terminated by Si−H bonds, which are easily oxidized and result in undesirable electrochemical properties. Therefore, it is unclear that the 60 % coverage seen on hydrosilylated vFc-terminated surfaces actually corresponds to 60 % coverage of the Si(111) atop sites. If there is polymerization occurring during this radical reaction, then the actual silicon surface coverage could be much lower. In fact, the reported effective ferrocene diameter is 0.66 nm, which would mean that a compact monolayer coverage of ferrocenyl moieties would be $4.4 \times 10^{-10} \, \mathrm{mol \, cm^{-2}}$, corresponding to 0.34 monolayers on a Si(111) surface.[51,52] This calculation indicates that there must be multilayers forming on this surface, and that 65 % of the Si atop sites are unfunctionalized. Our previous work showed that the formation of mixed methyl/functional monolayers allowed us to maintain the excellent photoelectronic properties of the methyl surface while incorporating relatively high coverage of functional moieties on
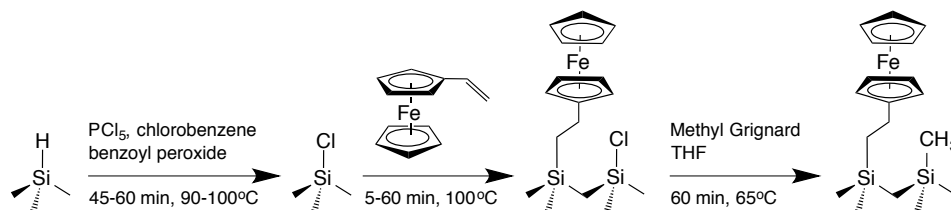
SCHEME 3.1: Reaction scheme for the formation of a mixed methyl/vFc monolayer on chlorinated Si(111) starting from a H-terminated Si(111) surface. Reprinted with permission from Lattimer et al.[34] Copyright 2013 American Chemical Society.

the surface as well. However, the steric requirements of the cross-coupling reactions described in Chapter 2 limited the ultimate surface coverage of redox-active groups. Our aim in the following chapter was to combine the high coverage of redox-active groups imparted by the hydrosilylation reaction with the passivation and high surface coverage of methylation to form a new class of mixed monolayers on silicon.

We describe herein the characterization of mixed monolayer surfaces that have been prepared via radical reaction of an olefin with the Cl−Si(111) surface, followed by functionalization of remaining reactive Si−Cl bonds with methyl groups via reaction with CH_3MgCl (Scheme 3.1). The approach is readily carried out with commercially available reagents and avoids sterically demanding reagents or intermediates that could limit the coverage of immobilized species. The method was demonstrated by incorporation of vinylferrocene into a mixed vinylferrocenyl/methyl monolayer on Si(111) surfaces. Vinylferrocene has been used frequently as a model redox couple for surface attachment due to the well-behaved electrochemistry of vinylferrocene, as well as the ease of attaching vFc to silicon surfaces via hydrosilylation.[47,48,53] In this work, we show that the two-step halogenation/alkylation method can be extended to allow the formation of a Si(111) surface that has electroactive groups directly bound to the surface prior to the backfill of the remaining Cl−Si sites with methyl groups, has a low interfacial charge-carrier recombination velocity, is protected against oxidation, and displays photoelectrochemical activity that confirms facile charge transfer from the silicon to the surface-attached redox species.

3.2 Methylation of H− and Cl−Si(111)

Methylation with a Grignard reagent requires a Cl−Si surface, while hydrosilylation requires a H−Si surface. The obvious way to form a mixed monolayer using both these reactions
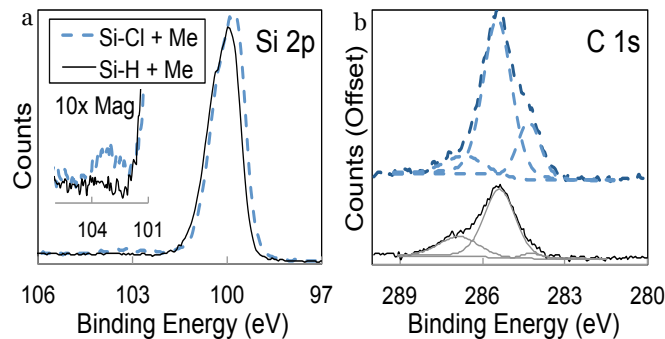
FIGURE 3.1: Comparison of the high-resolution XPS data for the a) Si 2p and b) C 1s signals of $CH_3-Si(111)$ surfaces produced by reaction of CH_3MgCl with a $Cl-Si(111)$ (blue, dashed) or $H-Si(111)$ (black, solid) surface. The oxide peak at $102\,eV$ in the Si 2p region is shown with 10x magnification in the inset. The C 1s peak at $284\,eV$ was ascribable to the carbon of the CH_3 group that was directly bound to atop $Si(111)$ sites. This peak on the surface formed on $H-Si(111)$ had an area of $\sim 8\,\%$ of the area of the peak for the $CH_3-Si(111)$ surfaces formed by reaction of CH_3MgCl with $Cl-Si(111)$. Adapted with permission from Lattimer et al.[34] Copyright 2013 American Chemical Society.

would be to perform both of these reactions on the same starting surface. We used methyl Grignard to functionalize both H- and Cl-terminated silicon to see if the reaction would be equally successful on both starting surfaces. The results are shown in Figure 3.1.[34] The Si 2p region of both surfaces had little sign of surface oxidation, based on the very small $Si-O$ peak at $103\,eV$, corresponding to <0.1 monolayer of surface oxide. Details of the surface coverage calculations using XPS can be found in Appendix B.1.1. The C 1s region (Figure 3.1b) exhibited three peaks, with the lowest binding-energy component, at $284\,eV$, corresponding to the carbon directly bound to silicon, and providing evidence that the surface had been functionalized with $Si-C$ bonds.[13,29] The higher binding-energy signal, at $285\,eV$, was ascribed to adventitious carbon bonded to carbon and/or hydrogen, and the $287\,eV$ peak was ascribed to adventitious carbon bonded to oxygen or other electronegative elements.[13,29] In contrast, $H-Si(111)$ surfaces that had been exposed to CH_3MgCl, without formation of the $Cl-Si(111)$ intermediate surface, showed C 1s signals at $284\,eV$ that had an area of $\sim 8\,\%$ of the corresponding peak on the $CH_3-Si(111)$ surfaces prepared by the two-step method (Figure 3.1b). Hence $H-Si(111)$ surfaces did not efficiently react with CH_3MgCl, and so the chlorination step was required under our reaction conditions to achieve a high yield of surface functionalization.
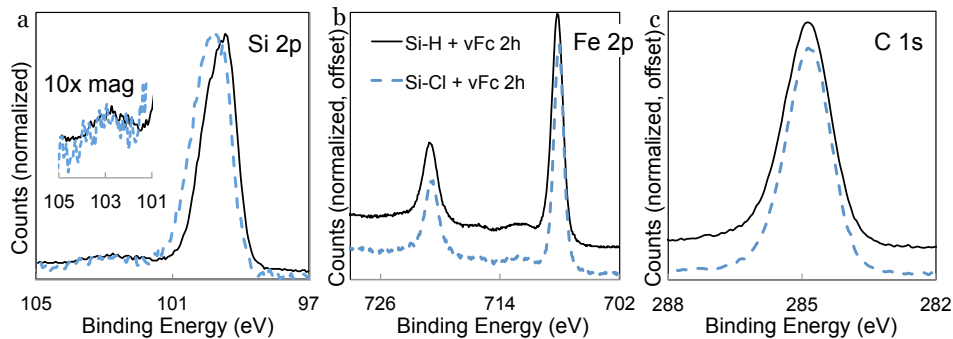
FIGURE 3.2: High-resolution XPS data of surfaces obtained by the thermal reaction of vFc with H−Si(111) (black, solid) and Cl−Si(111) (blue, dashed) surfaces. The silicon oxide component is shown expanded by 10x at 102–103 eV on both surfaces. The Fe 2p spectra exhibited large Fe(II) peaks at 708 and 721 eV that were ascribable to the presence of a ferrocene moiety. The C 1s spectra of both surfaces had a single, broad peak at 285 eV. Reprinted with permission from Lattimer et al.[34] Copyright 2013 American Chemical Society.

3.3 Thermal Reactions of H− and Cl−Si(111) with Vinylferrocene

Figure 3.2 shows the high-resolution Si 2p, Fe 2p, and C 1s XPS data for H−Si(111) and Cl−Si(111) surfaces that had been exposed to vFc for 3 h, followed by extensive rinsing and sonication after synthesis and prior to characterization.[34] Experimental details for the preparation of these surfaces is found in Appendix A.8. The predominant state of iron on both of these surfaces was Fe(II), with peaks arising from Fe(II)-derived ferrocene moieties detected at 708 and 721 eV, with very minor Fe(III)-derived contributions at 712 and 725 eV (Figure 3.2b).[47] Less than 10 % of a monolayer of Cl was detected on these surfaces. The C 1s region was best fit by a single peak at 285 eV (Figure 3.2c). No Fe was detected when H−Si(111) or Cl−Si(111) surfaces were exposed to unsubstituted ferrocene under otherwise the same reaction conditions.

The coverage of vinylferrocene-derived Fe on surfaces produced by the reaction of H−Si(111) and Cl−Si(111) surfaces with vFc was calculated to be $\eta_{\text{Fe}} = 0.8 \pm 0.1$ and $\eta_{\text{Fe}} = 1.1 \pm 0.1$ monolayers, or Fe atoms per Si atop site, respectively. Details of the surface coverage quantification using XPS can be found in Appendix B.4.1. Because the subtended area of a vFc molecule is much larger than the area of a Si atom on an unreconstructed Si(111) surface, the measured Fe coverage indicates that multiple layers of vFc were attached to the surface.[51] Both surfaces contained submonolayer levels of oxidized Si, as evidenced by

a broad signal at $102\,\mathrm{eV}$,[40] whose area corresponded to 0.3 ± 0.1 and 0.4 ± 0.1 monolayers for Cl−Si(111) and H−Si(111) surfaces, respectively, that had been exposed to vFc (Figure 3.2a). A large C 1s signal at $285\,\mathrm{eV}$ was observed for the vFc-exposed surfaces (Figure 3.2c), and this peak is attributable to a combination of the 12 carbon atoms from the ferrocene moiety, as well as to adventitious carbon on the functionalized surface. We did not see a distinct shoulder at $284\,\mathrm{eV}$ from surface-attached carbon, but the large peak at $285\,\mathrm{eV}$ may have obscured a small signal.

3.3.1   Electrochemistry of vFc-Terminated Si(111) Surfaces

The cyclic voltammetry of H−Si(111) and Cl−Si(111) surfaces that had been treated with vFc exhibited a reversible redox couple at $+0.1\,\mathrm{V}$ versus $\mathrm{Ag/AgNO_3}$ (Figure 3.3a,c). Under virtually identical electrochemical conditions, the $\mathrm{Fc/Fc^+}$ couple has been observed at $+0.08\,\mathrm{V}$ versus $\mathrm{Ag/AgNO_3}$ for vFc immobilized on Si(100) surfaces.[48] The anodic and cathodic peak current densities showed a linear dependence on the scan rate, indicating a surface-attached redox reaction (Figure 3.3b,d).[49] The total charge transferred was used to calculate the number of electroactive Fc groups on the surface, which corresponded to $\eta_{\mathrm{Fc}} = 0.9 \pm 0.1$ and $\eta_{\mathrm{Fc}} = 1.1 \pm 0.1$ Fc groups per Si atop site for H−Si(111) and Cl−Si(111) surfaces modified with vFc, respectively. The details of this surface coverage calculation can be found in Appendix B.4.1.

The separation of the anodic and cathodic peaks should be small, ideally equaling zero, for a surface-bound redox couple, but will increase with scan rate if the rate of interfacial charge-transfer is comparable to the voltammetric time scale.[54] At a scan rate of $200\,\mathrm{mV\,s^{-1}}$, the anodic and cathodic peak separation was 50 and $46\,\mathrm{mV}$ for H−Si(111) and Cl−Si(111) surfaces, respectively. As a control, methyl-terminated $\mathrm{p^+}$-Si(111) electrodes were prepared and used to investigate the electrochemistry of Fc in solution. These electrodes showed a peak current density that depended on the square root of the scan rate, as expected for freely diffusing redox couples in solution.[49] The peak-to-peak separation was several hundred mV at a scan rate of $100\,\mathrm{mV\,s^{-1}}$, and increased with scan rate. Hence, the semiconductor electrode contributed to the observed peak splitting for the ferrocene redox couple, precluding a rigorous analysis by conventional methods used for metal electrodes. Nonetheless, the small peak splitting observed on the vFc-modified H−Si(111) and Cl−Si(111) surfaces implied relatively rapid charge transfer on the surface on this voltammetric time scale ($\sim$50 mV at
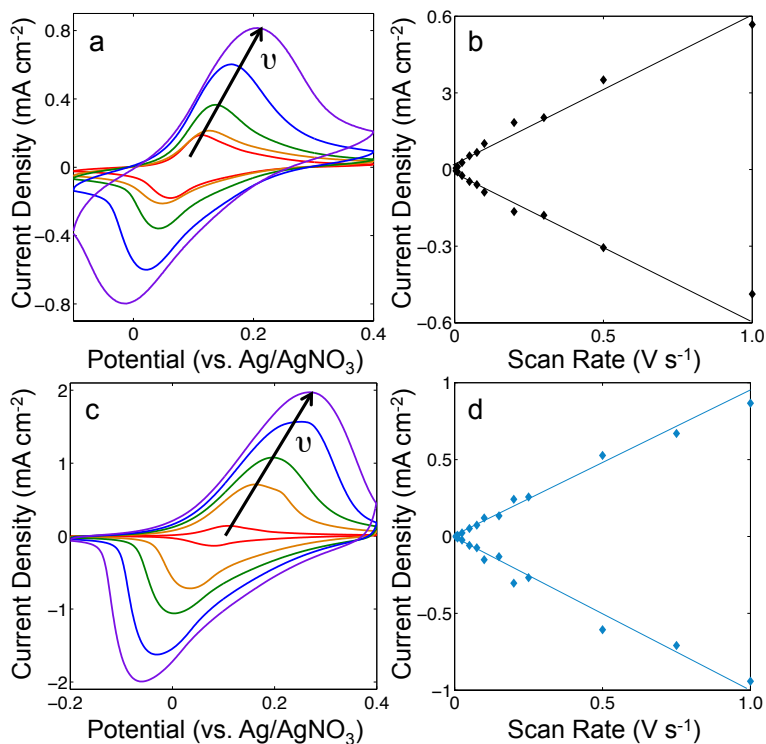
FIGURE 3.3: Dark cyclic voltammetry of electrodes formed from reaction of p^+-type H−Si(111) or Cl−Si(111) reacted with vFc for 2 h at 140 °C. a) Cyclic voltammetry of the H−Si(111) surface obtained at scan rates of 200 to 2000 mV s^{-1}, with increasing scan rate (v) indicated by the arrow. c) Cyclic voltammetry of the Cl−Si(111) surface obtained at scan rates of 150 to 3000 mV s^{-1}, with increasing scan rate indicated by the arrow. b,d) The linear relationship between maximum current density and scan rate on the H−Si(111) surface (b) and Cl−Si(111) surface (d) is consistent with the presence of a surface-bound redox couple. Adapted with permission from Lattimer et al.[34] Copyright 2013 American Chemical Society.

100 mV s^{-1}).

The similarity between these resultant surfaces indicated that the reaction between the vFc and both the H- and Cl-terminated silicon surfaces was efficient and likely occurred via similar mechanisms. The similarity of these surfaces suggested the presence of a mutually similar link between the Fc group and both of these surfaces. The high surface coverage of Fc on these surfaces suggested that the vFc polymerized on the surface. Polymerization of similar aryl-olefins has been seen in other work on attaching groups to surfaces using surface-initiated radical polymerization.[55,56] The presence of multilayers made it difficult to ascertain the exact termination of the silicon on these surfaces. We did not observe a C−Si peak at 284 eV on these surfaces, and there was not significant surface oxidation. This left the surface structure largely unknown, but the electrochemistry indicated that the vFc is attached
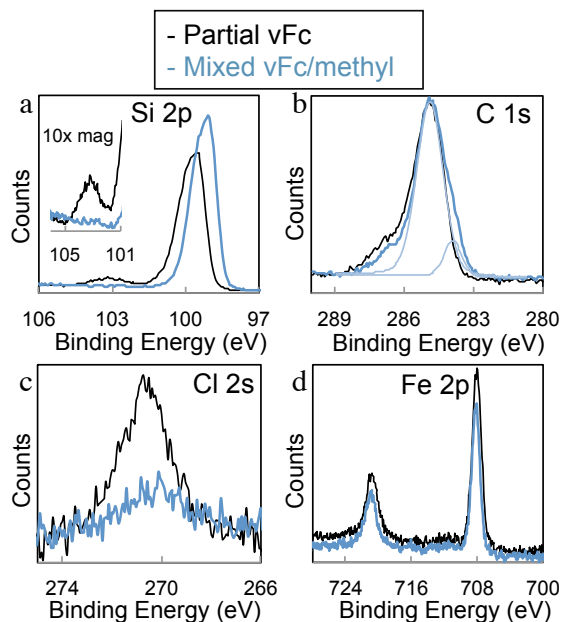
FIGURE 3.4: XPS data for partial vFc− (black) and mixed methyl/vFc− (blue) modified Si(111) surfaces. a) High-resolution Si 2p region. A Si−O peak at 103 eV was observed for the partial vFc−Si(111) surface but was not observed on the mixed methyl/vFc−Si(111) surface. b) High-resolution C 1s region. The mixed methyl/vFc−Si(111) surface had a peak at 284 eV ascribable to the Si-bound CH_3 group, shown in light blue, that was not resolved in the spectrum of the partial vFc−Si(111) surface. c) High-resolution Cl 2s region. More chlorine was observed on the partial vFc−Si(111)surface, as evidenced by the Cl 2s peak at 270 eV, than on the mixed methyl/vFc−Si(111)surface. d) High-resolution Fe 2p region, showing similar coverages of Fe on these two surfaces. Reprinted with permission from Lattimer et al.[34] Copyright 2013 American Chemical Society.

to the surface through a stable linker. This was supported by studies using unsubstituted ferrocene, which did not result in any surface attachment of the ferrocene moiety by XPS, suggesting that the vinyl group was necessary for surface attachment. Surfaces terminated by methyl groups prior to reaction with vFc showed no Fe signal by XPS, indicating that the reaction between the vFc and the Cl-terminated surface occurred through the Cl−Si bond and not by non-specific adsorption of the vFc group to the silicon. While these results were promising regarding the ability to use the Cl-terminated silicon surface as a starting point for the formation of mixed monolayers, we would have preferred a more controlled process for surface attachment that did not result in multilayers and poorly characterized surface species.

3.3.2 Mixed Methyl/Vinylferrocenyl Surfaces

Scheme 3.1 shows the reaction sequence for the formation of mixed methyl/vinylferrocenyl surfaces. These surfaces were chlorinated, and the Cl−Si(111) surface was then first reacted with vFc for a predetermined time period, followed by reaction with methyl Grignard. Figure 3.4 presents the high-resolution XPS data for a Cl−Si(111) surface that was reacted thermally with vFc for 30 min (partial vFc) as well as for a Cl−Si(111) surface that was reacted thermally with vFc for 20 min and then methylated using CH_3MgCl (mixed methyl/vFc). Fe(II) peaks at 708 and 721 eV were observed in the Fe 2p region in both cases, with Fe coverages of $\eta_{Fe} = 0.15 \pm 0.05$ and $\eta_{Fe} = 0.10 \pm 0.05$ monolayers for the partial vFc- and mixed methyl/vFc-terminated surfaces, respectively (Figure 3.4d). The lower coverage of Fe on these vFc-functionalized surfaces as compared to the vFc−Si(111) surfaces depicted in Figure 3.2 was consistent with only partial functionalization of the Si surface occurring with shorter reaction times (30 min vs. 3 h). The surface oxide coverage, measured from the Si−O peak at 102 eV from the Si 2p XPS signal, was $\eta_{Si-O} = 0.8 \pm 0.1$ monolayers on the partially vFc-terminated Si surface but was below the detection limit (<0.01 monolayer) on the mixed methyl/vFc surface (Figure 3.4a). The C 1s signal on the partial vFc-terminated Si(111) surface was a broad peak centered at 285 eV with a total area that corresponded to 4.0 ± 0.5 C per Si atop site. This would correspond to around 0.3 monolayers of ferrocene, which indicated that there was some adventitious carbon contribution on this surface. The mixed methyl/vFc−Si(111) surface C 1s signal also exhibited a large peak at 285 eV, corresponding to 3.0 ± 0.5 monolayers of C, with a shoulder at 284 eV that yielded upon curve-fitting analysis a best fit to 0.5 ± 0.1 monolayers of Si−CH_3 per Si atop site (Figure 3.4b). The peak at 284 eV indicates that there are methyl groups on the surface in addition to the vFc groups seen by the Fe 2p signal.[13,29] This indicates that we have successfully formed a mixed methyl/vFc monolayer on the surface. Based on the Cl 2s XPS signal at 270 eV, the partial vFc surface exhibited a Cl coverage of 0.5 ± 0.1 monolayers, compared to 0.1 ± 0.1 monolayers of Cl on the mixed methyl/vFc surface (Figure 3.4c). This was consistent with our reaction scheme wherein the remaining chlorine groups on the surface after partial reaction with vFc are available to react with methyl Grignard to form the mixed monolayer.
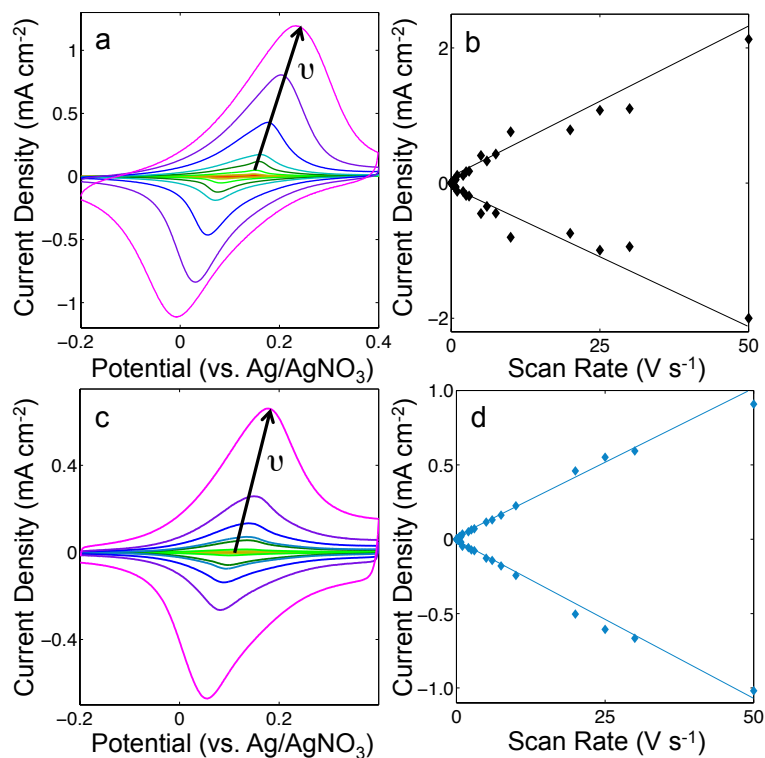
FIGURE 3.5: Cyclic voltammetry of partial vFc-terminated and mixed methyl/vFc-terminated p^+ Si(111) surfaces. a) Cyclic voltammetry of the partial vFc-terminated Si(111) surface at scan rates of 0.05 to $25\,\mathrm{V\,s^{-1}}$, with increasing scan rate (v) indicated by the arrow. c) Cyclic voltammetry of the mixed methyl/vFc surface at scan rates of 0.05 to $25\,\mathrm{V\,s^{-1}}$, with increasing scan rate indicated by the arrow. b,d) The linear relationship between maximum current density and scan rate on the partial vFc$-$Si(111) (b) and mixed methyl/vFc$-$Si(111) (d) electrodes is consistent with the presence of a surface-bound redox couple. Adapted with permission from Lattimer et al.[34] Copyright 2013 American Chemical Society.

3.3.3   Electrochemistry of Mixed Methyl/Vinylferrocenyl Surfaces

Figure 3.5 shows the cyclic voltammetric data for the partial vFc-functionalized and mixed methyl/vFc-functionalized Si(111) surfaces. Both surfaces had a reversible redox couple at $+0.10\,\mathrm{V}$ vs. Ag/AgNO$_3$, with a linear dependence of the peak current density on the scan rate, as expected for a surface-attached redox couple.[49] After background subtraction, integration of the anodic and cathodic current versus time was analyzed to obtain the total charge transferred, giving an electrochemically active surface coverage of vFc, η_{Fc}. The details of this calculation can be found in Appendix B.4.1. The average surface coverage of vFc on the partial vFc and mixed methyl/vFc surfaces at a variety of scan rates was $\eta_{\mathrm{Fc}} = 0.08 \pm 0.03$ and 0.03 ± 0.01 monolayers, respectively. The surface coverage did not vary with the scan rate or the scan number, but remained steady throughout the course of the electrochemical cycling, within experimental error, for both surfaces. This indicates that the surface functionalization was stable to the electrochemical conditions, and there was no loss of electroactive ferrocene from the surface due to the electrochemical cycling. The peak-to-peak splitting at $200\,\mathrm{mV\,s^{-1}}$ was $57\,\mathrm{mV}$ for the partial vFc-terminated Si(111) surface and $39\,\mathrm{mV}$ for the mixed methyl/vFc-terminated Si(111) surface, indicating rapid interfacial charge transfer on this time scale ($200\,\mathrm{mV\,s^{-1}}$).

Figure 3.6 shows the coverage of vFc incorporated into mixed methyl/vFc monolayers as a function of the reaction time between vFc and the Cl−Si(111) surfaces, as measured electrochemically by determination of η_{Fc}. The coverage of electroactive vFc groups incorporated into the mixed monolayers increased from 0.01 to 0.3 monolayers with the duration of the exposure to vFc from 10 to 60 min, and could be reproducibly controlled by variation in the duration of the exposure.

Figure 3.7a shows the Si 2p region of the partial vFc-terminated and mixed methyl/vFc-terminated Si(111) surfaces after >30 redox cycles had been performed on the electrode surfaces. The partial vFc-terminated Si(111) surface showed a large Si−O peak at $103\,\mathrm{eV}$, corresponding to 2.8 ± 0.5 monolayers of silicon oxide, which indicated that the surface had been extensively oxidized during electrochemical cycling (cf Figure 3.3a). In contrast, the mixed methyl/vFc-terminated Si(111) surface showed 0.4 ± 0.1 monolayers of surface oxide after redox cycling. The Fe 2p regions of both surfaces were largely unchanged from the spectra obtained before redox cycling (Figure 3.7b and Figure 3.4d). After electrochemistry,
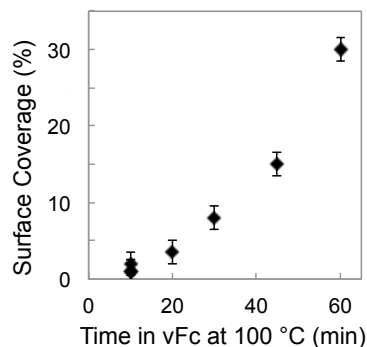
FIGURE 3.6: Plot of reaction time vs. surface coverage in % of a monolayer of the vFc group as measured electrochemically on p^+-type mixed methyl/vinylferrocenyl Si(111) surfaces. Reprinted with permission from Lattimer et al.[34] Copyright 2013 American Chemical Society.
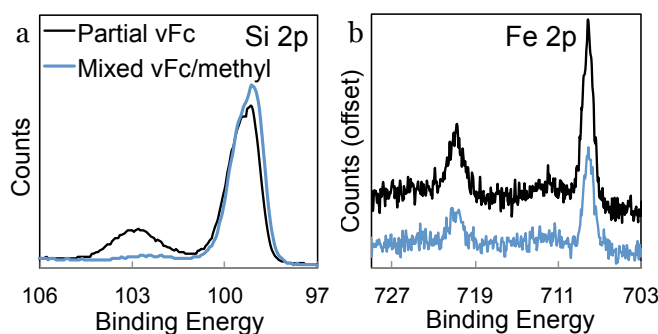
FIGURE 3.7: High-resolution XPS data of the Si 2p and Fe 2p regions of the partial vFc- (black) and mixed methyl/vFc- (blue) modified Si(111) surfaces after electrochemistry in contact with $(NEt_4)ClO_4$ electrolyte. a) The partial vFc$-$Si(111) surface showed a large Si$-$O peak in the Si 2p region, whereas the mixed methyl/vFc$-$Si(111) surface showed little to no Si oxide Si 2p signal. b) The Fe 2p region showed Fe(II) peaks at 708 and 721 eV from the ferrocene groups, with very little Fe(III) signal at 712 and 725 eV. Reprinted with permission from Lattimer et al.[34] Copyright 2013 American Chemical Society.

the Fe coverages calculated using the high-resolution Fe 2p and Si 2p XPS signals were $\eta_{Fe} = 0.08 \pm 0.02$ Fe per Si atop site on the partial vFc-terminated Si(111) surface and $\eta_{Fe} = 0.04 \pm 0.01$ Fe per Si atop site on the mixed methyl/vFc-terminated Si(111) surface. These values agreed well with the Fe coverages calculated using the electrochemical data, but are lower than the coverage calculated from the XPS data obtained on the surfaces prior to electrochemistry. This could be due to the loss of non-electroactive ferrocene from the surface during electrochemical cycling.

Surface modification	η_i[a]	η_{Si-o}[a]	η_{Fc}[b]	η_{Fe}[a,c]	η_{Si-o}[a,c]	Charge-carrier lifetime (ms)	S (cm s^{-1})
Methylation	1.0 ± 0.1 [d]	0.0 ± 0.1	—	—	—	0.54	33
Si−H + vFc 2 h	0.9 ± 0.1 [e]	0.4 ± 0.1	0.9 ± 0.1	—	—	0.03	640
Si−Cl + vFc 2 h	1.1 ± 0.1 [e]	0.3 ± 0.1	1.1 ± 0.1	—	—	0.01	2600
Partial vFc	0.20 ± 0.05[e]	0.4 ± 0.1	0.08 ± 0.03	0.08 ± 0.02	2.8 ± 0.5	0.01	2700
Mixed methyl/vFc	0.10 ± 0.05[e]	0.0 ± 0.1	0.03 ± 0.01	0.04 ± 0.01	0.4 ± 0.1	0.50	35
Si−Cl + 4F-Sty[f] 3 h	3.4 ± 0.5 [g]	0.0 ± 0.1	—	—	—	0.01	1300
Mixed methyl/4F-Sty[f]	0.20 ± 0.05[g]	0.5 ± 0.1	—	—	—	0.27	66

[a]Coverage per Si atop site determined by XPS. [b]Coverage per Si atop site determined by electrochemical analysis. [c]Determined after performing electrochemistry onsurface. [d]η_{Si-CH_3}. [e]η_{Fe}. [f]4F-Sty indicates 4-fluorostyrene. [g]η_F.

TABLE 3.1: Properties of modified silicon surfaces. Reprinted with permission from Lattimer et al. [34] Copyright 2013 American Chemical Society.

3.3.4 Charge-Carrier Lifetimes of Mixed Methyl/Vinylferrocenyl Mono-
layers

Table 3.1 presents the observed charge-carrier lifetimes and inferred S values for the surfaces described in this section. Details of the experimental set-up and S value calculations can be found in Appendix B.3. H$-$Si(111) and Cl$-$Si(111) surfaces modified by vFc exhibited photogenerated charge-carrier lifetimes of 27 ± 5 ms and 7 ± 5 ms, respectively, corresponding to $S = 640 \pm 20$ and $S = 2600 \pm 100$ cm s^{-1}, respectively. For comparison, CH$_3$$-$Si(111) surfaces had charge-carrier lifetimes of 550 ± 50 ms, corresponding to $S = 30 \pm 5$ cm s^{-1}. The partial vFc-terminated and mixed methyl/vFc-terminated Si(111) surfaces exhibited charge-carrier lifetimes of 10 ± 5 and 500 ± 50 µs, respectively, corresponding to $S = 2700 \pm 100$ and $S = 35 \pm 5$ cm s^{-1}, respectively. The 4-fluorostyrene-functionalized Si(111) surface exhibited a charge-carrier lifetime of 14 ± 5 µs, which corresponded to $S = 1300 \pm 100$ cm s^{-1}, whereas the mixed methyl/4-fluorostyrene-terminated Si(111) surface had a charge-carrier lifetime of 270 ± 50 µs, corresponding to $S = 66 \pm 5$ cm s^{-1}, which was similar to the value of S measured on the mixed methyl/vFc-terminated Si(111) surface. Experimental details for the formation of the 4-fluorostyrene modified surfaces can be found in Appendix A.9.

The low SRVs measured on the mixed methyl/vFc and mixed methyl/4-fluorostyrene surfaces were comparable to the SRV of the methyl-terminated surface. This indicated that these surfaces had good photoelectronic properties and did not facilitate fast charge-carrier recombination at the surface. However, if holes were to transfer to the attached Fc upon illumination of intrinsic silicon, the reduced concentration of holes on the surface could result in extended charge-carrier lifetimes. 4-Fluorostyrene, which is chemically similar to the vinyl-appended cyclopentadienyl (Cp) ring in vFc, is not redox active and cannot act as a Faradaic hole acceptor. Mixed 4-fluorostyrene/methyl Si(111) surfaces also showed the relatively long charge-carrier lifetimes and low S values characteristic of a well-passivated and stable Si surface. Thus the low S values of the mixed methyl/vFc-terminated Si(111) surfaces can be attributed to low rates of charge-carrier recombination on a well-passivated surface, rather than the redox properties of the Fc molecule on the surface. These long charge-carrier lifetimes should therefore make these electrons and holes available for chemical reactions on these surfaces under photoelectrochemical conditions.

3.3.5 Photoelectrochemistry of Mixed Methyl/Vinylferrocenyl Surfaces on n-type Si

Figure 3.8 shows cyclic voltammetric data in the dark and under illumination of a mixed methyl/vinylferrocenyl n-type Si electrode in CH_3CN. Details of the photoelectrochemical experiment can be found in Appendix B.4. In the dark, the ferrocene redox couple was observed at $\sim 0.1\,V$ vs. $Ag/AgNO_3$, similar to mixed methyl/vinylferrocenyl surfaces on p^+-type silicon (Figure 3.5). The potential of the ferrocene redox couple was taken as the average of the potentials of the anodic and cathodic peak currents. On n-type silicon at a scan rate of $1\,V\,s^{-1}$ the peak separation was $\sim 400\,mV$ in the dark, due to slow charge-transfer kinetics (Figure 3.8). When the sample was illuminated by visible light, the ferrocene redox couple became more reversible and the redox peak shifted to $-0.3\,V$ vs. $Ag/AgNO_3$, indicating a photovoltage generated by the Si(111) of $\sim 0.4\,V$. The peak-to-peak separation under illumination was $10\,mV$ at $1\,V\,s^{-1}$, indicating facile charge transfer to the surface-attached ferrocene. The average photovoltage generated on this surface at a variety of scan rates was $360 \pm 50\,mV$, as determined by the difference between the redox potential of the Fc couple on illuminated n-type Si and the redox potential observed on p^+-type Si in the dark ($0.10\,V$ vs. $Ag/AgNO_3$ on all the samples studied herein).[57] This comparison is illustrated in Figure 3.9, which shows representative cyclic voltammetric scans of mixed methyl/vinylferrocenyl surfaces on p^+-type Si in the dark and n-type Si under illumination, at $10\,V\,s^{-1}$. The photovoltage decreased by $\sim 20\,\%$ over several hours of scanning, although the coverage of electrochemically active ferrocene groups remained stable.

We have developed a new method for forming mixed methyl/vinylferrocene monolayers on Si(111) surfaces with relative ease and with a potentially large substrate scope. As an example reaction system, vinylferrocene was attached at up to a ratio of $30\,\%$ of the Si(111) atop sites. The functionalized surfaces were resistant to oxidation and permitted relatively rapid interfacial charge transfer to the attached ferrocene group. The mixed monolayers maintained the favorable electronic properties of the underlying silicon, as evidenced by the low surface recombination velocities measured on the functionalized surfaces, as well as the 0.4 V photovoltage generated on n-type silicon. However, this method required a relatively large amount (grams) of a thermally-stable, olefin-appended liquid substrate for functionalization of the silicon. While vinylferrocene was an excellent test substrate that
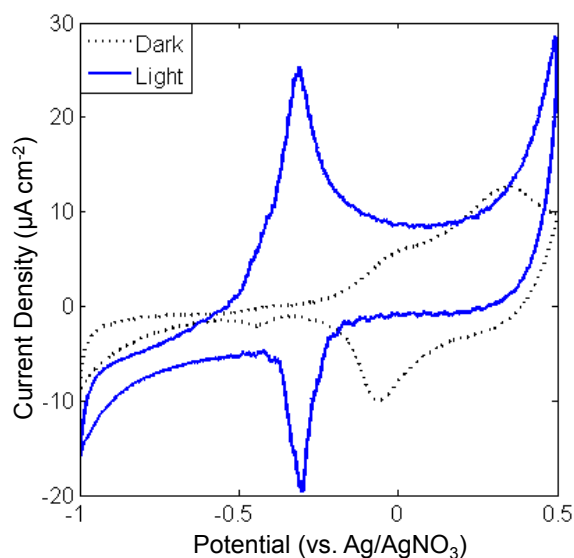
FIGURE 3.8: Cyclic voltammetry (scan rate of $1\,V\,s^{-1}$) of a mixed methyl/vinylferrocenyl n-type Si(111) electrode under illumination (blue) and in the dark (black). The photovoltage was $0.4\,V$, as determined by the shift in the average of the anodic and cathodic peak positions on illuminated n-Si relative to the position on p^{+}-Si in the absence of illumination. Reprinted with permission from Lattimer et al.[34] Copyright 2013 American Chemical Society.
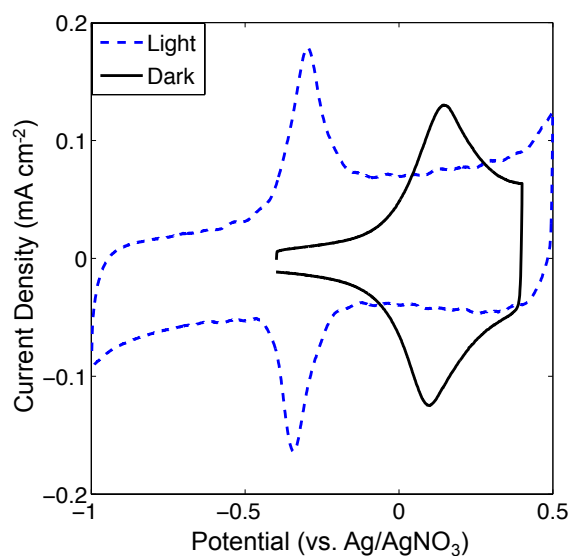
FIGURE 3.9: Cyclic voltammetry (scan rate of $10\,V\,s^{-1}$) of mixed methyl/vinylferrocenyl electrode surfaces on n-type Si(111) under illumination (blue) and on p^{+}-type Si(111) in the dark (black). The photovoltage observed was $0.44\,V$. Reprinted with permission from Lattimer et al.[34] Copyright 2013 American Chemical Society.

fulfilled these requirements, most molecular proton-reduction catalysts that could be used in a solar fuel device will not.

3.4 UV-Light Induced Reaction of Vinylferrocene with H- and Cl-Si(111)

Having established the ability to form mixed methyl/vinylferrocenyl surfaces with excellent photoelectrochemical properties, we wanted to make this reaction more universally applicable. To this end, we began to investigate extending the reactivity of the Cl−Si(111) surface with solution species, using UV-light rather than heat to induce the reaction. This would require much less substrate (milligrams) and ease the thermal stability requirements.

We began again with vinylferrocene, as it still fulfilled the requirements for a test complex. It was necessary to find conditions where there would be efficient reactivity between the solution vinylferrocene and the Cl−Si(111) surface. We used the H−Si(111) surface as a control because it has demonstrated reactivity with vFc under UV illumination.[48] We assumed that if the H−Si(111) surface was not reactive, the then Cl−Si(111) surface would not be reactive either under identical conditions, if they followed a similar reaction mechanism; a more detailed discussion of the mechanism involved in these reactions can be found in Chapter 5. We initially used THF as the solvent because it was used for the methylation reaction and so we knew that it would not damage the surface.

The experimental details for the UV-light induced reaction of vFc with H− and Cl−Si(111) can be found in Appendix A.10. In short, the H- or Cl-terminated surface was placed polished-side down into a glass dish with a flat, quartz bottom filled with a solution of 50–100 mg vFc in 2–3 mL THF in a N_2-purged flush box. The dish was placed atop a UV-light tungsten-halogen lamp for reading chromatography plates and covered with aluminum foil. The 254-nm UV-light source was switched on for the desired length of time. After the reaction, the wafer was rinsed with THF and then either removed from the box and cleaned as usual, or subjected to additional reactions.

Figure 3.10 shows the XPS of H- and Cl-terminated silicon surfaces reacted with vFc in THF after illumination by 254 nm light for 3 h. The Fe 2p XPS (Figure 3.10a) clearly showed significantly more iron on the Si−H surface (black) than on the Si−Cl (blue) surface, corresponding to 0.15 ± 0.05 and 0.03 ± 0.01 monolayers, respectively. This suggested that
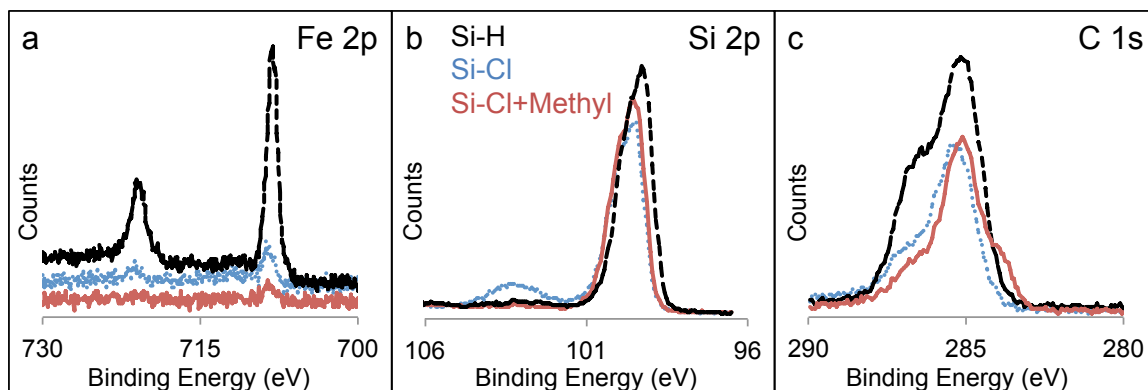
FIGURE 3.10: XPS of Si−H and Si−Cl surfaces modified by reaction with vinylferrocene in THF under illumination by UV light for 3 h. a) The high-resolution Fe 2p XPS of the Si−H surface after reaction with vFc (black), the Si−Cl surface after reaction with vFc (blue), and the Si−Cl surface after reaction with vFc and methyl Grignard (red). There was significantly more iron on the Si−H surface than the two Si−Cl surfaces, indicating that the Si−H surface was more reactive under these conditions. b) The high-resolution Si 2p XPS of the Si−H surface, in black, the Si−Cl surface, in blue, and the Si−Cl surface with addition reaction with methyl Grignard, in red. The Si−Cl surface was extensively oxidized, as shown by the peak at 103 eV, likely due to the lack of surface coverage by the vFc group leaving many unfunctionalized Si atop sites. The lack of surface oxidation on the Si−Cl surface reacted with both vFc and methyl Grignard indicated that the surface coverage on this surface was higher. c) The high-resolution C 1s XPS of the Si−H surface, in black, the Si−Cl surface, in blue, and the Si−Cl surface with additional reaction with methyl Grignard, in red. The shoulder at 284 eV, which was only present on the Si−Cl surface reacted with both vFc and methyl Grignard, indicated that a mixed methyl/vFc surface had been formed.

under the same conditions, the Si−H surface was more reactive than the Si−Cl surface. This was not unexpected, based on the relatively long history of work on Si−H surface functionalization.[8] However, the attachment of any vFc to the Si−Cl surface allowed us to use this reaction for mixed monolayer formation with methyl Grignard, which cannot be done using the Si−H surface. This is shown in Figure 3.10, in red. The mixed monolayer was formed by reacting the Si−Cl surface first with vFc for 3 h under UV illumination, and then with methyl Grignard for 2 h. The Fe 2p XPS showed even less iron on this surface than for the Cl−Si surface reacted with vFc without subsequent methylation, but there was still some reactivity with vFc. The amount of Fe on this surface corresponded to 0.01 ± 0.01 monolayers.

The C 1s XPS of these three surfaces, shown in Figure 3.10b, looked very similar, with more carbon on the Si−H surface (black) than the Si−Cl surfaces (blue and red) because the vFc reacted more efficiently with that surface. However, the Si−Cl surface reacted with both vFc and methyl Grignard (red) had a shoulder at 284 eV, which was missing in the other two spectra. This extra peak was assigned to the methyl groups in this mixed monolayer.[13,29]

The Si 2p XPS of the three surfaces is shown in Figure 3.10c. The Si−H surface did not show any sign of surface oxidation, but the Si−Cl surface had a significant peak at 103 eV. This was likely due to the poor functionalization of the Si−Cl surface with vFc, which left many surface sites chlorine-terminated; these sites are prone to oxidation in air. This was confirmed with the Si−Cl surface reacted with both vFc and methyl Grignard, which had no peak at 103 eV, indicating that the methylation of the partially vFc-modified surface prevented oxidation.

3.4.1 Electrochemistry of Surfaces Functionalized by UV Light

Electrochemical experiments performed using these three types of surfaces confirmed the successful immobilization of vFc. All three had a reversible, non-diffusional redox couple at $+0.1$ V vs. Ag/AgNO$_3$ in CH$_3$CN with 0.1 M (NEt$_4$)ClO$_4$ as the electrolyte, consistent with our previous work on thermal immobilization of vFc on silicon. The surface coverage of electroactive ferrocene calculated from the electrochemical data was 0.04 ± 0.01 monolayers on the Si−H surface, and 0.002 ± 0.001 monolayers on the two Si−Cl surfaces.

The XPS and electrochemical results here indicate that while the UV-induced reaction did work on the chloride-terminated silicon surface, it did not proceed quickly under the initial
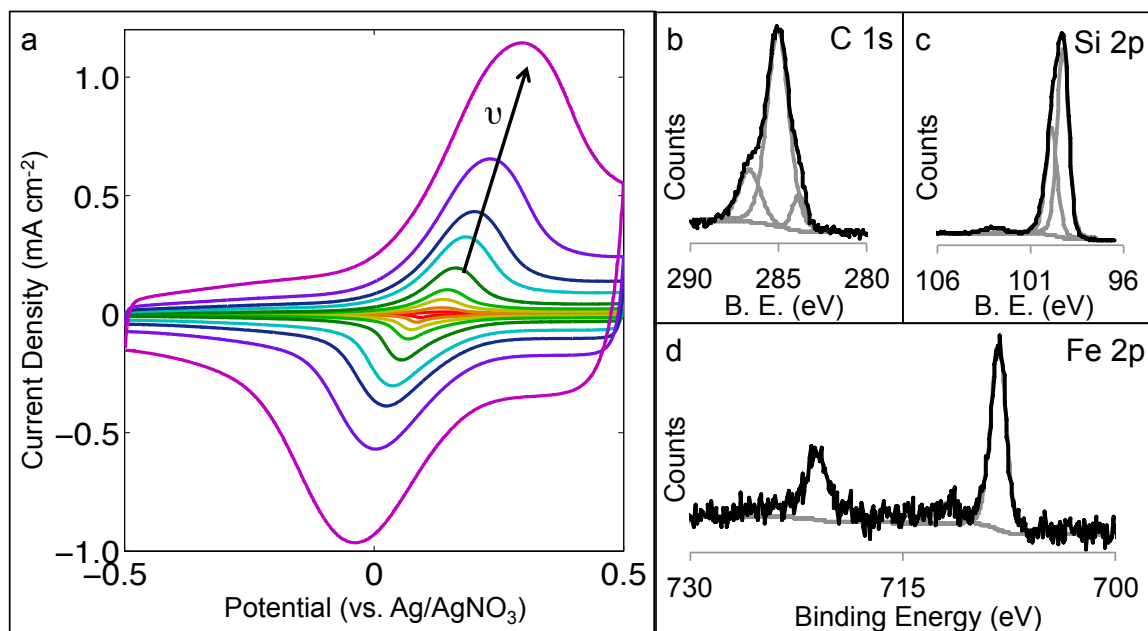
FIGURE 3.11: The electrochemistry and XPS of a mixed vFc/methyl surface produced by reaction with vFc in THF under UV light for 18 h, followed by reaction with methyl Grignard. a) Cyclic voltammetry showing the surface-attached ferrocene redox couple. Increasing scan rate from 0.3 to $100\,\mathrm{V\,s^{-1}}$ is indicated by the black arrow. b) The high-resolution C 1s XPS of the surface, showing the methyl peak at 284 eV. c) The high-resolution Si 2p XPS of the surface, showing a small surface oxide peak at 103 eV. d) The high-resolution Fe 2p XPS showing the Fe(II) doublet at 708 and 721 eV, with little to no Fe(III) visible at 712 and 725 eV.

test conditions. We screened a variety of conditions to improve the coverage of vFc. One such modification was increasing the reaction time in vFc to 18 h followed by methylation, and the results are shown in Figure 3.11. The cyclic voltammetry showed a reversible redox couple at $+0.1$ V vs. $Ag/AgNO_3$, as expected for ferrocene. The peak current density was linear with the scan rate, as expected for a surface-attached redox couple. Shown in Figure 3.11a are cyclic voltammograms at various scan rates between 0.3 and $100\,V\,s^{-1}$. The peak separation at $300\,mV\,s^{-1}$ was $52\,mV$, indicating that there was rapid charge transfer at the surface at this time scale. Integration of the current vs. time plots gave an electroactive ferrocene coverage of 0.03 ± 0.01 monolayers. The high-resolution XPS of this surface is shown in Figure 3.11b-d. The C 1s spectrum had a peak at $284\,eV$, assigned to the methyl groups on the surface.[13,29] The Si 2p spectrum had a small silicon oxide peak at $103\,eV$, possibly because of the increased time under UV illumination. The Fe 2p spectrum had an Fe(II) doublet at 708 and $721\,eV$, with no apparent Fe(III) component at 712 and $725\,eV$, indicating that the ferrocene was intact and had not decomposed during surface functionalization. The iron coverage by XPS corresponded to 0.07 ± 0.02 monolayers.

High-purity, intrinsically doped silicon was used to prepare two surfaces by reaction with vFc in THF under UV light for 18 h, one of which was then reacted with methyl Grignard for 2 h. The SRV measured on the purely vFc surface was $870\,cm\,s^{-1}$, while the SRV on the mixed vFc/methyl surface was $48\,cm\,s^{-1}$ (Table 3.2). This suggested that the mixed surface had good photoelectronic properties, and that the formation of the mixed monolayer increased the surface passivation, allowing the charge carriers to have an extended lifetime before recombination. Therefore, it seemed likely that we could use these surfaces formed by the reaction under UV light for photoelectrochemical experiments as well. However, the surface coverage even after 18 h of illumination was still quite low (<0.05 monolayers), and so further experiments were performed to increase surface coverage of vFc without damaging the photoelectronic properties of the surface.

3.4.2 Radical Initiation with Benzoyl Peroxide

We wanted to increase the surface coverage of electroactive ferrocene without damaging the surface with excessive time under UV illumination. Because the mechanism of the reaction under UV light is most likely a radical process, adding a radical initiator like benzoyl peroxide (BP) to the solution should accelerate the reaction rate. BP was chosen because it was used

in the chlorination reaction, and so it was readily available and did not show any indication of deleterious side reactions with the silicon surface. There is some evidence that THF can react with silicon surfaces, possibly through a ring-opening reaction that results in addition of the THF to the surface through its oxygen atom.[58] We therefore changed the solvent to dichloromethane (CH_2Cl_2) or acetonitrile (CH_3CN) to minimize surface oxidation and because of the increased solubility of BP in those solvents. A highly-doped, n-type Si−Cl surface, with resistivity of 0.004–$0.006 \, \Omega \cdot cm$, was placed in a solution of 50–$100 \, mg$ vFc in CH_2Cl_2 and illuminated by UV light for $30 \, min$, then rinsed with CH_2Cl_2 and reacted with methyl Grignard for $2 \, h$. The XPS and electrochemistry of this surface are shown in Figure 3.12.

Shown in Figure 3.12a are cyclic voltammograms at various scan rates between 0.1 and $10 \, V \, s^{-1}$. The cyclic voltammetry showed a reversible redox couple at $+0.1 \, V$ vs. $Ag/AgNO_3$, as expected for ferrocene. The peak current density was linear with the scan rate, as expected for a surface-attached redox couple. Integration of the current vs. time plots gave an electroactive ferrocene coverage of 0.2 monolayers. The peak separation at $100 \, mV \, s^{-1}$ was only $20 \, mV$, indicating that there was rapid charge transfer at the surface at this time scale. It was unclear that we would see rapid electron transfer on an n-type surface as opposed to a p-type surface, because the concentration of holes in an n-type semiconductor is limited. However, the high dopant density of this silicon made it very conductive (resistivity of $<0.01 \, \Omega \cdot cm$), and so charge transfer did not appear to be inhibited with this type of silicon, even in the dark. This will be important when we are doing photoelectrochemical measurements.

The high-resolution XPS of this surface is shown in Figure 3.12b-d. The C 1s spectrum was fit to a single peak at $285 \, eV$. There did not appear to be a separate shoulder at $284 \, eV$ from the methyl groups, though it could have been obscured by the large peak at $285 \, eV$. The Si 2p spectrum showed no silicon oxide peak at $103 \, eV$, indicating that reducing the reaction time and changing the solvent improved the quality of the surface produced. The Fe 2p spectrum had an Fe(II) doublet at 708 and $721 \, eV$, and no Fe(III) component at 712 and $725 \, eV$, indicating that the ferrocene was intact. The iron coverage by XPS corresponds to 0.7 ± 0.1 monolayers, which may have been an overestimate, compared to the electrochemical data. With such high coverage, it is likely that some multilayer formation occurred,[51] and the discrepancy between XPS and electrochemical coverage calculations

62
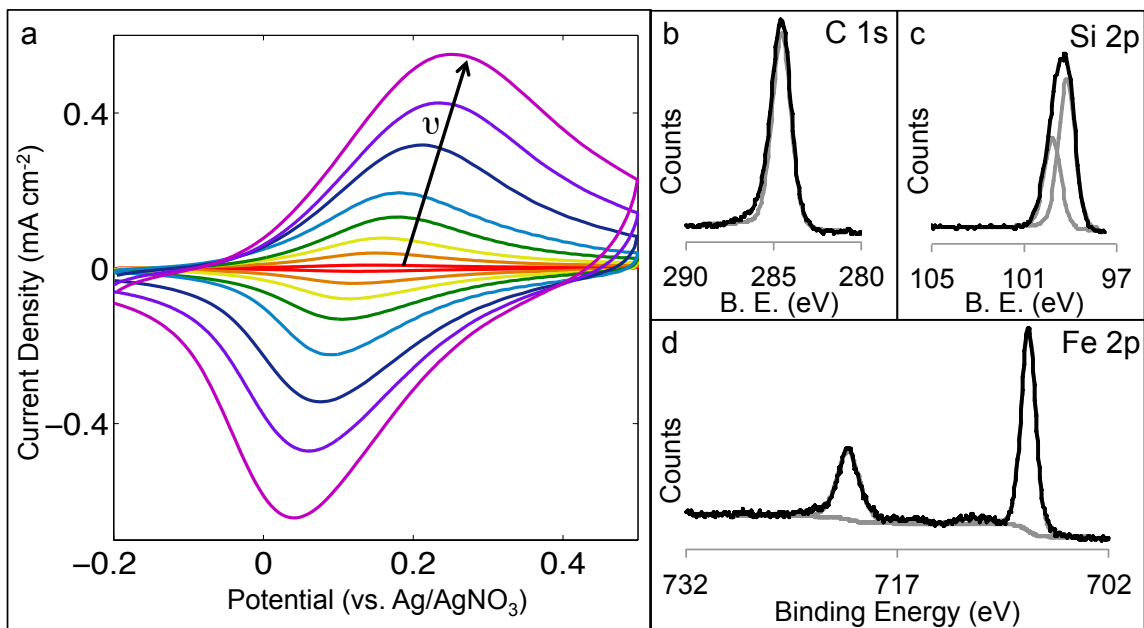
FIGURE 3.12: The electrochemistry and XPS of a mixed vFc/methyl surface produced by reaction with vFc in CH_2Cl_2 with BP, illuminated by UV light for 30 min, followed by reaction with methyl Grignard. a) Cyclic voltammetry showing the surface-attached ferrocene redox couple. Increasing scan rate from 0.1 to $10\,V\,s^{-1}$ is indicated by the black arrow. b) The high resolution C 1s XPS of the surface. This peak was fit to a single large peak around 285 eV, suggesting that any methyl peak at 284 eV was obscured by the large carbon component from the ferrocene groups. c) The high-resolution Si 2p XPS of the surface, showing little to no surface oxide peak at 103 eV. d) The high-resolution Fe 2p XPS showing the Fe(II) doublet at 708 and 721 eV, with little to no Fe(III) visible at 712 and 725 eV.

Solvent	THF	THF	CH_2Cl_2	CH_3CN	CH_3CN
Time under UV	2 h	2 h	30 min	2 h	2 h
BP (y/n)	no	no	yes	yes	yes
Methyl (y/n)	no	yes	yes	no	yes
Charge-carrier lifetime (ms)	0.02	0.37	0.38	0.05	0.40
S ($cm\,s^{-1}$)	870	48	46	350	43
η_{Fe}[a]	0.05 ± 0.02	0.01 ± 0.01	0.6 ± 0.1	0.3 ± 0.1	0.3 ± 0.1

[a]coverage of Fe per atop site determined by XPS.

TABLE 3.2: Properties of vFc-modified Cl-terminated Si surfaces using UV-light induced reaction.

could be due to non-electroactive ferrocene sitting on the surface. This phenomenon has been seen previously on vFc-modified silicon surfaces, where the surface coverage measured using XPS was higher than the coverage measured electrochemically.[47] Some of this ferrocene could be non-electroactive because there was not a suitable pathway for the charges to reach the redox center, or it could simply have fallen off the surface after immersion in electrolyte because it was not actually covalently bound to the surface.

We wanted to ensure that the photoelectronic properties of these surfaces were not affected by the addition of BP to the reaction solution or by changing the solvents. To this end, several surfaces were prepared using intrinsically doped silicon under a variety of conditions for SRV measurements. The results of these experiments are displayed in Table 3.2. All starting surfaces were chlorine-terminated. The surfaces prepared using THF as the solvent, without BP in solution, had low vFc surface coverage, as discussed above. The SRVs on these surfaces that were not methylated with methyl Grignard were high, with $S = 870 \pm 50\,cm\,s^{-1}$. When these surfaces were methylated following reaction with vFc in THF, the SRVs were much lower, with $S = 48 \pm 5\,cm\,s^{-1}$. Changing the solvent to CH_2Cl_2 and adding BP to the vFc solution greatly increased the vFc surface coverage, as discussed above. One surface modified with vFc in CH_2Cl_2 with BP in solution under UV illumination for 30 min, followed by methylation with methyl Grignard, had $S = 46\,cm\,s^{-1}$. Several other surfaces functionalized with vFc by illumination with UV light in CH_2Cl_2 with BP for between 20 and 180 min, followed by methylation, also had SRVs of between 40 and 70 $cm\,s^{-1}$, depending on the time spent under UV illumination (not shown in table). When CH_3CN was used as the solvent, surface coverage of vFc was also high, with the results shown in Table 3.2. For surfaces prepared with vFc in CH_3CN with BP under illumination for 2 h, surface coverage of Fe was 0.30 ± 0.05 monolayers. When these surfaces were methylated following UV illumination,

$S = 43 \pm 5\,\mathrm{cm\,s^{-1}}$, whereas when methylation did not occur, $S = 350 \pm 50\,\mathrm{cm\,s^{-1}}$. These results made it clear that the addition of BP to the reaction solution and the use of CH_2Cl_2 or CH_3CN as the solvent did not adversely affect the photoelectronic properties of the surfaces. Rather, using these solvents and adding BP to the reaction solution greatly increased the surface coverage of vFc at moderate illumination times (30 to 120 min) without adversely affecting the photoelectronic properties of the surfaces.

3.4.3 Photoelectrochemistry

Photoelectrochemical experiments were carried out on silicon wafers with various levels of doping, which changed the resistivity of the wafers. Details of the photoelectrochemistry experiments can be found in Appendix B.4. We wanted to determine whether changing the dopant density of the silicon would have an effect on the photovoltages or electron transfer rates measured on these surfaces. Beginning with highly doped n^+-Si(111), with resistivity 0.004–0.006 $\Omega \cdot$ cm, we functionalized a series of silicon wafers with mixed methyl/vinylferrocenyl monolayers and measured their photoelectrochemical properties. The results are summarized in Table 3.3. There does not appear to be a clear correlation between dopant density and photovoltage. Except for the highly doped sample (resistivity 0.004–0.006 $\Omega \cdot$ cm), all the wafers generated photovoltages of 400 ± 50 mV. The highly doped n-type silicon had a small photovoltage of 50 mV, suggesting that it may not actually be degenerate.

The charge transfer rates (k_{et}) on the surfaces were measured using potential-step chronoamperometry experiments.[49] The details of these experiments and calculations can be found in Appendix B.4.2. Independent measurements were made for the oxidation and reduction reactions, allowing us to measure k_{et} for both the oxidation ($k_{et,ox}$) and reduction ($k_{et,red}$) of the vFc on the surface. These rates were measured both in the dark ($k_{et,dark}$) and under illumination ($k_{et,light}$), allowing us to compare the efficacy of interfacial charge transfer under these conditions. The relative magnitude of the charge transfer rate can also be estimated using E_{pp}, the peak-to-peak separation of the redox couple. For a surface attached redox couple, E_{pp} should be small, ideally zero. However, E_{pp} will increase with the scan rate if k_{et} is comparable to the voltammetric time scale. A large E_{pp} (>100 mV) indicates slower charge transfer, and small E_{pp} (<50 mV) indicates faster charge transfer, on the timescale of the scan rate used for these experiments (100 mV s^{-1} for the samples described in Table 3.3).[54]

The charge transfer rate showed a moderate correlation with the dopant density of the silicon wafers. The degenerately doped sample showed fast charge transfer ($k_{et} = 30 \pm 10\,\text{s}^{-1}$) and small E_{pp} ($20 \pm 5\,\text{mV}$) in the light and the dark, as one would expect for a highly conductive sample. All other samples had low charge transfer rates for ferrocene-oxidation in the dark ($k_{et,ox,dark} \leq 5 \pm 5\,\text{s}^{-1}$), and fast charge transfer under illumination ($k_{et,light} = 30 \pm 10\,\text{s}^{-1}$). Most interestingly, moderately doped n-type silicon (resistivity of $0.01\text{--}10\,\Omega \cdot \text{cm}$) had fast ferrocenium-reduction kinetics in the dark ($k_{et,red,dark} = 20 \pm 10\,\text{s}^{-1}$). This indicated that the ferrocenium-reduction reaction was not limited by electron availability on these samples, though ferrocene-oxidation was limited by hole availability. However, for samples with resistivity of $>20\,\Omega \cdot \text{cm}$, both ferrocene-oxidation and ferrocenium-reduction were slow in the dark ($k_{et,dark} < 5 \pm 5\,\text{s}^{-1}$), indicating that both electron and hole availability were limiting factors for the charge transfer reaction. This agreed fairly well with predicted behavior for n-type silicon.

Resistivity $\Omega \cdot cm$	η_{Fc} [a]	V^0_{dark} [b]	V^0_{light} [b]	$k_{et,ox,dark}$ [c] s^{-1}	$k_{et,red,dark}$ [c] s^{-1}	$k_{et,light}$ [c] s^{-1}	$E_{pp,dark}$ [d] mV	$E_{pp,light}$ [d] mV
0.004–0.006	0.2	0.12	0.05	30 ± 10	30 ± 10	30 ± 10	20 ± 5	20 ± 5
0.019–0.023	0.3	0.12	−0.30	1 ± 5	30 ± 10	30 ± 10	150 ± 10	20 ± 5
0.8–1.5	0.02	—	−0.20	—	—	30 ± 10	350 ± 10	20 ± 5
1–10	0.05	0.12	−0.35	5 ± 5	20 ± 10	30 ± 10	70 ± 10	20 ± 5
23–34	0.1	0.12	−0.30	2 ± 5	3 ± 5	30 ± 10	260 ± 10	10 ± 5
63–77	0.05	0.12	−0.30	—	—	—	100 ± 10	10 ± 5

[a]Surface coverage in monolayers, determined electrochemically. All values ±0.05 monolayers. [b]V^0 is the ferrocene redox potential vs. Ag/Ag(NO$_3$). All values ±0.05 V. [c]Charge transfer rates determined by potential step chronoamperometry. [d]E_{pp} is the peak-to-peak potential difference between the anodic and cathodic peak current densities.

TABLE 3.3: Properties of n-type silicon electrodes modified by mixed methyl/vinylferrocenyl monolayers.

3.4.4 Stability Testing

While the surface-attached ferrocene was well behaved in non-aqueous solvents and at moderate potentials under illumination, a water-splitting device will be used under quite different conditions. Previous electrochemical experiments showed that mixed methyl/vinylferrocenyl surfaces degraded rapidly at potentials more oxidizing than $+0.4\,\mathrm{V}$ vs. Fc/Fc^+, resulting in significant oxidation of the surface and loss of the ferrocene moiety. The silicon surface, however, is predicted to be reductively stable. We tested this by cycling a mixed methyl/vinylferrocenyl surface between $+0.4$ and $-2.0\,\mathrm{V}$ vs. Fc/Fc^+ for an hour at a variety of scan rates. The scan rate dependence of the peak current density was linear, indicating that the ferrocene was surface-bound.[49] Figure 3.13 shows the first and final CVs taken on this surface. The scans were very similar, corresponding to 0.81 ± 0.05 and 0.74 ± 0.05 monolayers of ferrocene, respectively, indicating that the mixed monolayer is reductively stable.

We also tested the stability of the surface under acidic conditions that would be used for studies of proton reduction. We first soaked a mixed methyl/vinylferrocenyl surface in a solution of $0.1\,\mathrm{M}$ electrolyte and $40\,\mathrm{mM}$ p-toluenesulfonic acid (tosic acid, Sigma, $\geq 98.5\,\%$) in acetonitrile for $2\,\mathrm{h}$ to simulate model electrochemical conditions. XPS of the surface before and after treatment resulted in a small decrease in iron coverage (0.08 monolayers to 0.06 monolayers). This could indicate some acid instability, or could simply be due to the additional handling, rinsing, and sonication to which the wafer was subjected after acid treatment. Additionally, this experiment was performed under ambient conditions, and so was exposed to oxygen from the air and in the solvent for the duration of the experiment. To further explore the stability of the surface under acidic conditions, electrochemical experiments were performed.

Figure 3.14 shows a series of cyclic voltammograms collected on a mixed methyl/ferrocenyl surface as the acid concentration of the electrolyte solution was increased from 0 to $17\,\mathrm{mM}$ Tosic acid. This experiment was performed under inert atmospehere (N_2) in nonaqueous solvent (CH_3CN, anhydrous). The shape and size of the ferrocene redox signal did not change as the acid concentration was increased. Over the course of the experiment, the electroactive ferrocene coverage on the surface remained essentially constant, with a decrease in ferrocene coverage from the first to final scan of less than 0.01 monolayers. There was an increase
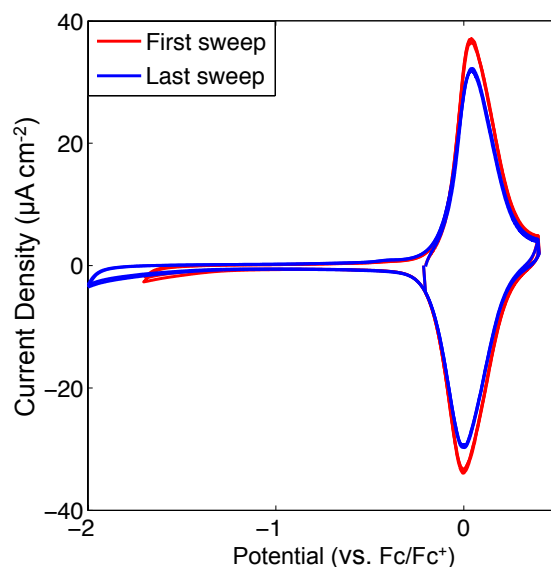
FIGURE 3.13: Cyclic voltammetry of a mixed methyl/vinylferrocenyl surface in acetonitrile. This surface is reductively stable to $-2\,\mathrm{V}$ vs. $\mathrm{Fc/Fc^+}$ with trace losses of electroactive material from the surface after an hour of cycling. In red, the first CV sweep performed on the surface. In blue, the final CV sweep performed on the surface. These two CVs are nearly identical, corresponding to 0.80 ± 0.05 and 0.75 ± 0.05 monolayers of surface-attached ferrocene, respectively.
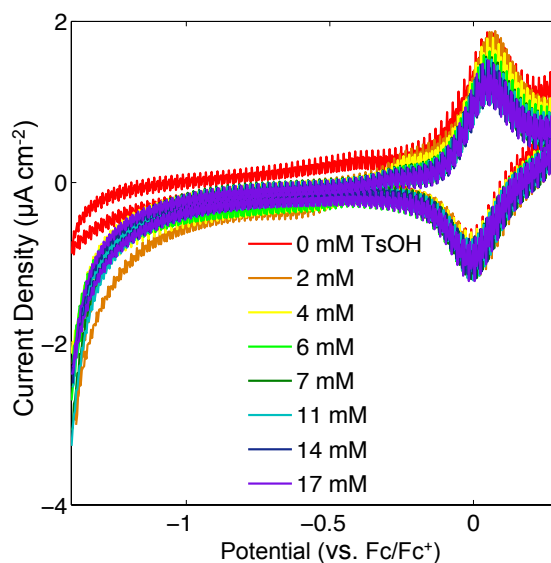
FIGURE 3.14: Cyclic voltammetry of a mixed methyl/vinylferrocenyl silicon surface under acidic conditions. This experiment was performed under inert atmosphere in anhydrous MeCN with $0.1\,\mathrm{M}$ $(\mathrm{NEt_4})\mathrm{ClO_4}$ as the electrolyte and Tosic acid (TsOH) as the proton source. The acid concentration was increased from 0 to $17\,\mathrm{mM}$ and sequential CVs were collected at a scan rate of $100\,\mathrm{mV\,s^{-1}}$.

in reductive current starting around $-1.1\,\text{V}$ vs. Fc/Fc^+ after tosic acid was added to the solution, indicating that the silicon surface was performing proton reduction. This reductive current did not increase with acid concentration, however, which could indicate that the reaction rate plateaued by $2\,\text{mM}$ tosic acid. From these results, it appeared that this surface functionalization was stable under both acidic and reductive conditions, in nonaqueous solvent under inert atmosphere.

3.4.5 Aqueous Electrochemistry of Mixed Methyl/vFc Surfaces

A water-splitting device will be run in aqueous solvent, so it was necessary to test the stability of the mixed monolayer surface in water. We studied the electrochemistry of a mixed methyl/ferrocenyl surface in water using $1.0\,\text{M}$ potassium phosphate, pH 4.2, as the electrolyte, and performed the electrochemistry under ambient atmosphere. Experimental details of the aqueous electrochemistry can be found in Appendix B.4.3. Figure 3.15 shows the cyclic voltammetry of the mixed methyl/vinylferrocenyl surface at various scan rates between 10 and $1000\,\text{mV}\,\text{s}^{-1}$. The scan rate dependence of the mixed methyl/vinylferrocenyl surface in water, as well as the coverage of electroactive ferrocene as a function of scan number, are also shown in this figure. The reversible Fc/Fc^+ couple was at $170\,\text{mV}$ vs. $K_4Fe(CN)_6/K_3Fe(CN)_6$. This corresponded to $0.53\,\text{V}$ vs. SHE, which was similar to previous electrochemical studies of ferrocene immobilized on silicon substrates in aqueous solvent.[47] The peak current density was linear with the scan rate, indicating that the ferrocene was surface-bound. However, the surface coverage of ferrocene did decrease over the course of the experiment; much of the loss occurred during the first few scans. Overall, the electroactive ferrocene coverage decreased by about $25\,\%$ over the course of the experiment, from 0.80 ± 0.05 to 0.60 ± 0.05 monolayers. Details of the surface coverage calculations using electrochemical data can be found in Appendix B.4.1. In addition, XPS of the surface after electrochemical cycling showed significant surface oxidation in the Si 2p region. This indicated that the mixed methyl/vinylferrocenyl surface had limited stability under aqueous conditions. However, ferrocene is not normally soluble in water, and so the electrochemistry of ferrocene in aqueous solvents is limited. Despite the limited stability observed in this system, it could provide a platform for studying the aqueous electrochemistry of other insoluble species.
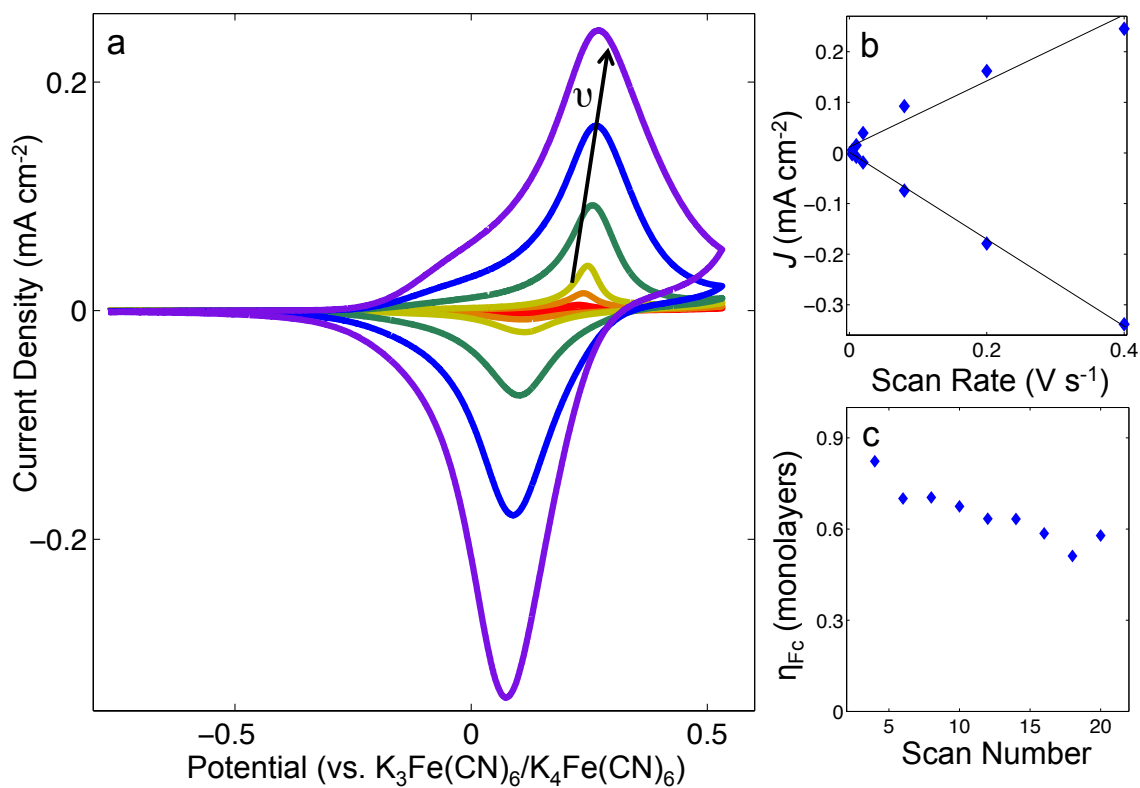
FIGURE 3.15: Electrochemistry of a mixed methyl/vinylferrocenyl surface in water. a) Cyclic voltammetry of the surface from 10 to $1000\,\text{mV s}^{-1}$, with increasing scan rate indicated by the black arrow. b) Peak current density as a function of scan rate, showing a linear dependence as expected for a surface-attached redox couple. c) Surface coverage of electroactive ferrocene as a function of scan number. The surface coverage decreased from 0.80 ± 0.05 to 0.60 ± 0.05 monolayers, which meant that approximately $25\,\%$ of the ferrocene was lost from the surface over the course of the experiment.

3.5 Conclusion

Mixed methyl/vinylferrocene monolayers have been formed on Si(111) surfaces via a straightforward route. Our methodology has a potentially large substrate scope and applicability to other redox-active molecules. The UV-light initiated reaction allowed us to dramatically decrease the amount of vinylferrocene necessary for surface attachment, and the addition of BP to the reaction solution drastically decreased the reaction time necessary for high surface coverage. The electroactive surface coverage of the ferrocene in these mixed monolayers could be varied from <1 to 100 % of the silicon atop sites. The functionalized surfaces were resistant to oxidation and permitted relatively rapid interfacial charge transfer to the attached ferrocene group. The mixed monolayers maintained the favorable electronic properties of the underlying silicon, as evidenced by the low surface recombination velocities measured on the functionalized surfaces, as well as the $400 \pm 50\,\mathrm{mV}$ photovoltage generated on n-type silicon. This method is therefore an attractive approach for the attachment of electrocatalysts and other functional groups to silicon surfaces, without introducing deleterious surface recombination sites or chemical instability to the resulting Si/organic interface.

Portions of the preceding chapter have been adapted with permission from Lattimer et al.[34] Copyright 2013 American Chemical Society.

Chapter 4

Assembly, Characterization, and Electrochemical Properties of Immobilized Metal Bipyridyl Complexes on Silicon(111) Surfaces

4.1 Introduction

The ability to prepare a catalyst-functionalized silicon surface that is free of both electronic defects and chemically reactive sites will be a necessary development for the advancement of any silicon-based solar-fuels device. If complex organometallic catalysts can be immobilized on semiconductor-electrode surfaces without loss of catalytic activity, these assembled photocathodes could perform reductive, fuel-forming reactions, such as the conversion of protons to dihydrogen, or the reduction of CO_2 to liquid fuels.[59][60][61] Retaining the activity of surface-bound molecular catalysts remains challenging due to the limited compatibility of most molecular catalysts with conditions that are suitable for covalently attaching ligands to the silicon surface.[56] Furthermore, the proper coordination environment around the metal center must be maintained during electrochemical cycling to prevent ligand-exchange processes which may cause either the loss of catalyst molecules from the surface, or the formation of secondary heterogeneous materials.[62][63]

We used the method for preparing mixed monolayers on Si(111) that combines the chlorine-termination route with UV light-induced attachment of vinyl-tagged reagents discussed in Chapter 3 to form a new class of mixed monolayers suitable for catalyst attachment, as shown in Scheme 4.1. We used this method based on the structural similarity between vinylferrocene
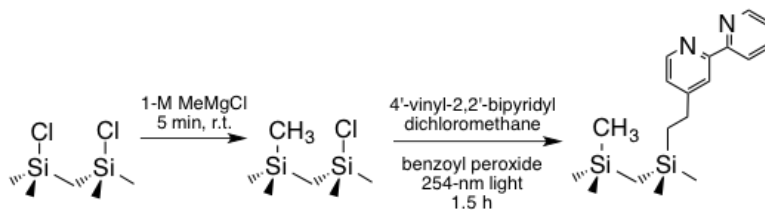
SCHEME 4.1: Route for formation of mixed methyl/vbpy monolayer. Reproduced by permission of The Royal Society of Chemistry (RSC).[64]
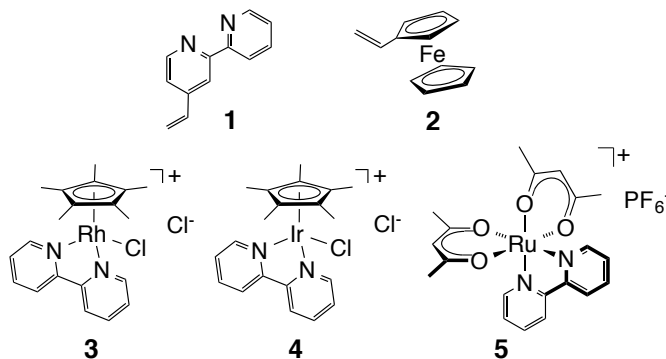
FIGURE 4.1: Structures of **1-5**. **1)** 4′-vinyl-2,2′-bipyridyl, vbpy. **2)** vinylferrocene, vFc. **3)** [Cp*Rh(bipy)Cl]Cl. **4)** [Cp*Ir(bipy)Cl]Cl. **5)** [Ru(acac)$_2$(bpy)]PF$_6$. Reproduced by permission of The Royal Society of Chemistry (RSC).[64]

(**2**) and 4′-vinyl-2,2′-bipyridyl (vbpy, **1**, see Figure 4.1), which we anticipated would result in similar reactivity with the silicon surface. The chlorinated surface (i.e., all atop sites terminated as Si−Cl) was briefly exposed to CH$_3$MgCl to yield a predominantly methyl-terminated surface with some remaining unreacted Si−Cl bonds. This partially methylated surface was then reacted with vbpy under UV light to produce a mixed methyl/vbpy monolayer on the silicon surface. This surface was characterized and shown to display good photoelectronic properties, low surface oxidation, and high bipyridine (bipy) coverages (between 0.1 and 0.35 monolayers).

Using these surfaces, we subsequently demonstrated that this immobilized ligand can form complexes with metal reagents on the surface. We assembled immobilized analogues of pentamethylcyclopentadienyl (Cp*) rhodium (**3**) and iridium (**4**) complexes of bipyridine, as well as a ruthenium complex (**5**, Figure 4.1) on the surface. As the rhodium complexes have been shown by Grätzel, Kölle, and others to serve as proton-reduction catalysts,[65–70] we investigated the stability of the Rh system in the presence of p-toluenesulfonic acid. Much of the work discussed in this chapter was done in collaboration with Dr. James Blakemore.
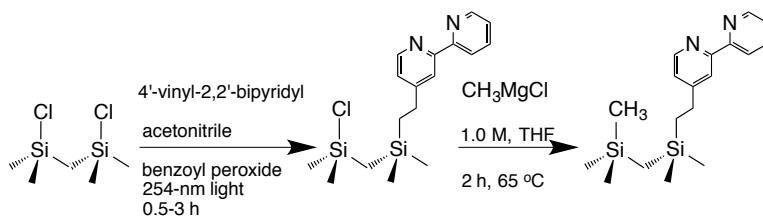
SCHEME 4.2: Initial route used for the formation of mixed vbpy/methyl monolayer.

4.2 Mixed Vinylbipyridyl/Methyl Surfaces

We formed our first mixed vinylbipyridyl/methyl monolayers by mimicking the reaction sequence used for forming mixed methyl/vinylferrocenyl monolayers. This was done by chlorinating a H−Si(111) surface, placing the wafer in a solution of vbpy in acetonitrile (CH_3CN) with benzoyl peroxide (BP) added as a radical initiator, and exposing it to UV light for 30 to 180 min. The surface was then rinsed with CH_3CN to remove residual reactant and placed in 1 M CH_3MgCl in THF at $60\,°C$ for $2\,h$. This reaction scheme is shown in Scheme 4.2. Experimental details can be found in Appendix A.11. The surfaces formed by this method had between 0.1 and 0.9 ± 0.1 monolayers of bipy and showed significant surface oxidation. The surface coverage of silicon oxide and bipy for mixed monolayers prepared by varying the reaction time with vbpy is shown in Table 4.1. Bipy coverage was quantified using the N 1s signal, with two nitrogen atoms per bipy molecule. Details of the quantification methodology can be found in Appendix B.1.1.

High-resolution XPS of a typical mixed vbpy/methyl surface formed using this reaction sequence is shown in Figure 4.2. These mixed vbpy/methyl surfaces all had some surface oxidation, as seen by the Si 2p peak at $103\,eV$. This peak increased in intensity with reaction time in the vbpy solution under UV illumination. The C 1s region for all these surfaces had a distinct peak at $284\,eV$, indicating that there are methyl groups on the surface, and a larger, broader peak at $285\,eV$ from the vbpy moiety on the surface, as well as adventitious carbon contributions. The N 1s region of these surfaces had a single peak at $399.8\,eV$ from the bipy groups, indicating that the attachment of the vbpy group was successful. This nitrogen signal increased with reaction time in the vbpy solution, indicating increased attachment of vbpy to the surface.
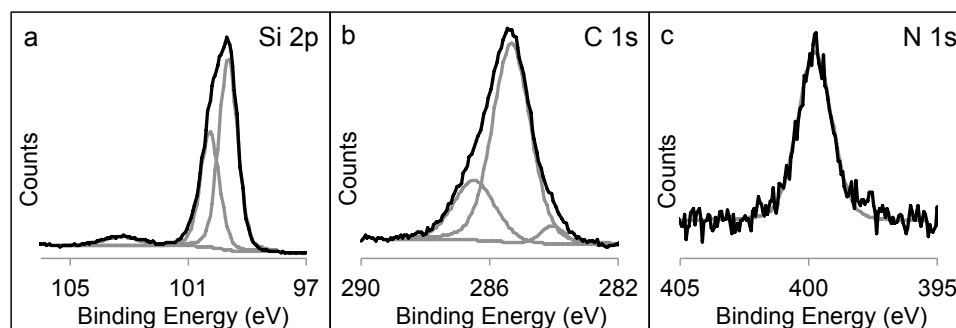
FIGURE 4.2: High-resolution XPS of a mixed vbpy/methyl surface. a) The Si 2p region had a small oxide peak at 103 eV. b) The C 1s region had a peak at 284 eV from the methyl groups and a larger components at 285 and 287 eV from the vbpy groups and adventitiously adsorbed carbon. c) The N 1s region had a single peak at 399.8 eV from the bipy groups attached to the surface through the vinyl moiety.
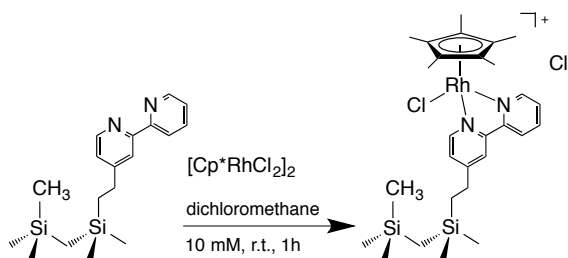
SCHEME 4.3: Proposed reaction scheme for the ligation of $[Cp^*RhCl_2]_2$ by surface-bound bipy in a mixed vbpy/methyl monolayer.

4.2.1 Metallation with Rhodium Complexes

These surfaces were then metallated by submersion in a solution of 10 mM $[Cp^*RhCl_2]_2$ in dichloromethane (CH_2Cl_2) for 1 h, followed by sonication for 10 min each in CH_2Cl_2, methanol (CH_3OH), and water. The proposed reaction scheme for the ligation of $[Cp^*RhCl_2]_2$ by surface-bound bipy is shown in Scheme 4.3. $[Cp^*RhCl_2]_2$ was prepared following published methods by J. Blakemore.[71] These surfaces were then analyzed using XPS to quantify the Rh that was bound to the surface through the bipy ligand. Table 4.1 shows the quantification of selected elements for a series of mixed vbpy/methyl surfaces that were formed by varying the time of exposure to vbpy under UV light. These surfaces were subsequently metallated by $[Cp^*RhCl_2]_2$, and the amount of Rh bound to the bipy ligand is displayed in the table. Details of the quantification methodology can be found in Appendix B.1.1.

Based on the surface coverages of >0.6 monolayers of bipy measured on some of the surfaces, it is likely that multilayers of vbpy are forming. Bipy is a relatively large molecule

	Reaction time in vbpy (min)			
	30	**60**	**120**	**180**
	mixed vbpy/methyl surfaces			
Si−O	0.2 ± 0.1	0.6 ± 0.1	0.9 ± 0.1	1.1 ± 0.1
bipy	0.11 ± 0.05	0.16 ± 0.05	0.65 ± 0.05	0.85 ± 0.05
	after reaction with [Cp*RhCl$_2$]Cl$_2$			
Si−O	1.9 ± 1.0	1.9 ± 0.1	1.6 ± 0.1	1.6 ± 0.1
bipy−Rh	0.17 ± 0.05	0.24 ± 0.05	0.25 ± 0.05	0.28 ± 0.05
bipy-free	0.03 ± 0.01	—	0.39 ± 0.05	0.66 ± 0.05
Rh	0.17 ± 0.05	0.21 ± 0.05	0.28 ± 0.05	0.33 ± 0.05

TABLE 4.1: Surface coverage in monolayers of selected elements on mixed vbpy/methyl surfaces, quantified by XPS. Si−O is the coverage of silicon oxide on the surface calculated from the Si 2p peak at $103\,\mathrm{eV}$. Bipy-free is the coverage of bipy on the surface calculated from the N 1s peak at $399.8\,\mathrm{eV}$. Bipy−Rh is the coverage of metallated bipy on the surface calculated from the N 1s peak at $400.7\,\mathrm{eV}$. Rh is the coverage of Rh(III) on the surface calculated from the Rh 3d peaks at 310.1 and $314.8\,\mathrm{eV}$.

and, like vFc, cannot fit on every Si atop site.[51] This implies that there will be some bipy that is buried or solvent-inaccessible, which could explain the relatively low coverage of Rh (0.3 monolayers) measured on surfaces with high bipy coverage (0.9 monolayers). This is further supported when comparing the surface coverage of Rh to the surface coverage of metallated bipy (calculated from the N 1s peak at $400.7\,\mathrm{eV}$). These values generally agree within experimental error, suggesting that the N 1s component at $400.7\,\mathrm{eV}$ results from Rh-ligated surface-attached bipy. The remaining unmetallated free-base bipy on the surfaces is likely from surface-attached bipy that cannot be ligated by the Rh complex for steric reasons. These multilayers of bipy may also explain why there was such a large Si−O signal on these surfaces. It was possible that the methyl Grignard could not reach the surface to react efficiently with the remaining Cl−Si sites on the surface, leaving them available for surface oxidation after the wafers were removed from the flush box and exposed to atmosphere and water during the cleaning procedure.

High-resolution XPS of a mixed vbpy/methyl surface metallated with Rh is shown in Figure 4.3. The Si 2p region showed some surface oxidation, similar to the amount seen prior to metallation (see Table 4.1). This indicated that the surface oxidation occurred during the initial surface functionalization and not as a result of the metallation procedure. The N 1s region was composed of two peaks, at 399.8 and $400.7\,\mathrm{eV}$, corresponding to free-base and bound bipy, respectively. The Rh 3d region had a doublet of peaks at 310.1 and $314.8\,\mathrm{eV}$,
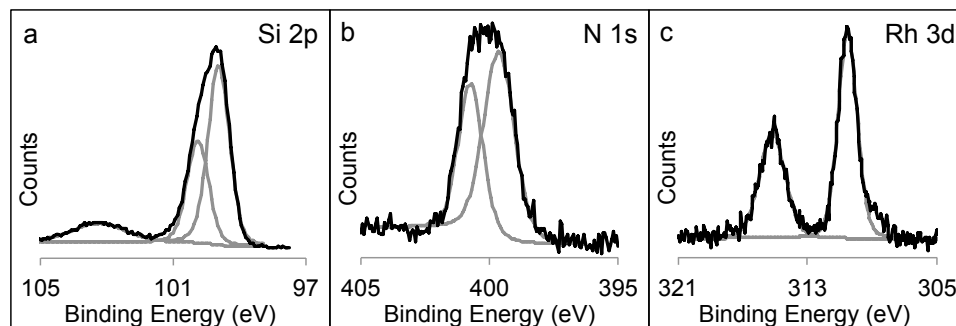
FIGURE 4.3: High-resolution XPS of a mixed vbpy/methyl surface after metallation with [Cp*RhCl$_2$]$_2$. a) The Si 2p region showed an increased silicon oxide peak at 103 eV after metallation. b) The N 1s region had two peaks, at 399.8 and 400.7 eV. The peak at 399.9 eV was from free bipy on the surface, while the new peak at 400/7 eV was from metallated bipy. c) The Rh 3d region had a doublet of peaks at 310.1 and 314.8 eV, consistent with Rh(III).

with the 4.7 eV spit-orbit splitting and area ratio of 3:2 expected for a Rh 3d doublet. These peak positions were consistent with rhodium in the +3 oxidation state, and were each fit to a single component, indicating that there was a single species of rhodium on the surface. In addition, [Cp*Rh(bipy)Cl]Cl was prepared using published methods from [Cp*RhCl$_2$]$_2$ and bipy by J. Blakemore, and characterized by XPS.[65] This Rh 3d region of this complex consisted of a doublet of peaks at 310.1 and 314.8 eV with an area ratio of 3:2, which agreed well with the Rh 3d region of our surface-attached complex.

4.2.2 Control Reactions

Several control experiments were performed to ensure that the rhodium was bound to the surface through the bipy moiety, rather than nonspecifically adsorbed onto the surface. Methyl-terminated silicon was immersed in a 10 mM solution of [Cp*RhCl$_2$]$_2$ in CH$_2$Cl$_2$ for 1 h, and then cleaned as described previously. XPS of this surface, shown in Figure 4.4, revealed no rhodium or nitrogen signals. High-resolution XPS of the N 1s and Rh 3d regions of the methyl surface also showed no above background signal, indicating that there was no surface adsorption of the rhodium complex. Also shown in Figure 4.4 is a mixed methyl/vbpy surface after metallation with [Cp*RhCl$_2$]]$_2$. This surface had Rh 3d and N 1s signals at 312 and 400 eV, respectively, from the Rh-complex bound to the surface through the bipy ligand. This implied that the bipy on the surface was necessary to bind the rhodium complex to the surface.

A mixed methyl/vbpy surface was immersed in 20 mM [Cp*Rh(bipy)Cl]Cl (instead of
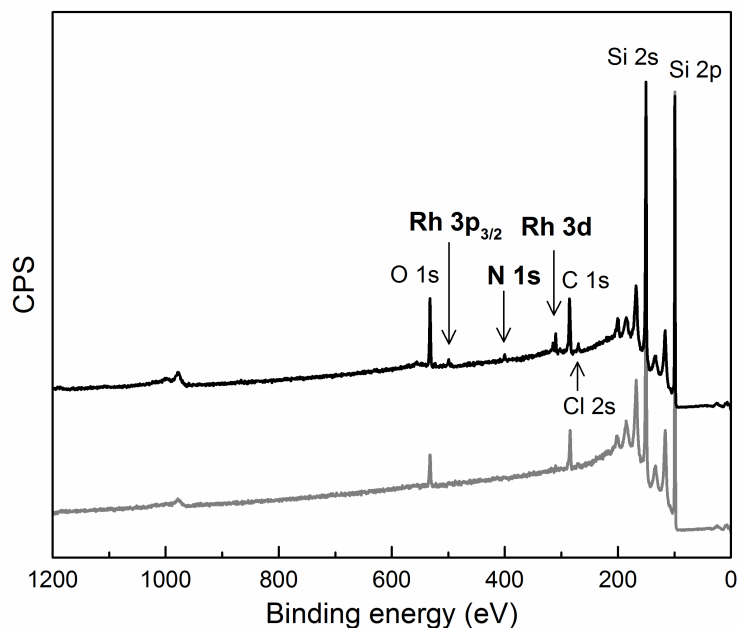
FIGURE 4.4: XPS of a mixed methyl/vbpy surface (black line) and a methyl surface (gray line) after metallation with $[Cp^*RhCl_2]_2$. Peaks in the Rh 3d region at 312 eV and N 1s region at 400 eV were clearly visible in the survey scan for the mixed methyl/vbpy surface only. Reproduced by permission of The Royal Society of Chemistry (RSC).[64]

10 mM $[Cp^*RhCl_2]_2$) in CH_2Cl_2 for 1 h. This complex already had a bipy bound to the Rh center and therefore had no available sites for ligation by another bipy ligand. This surface showed only 0.02 ± 0.01 monolayers of Rh coverage, suggesting that nonspecific adsorption did not occur and that ligand exchange was relatively slow.

Additional evidence for the ligation of the $[Cp^*RhCl_2]_2$ complex by the surface-bound bipy ligand is found in the high-resolution N 1s XPS, shown in Figure 4.5. Prior to metallation, the mixed vbpy/methyl surface had a N 1s signal dominated by the peak at 399.7 eV. Upon reaction with $[Cp^*RhCl_2]Cl_2$, the predominant peak shifted to 400.6 eV. High-resolution N 1s XPS of the free $[Cp^*Rh(bipy)Cl]Cl$ complex had a single peak at 400.4 eV. Therefore we assigned this higher binding energy peak at 400.6 eV to bipy bound to rhodium on our assembled surface, while the lower binding energy peak at 399.7 eV was assigned to free-base bipy.
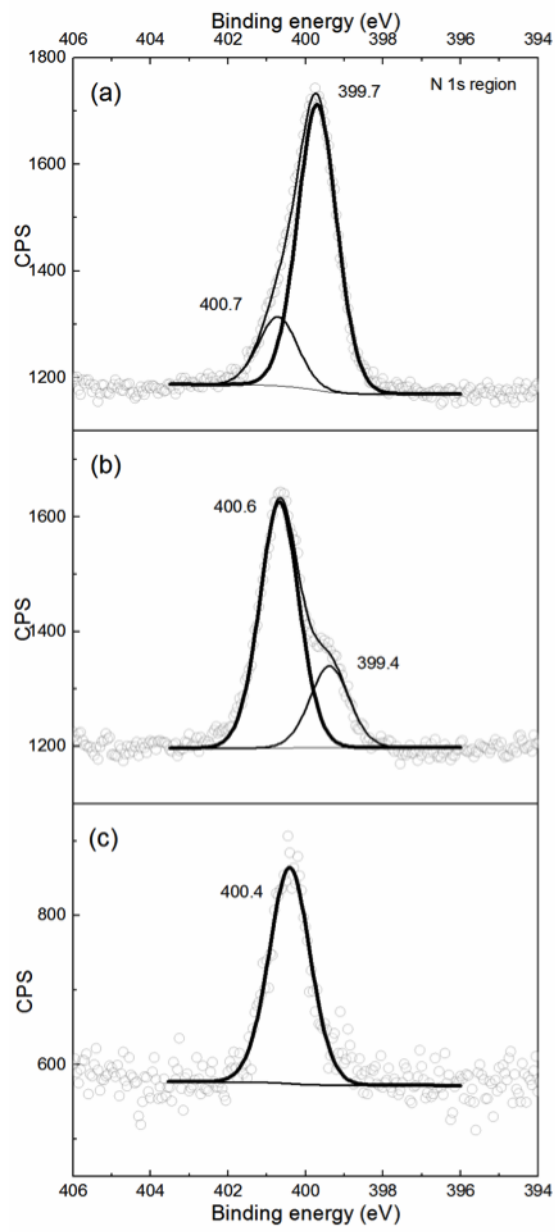
FIGURE 4.5: Comparison of N 1s XPS of a mixed methyl/vbpy surface before (upper panel, a) and after (middle panel, b) metallation with $[Cp^*RhCl_2]_2$. Lower panel c: N 1s XPS of $[Cp^*Rh(bipy)Cl]Cl$. Reproduced by permission of The Royal Society of Chemistry (RSC).[64]
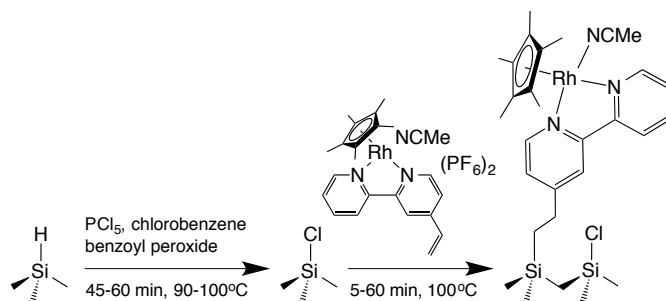
SCHEME 4.4: Reaction sequence for the attachment of $[Cp^*Rh(vbpy)CH_3CN](PF_6)_2$ to Cl$-$Si(111).

4.2.3 Attachment of $[Cp^*Rh(vbpy)CH_3CN](PF_6)_2$

In addition to metallation of the bound bipy ligand by Rh complexes, we simultaneously pursued the direct attachment of the complete Rh catalyst to the surface. This was done using the vinyl-tagged analog of the $[Cp^*Rh(bipy)Cl]Cl$ species. $[Cp^*Rh(vbpy)CH_3CN](PF_6)_2$ was prepared by J. Blakemore using vbpy synthesized by W. Sattler. The chlorinated Si(111) surface was reacted with this complex under UV light for 2 h in CH_3CN with trace BP, as shown in Scheme 4.4. Experimental details can be found in Appendix A.12.

Figure 4.6 shows the high-resolution XPS of $[Cp^*Rh(vbpy)CH_3CN](PF_6)_2$ after attachment to the silicon surface. The Si 2p region showed some surface oxidation at 103 eV, corresponding to <1 monolayer of silicon oxide. The N 1s region had a predominant peak at 400.7 eV, corresponding to 0.35 ± 0.05 monolayers of nitrogen, with a shoulder at 399.8 eV, corresponding to 0.06 ± 0.05 monolayers of nitrogen. This complex had three nitrogens bound to the Rh center, and so 0.35 monolayers of nitrogen corresponds to 0.12 ± 0.03 monolayers of the complex on the surface. The shoulder at 399.8 eV, corresponding to free-base bipy, could be from vbpy that attached to the surface and subsequently lost its Rh center. The Rh 3d region had two sets of doublets, at 308.5 and 312.8 eV and 310.5 and 315.1 eV. This indicates that there were two kinds of Rh on the surface, most likely a Rh(I) and a Rh(III) species. The Rh(III) is probably the same complex we have seen previously on similar surfaces, but the Rh(I) species is unknown. The Rh(III) component, at 310.5 and 315.1 eV, corresponded to 0.12 ± 0.02 monolayers, while the Rh(I) component, at 308.5 and 312.8 eV, corresponded to 0.05 ± 0.02 monolayers. This agreed well with the quantification of the nitrogen signal. There should be 12 F atoms per Rh atom (6 from each of the two PF_6^- groups). Analysis of the F 1s region gave 0.15 ± 0.05 monolayers, which corresponded to only 0.013 monolayers
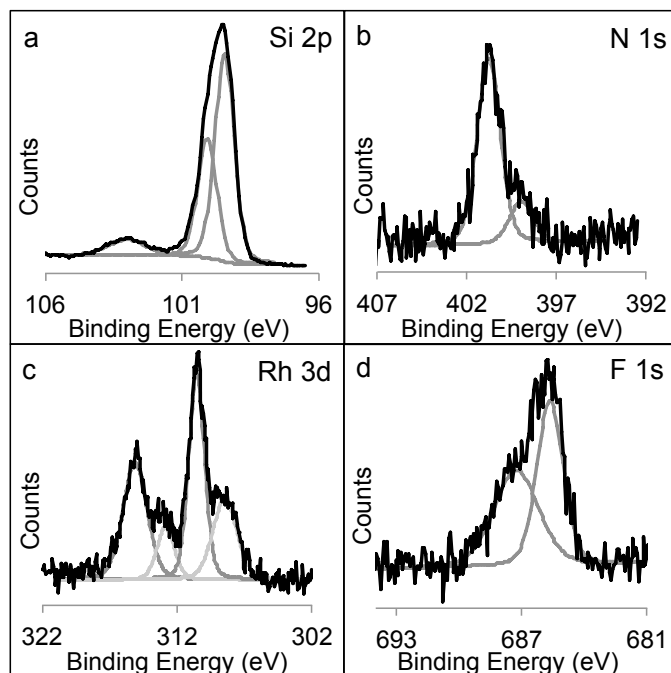
FIGURE 4.6: High-resolution XPS of $[Cp^*Rh(vbpy)CH_3CN](PF_6)_2$ after attachment to Cl−Si(111). a) The Si 2p region had a silicon oxide peak at 103 eV. b) The N 1s region had a dominant peak at 400.7 eV and a shoulder at 399.8 eV, corresponding to metallated and free-base bipy, respectively. c) The Rh 3d region showed two doublets of peaks, at 308.5 and 312.8 eV and 310.5 and 315.1 eV. These peak positions corresponded to Rh(I) and Rh(III), respectively, suggesting that we had reduced some of the Rh on the surface. d) The F 1s region had two peaks at 686 and 688 eV, likely from the PF_6^- counter anions associated with the Rh complex.

of complex. This indicated that the PF_6^- anion was lost from the surface, possibly through anion-exchange in solution, or because the complex has decomposed. Electrochemistry on this surface was performed, but we did not observe any redox events. Our inability to see an electrochemical signal for the redox couple on this surface suggested that decomposition may be an issue.

4.3 Modification to Mixed Methyl/Vinylbipyridyl Monolayer Formation

Our difficulty in preventing multilayer formation of the vbpy ligand and the significant surface oxide observed on the resultant surfaces led us to modify the reaction sequence used to form mixed methyl/vbpy monolayers. Following the reaction sequence shown in Scheme 4.1, we first did a partial methylation of the Cl−Si(111) surface by immersing the wafer in 1 M CH_3MgCl in THF at room temperature (r.t.) for 5 min, followed by rinsing with THF. The wafer was then placed in a solution of vbpy in CH_2Cl_2 with trace BP under UV illumination for 1–2 h. Experimental details can be found in Appendix A.13.

This method resulted in better control over bipy surface coverage and lower surface oxidation, as seen in Figure 4.7. The Si 2p region had no surface oxide, as evidenced by the lack of a peak at 103 eV. The C 1s region had a broad peak at 285 to 288 eV with a small shoulder at 284 eV, corresponding to carbon directly bound to silicon, assigned to the methyl groups on the surface.[29][13] The larger peak was a mixture of the carbon signals from the vbpy group and any adventitious carbon on the surface. The N 1s region had a predominant peak at 399.8 eV corresponding to 0.40 ± 0.05 monolayers of bipy, and a smaller shoulder at 400.7 eV corresponding to 0.13 ± 0.05 monolayers of bipy. The peak at 399.8 eV was from the free bipy ligand on the surface, and the higher energy component was likely bipy metallated by trace contaminants on the surface.

4.3.1 Metallation of Mixed Methyl/vbpy Surfaces with $[Cp^*RhCl_2]_2$

Having established a reproducible method of forming mixed methyl/vbpy surfaces with low surface oxidation and high bipy coverage, metallation of the bipy ligand to form metal complexes and catalysts on the surface could proceed. Mixed methyl/vbpy surfaces were immersed in 10 mM $[Cp^*RhCl_2]_2$ in CH_2Cl_2 for 1 h, with the results shown in Figure 4.8.
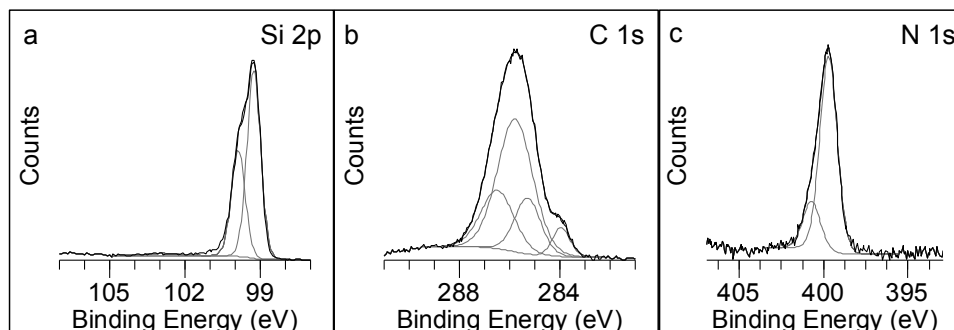
FIGURE 4.7: High-resolution XPS of a mixed methyl/vbpy surface. a) The Si 2p region did not have a peak at 103 eV, indicating that the surface was not oxidized during the formation of this mixed monolayer. b) The C 1s region had a large, broad peak between 285 and 288 eV, with a distinct shoulder at 284 eV. c) The N 1s region had a predominant peak at 399.8 eV and a shoulder at 400.7 eV.

The Si 2p region did not have a surface oxide peak at 103 eV, indicating that the metallation did not damage the surface. The N 1s region had a predominant peak at 400.7 eV and a smaller peak at 399.6 eV, corresponding to metallated and free-base bipy, respectively. Quantification of these peaks gave 0.40 ± 0.05 monolayers of metallated bipy and 0.13 ± 0.05 monolayers of free-base bipy. The Rh 3d region showed a doublet of peaks at 310.1 and 314.8 eV, each fit to a single component which corresponded to 0.5 ± 0.1 monolayers. The peak positions were consistent with Rh(III) and agreed well with the values seen previously for the [Cp*Rh(bipy)Cl]Cl complex in XPS. The amount of Rh and metallated bipy measured on this surface agreed within experimental error, suggesting that the complex was intact on the surface. In addition, there was a distinct Cl 2s peak visible in the survey and high-resolution Cl 2s spectra (not shown), indicating that the inner-sphere Cl^- ligand and outer-sphere Cl^- anion remained bound to the surface with the complex. The C 1s spectrum (not shown) still had a small shoulder at 284 eV from the methyl groups, but the signal was dominated by a broad peak at 286 eV which contained the carbon signals from the bipy groups and the metal complex, as well as any adventitious carbon on the surface.

4.3.2 Charge-Carrier Lifetimes of Mixed Methyl/vbpy Surfaces

Intrinsically-doped silicon was used to form mixed methyl/vbpy surfaces for SRV experiments. The experimental details of the SRV set-up can be found in Appendix B.3. On a mixed methyl/vbpy surface, the charge-carrier lifetime was 0.38 ± 0.01 ms, corresponding to an SRV of 46 ± 5 cm s^{-1}. This compared well to a methylated silicon surface, prepared and
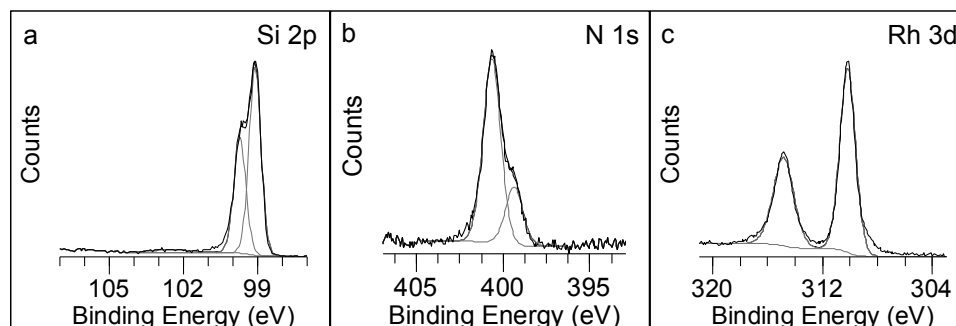
FIGURE 4.8: High-resolution XPS of a mixed methyl/vbpy surface after metallation with [Cp*RhCl$_2$]$_2$. a) The Si 2p region did not have a peak at 103 eV, indicating that the surface was not oxidized during metallation. b) The N 1s region had a predominant peak at 400.7 eV with a shoulder at 399.6 eV, corresponding to metallated and free-base bipy, respectively. c) The Rh 3d region contained a doublet of peaks at 310.1 and 314.8 eV, consistent with Rh(III). These peaks were each fit to a single component, suggesting that we have one Rh(III) species on the surface.

measured simultaneously for comparative purposes. The methylated silicon surface had a charge-carrier lifetime of 0.77 ± 0.01 ms, corresponding to an SRV of 23 ± 5 cm s^{-1}. The mixed methyl/vbpy was metallated with [Cp*RhCl$_2$]$_2$ and had a charge-carrier lifetime of 0.43 ± 0.01 ms, corresponding to an SRV of 41 ± 5 cm s^{-1}. These numbers were all well below the 100 cm s^{-1} limit indicative of good photoelectronic properties for Si(111) surfaces, implying that these surfaces had good photoelectrochemical properties.

4.3.3   Electrochemistry of Surface-Bound [Cp*Rh(bipy)Cl]Cl

Electrochemistry of the rhodium complexes was carried out in a N$_2$-purged glovebox. All solvents were anhydrous and all materials were furnace-dried before being brought into the box. These experiments were carried out using 0.10 M (NBu$_4$)PF$_6$ in CH$_3$CN as the electrolyte solution. Experimental details can be found in Appendix B.4.

In acetonitrile solution, [Cp*Rh(bipy)Cl]Cl undergoes a chemically-reversible net two-electron reduction from the starting rhodium(III) state to form a low-valent rhodium(I) complex with loss of coordinated counterions or solvent.[62,72] This complex shows a well-behaved, reversible redox couple near -1.2 V vs. Fc/Fc$^+$, with basal-plane graphite as the working electrode, shown in Figure 4.9. A plot of the peak current density vs. the square root of the scan rate is linear, as expected for a freely-diffusing redox couple in solution.[49] Similar CVs were collected using methyl-terminated silicon as the working electrode, with a small shift in the redox couple to -1.1 V vs. Fc/Fc$^+$.
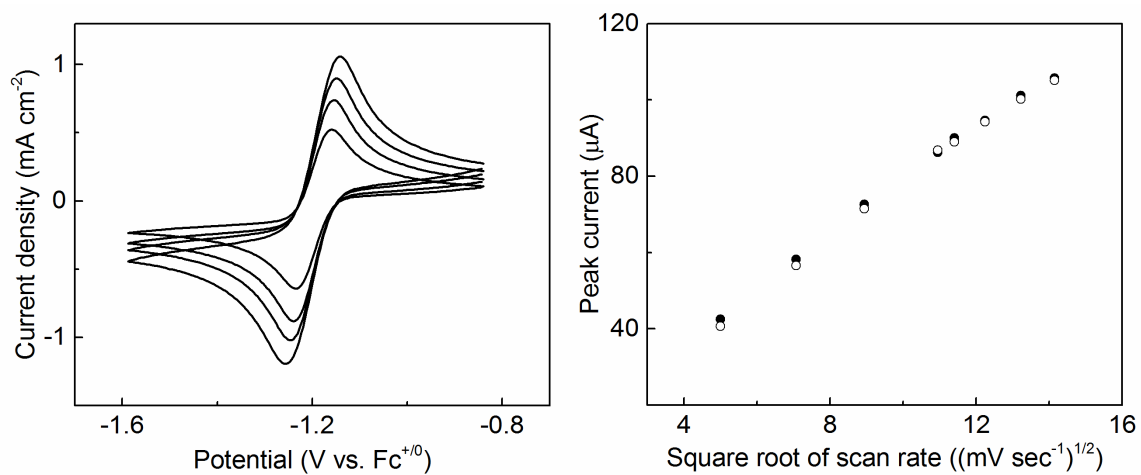
FIGURE 4.9: Solution Electrochemistry of [Cp*Rh(bipy)Cl]Cl. Reproduced by permission of The Royal Society of Chemistry (RSC).[64]
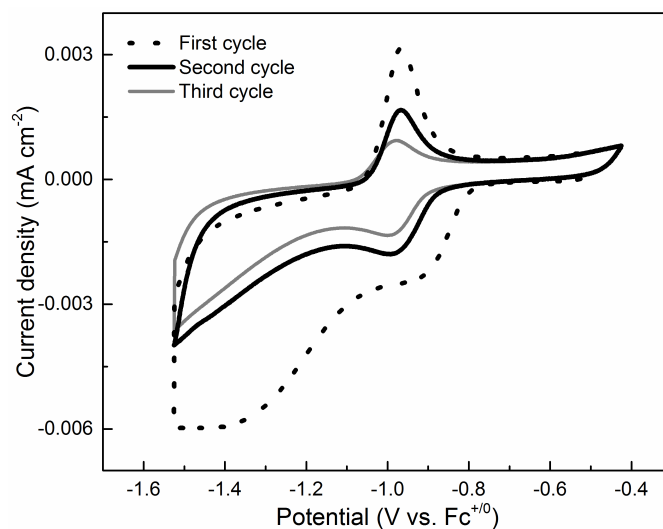
FIGURE 4.10: Electrochemistry of a mixed methyl/vbpy surface after metallation with [Cp*RhCl$_2$]$_2$. Reproduced by permission of The Royal Society of Chemistry (RSC).[64]
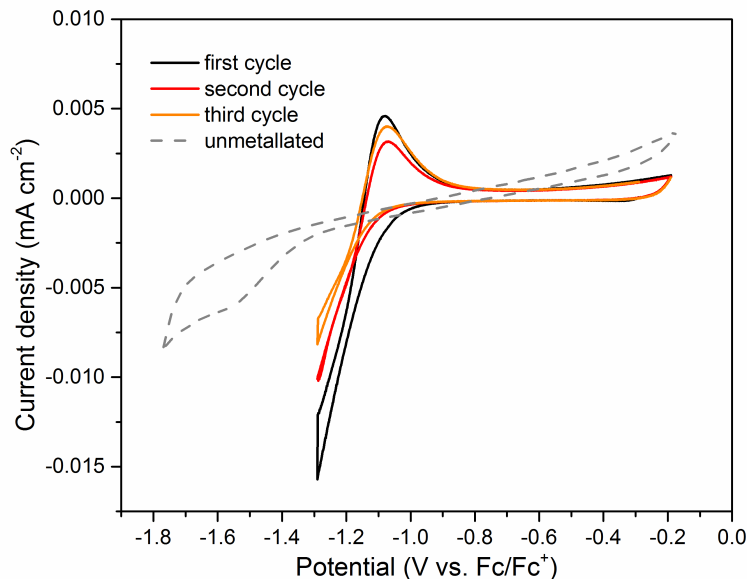
FIGURE 4.11: Electrochemistry of surface-attached [Cp*Rh(bipy)Cl]Cl scanned over a limited potential range, from -0.2 to $-1.3\,\text{V}$ vs. Fc/Fc$^+$. An unmetallated mixed methyl/vbpy surface is shown in gray for comparative purposes. This suface did not display any redox activity at potentials more positive than $-1.4\,\text{V}$ vs. Fc/Fc$^+$. Reproduced by permission of The Royal Society of Chemistry (RSC).[64]

Figure 4.10 shows the first three cyclic voltammograms collected on a mixed methyl/vbpy surface metallated by [Cp*RhCl$_2$]$_2$. There was a redox couple at $-1.0\,\text{V}$ vs. Fc/Fc$^+$ with a peak-to-peak separation of $10\,\text{mV}$. This small peak separation was indicative of a surface-bound, non-diffusive redox couple.[49] The couple at $-1.0\,\text{V}$ vs. Fc/Fc$^+$ was consistent with the solution electrochemistry of [Cp*Rh(bipy)Cl]Cl. On the very first voltammetric scan from -0.4 to $1.5\,\text{V}$, there was background current flow in a second redox process around $-1.3\,\text{V}$ (possibly reduction of free bipyridine). On the return anodic scan, there was a non-diffusional wave near $-1\,\text{V}$. Upon continued cycling, the current flow in the key redox process decreased precipitously, suggesting that the species was lost from the electrode surface during cycling. On the fourth and subsequent cycles, very low above-background current was visible. If the scan limits were changed such that the potential was scanned only from -0.2 to $-1.3\,\text{V}$, the observed process was more stable and was observed for up to six complete cycles of voltammetry (see Figure 4.11). This figure also shows a CV collected on an unmetallated mixed methyl/vbpy surface, for comparative purposes. This surface did not show any redox activity prior to the free-base bipy reduction at $-1.4\,\text{V}$ vs. Fc/Fc$^+$.

The surface coverage of electroactive Rh was estimated to be 0.002 ± 0.001 of a monolayer

using integrated current-time data from the cyclic voltammetry (averaging both the anodic and cathodic currents over three complete cycles). Details of this surface coverage calculation can be found in Appendix B.4.1. This was only ∼1 % of the coverage estimated from the XPS data (0.21 monolayers), suggesting that not all of the metal present on the surface was electroactive. The XP spectra collected after electrochemical cycling for the Rh-treated mixed surface showed no signal in the Rh 3d region and a trace nitrogen signal in the N 1s region. This indicated that both rhodium and bipyridine were lost from the surface upon redox cycling. Notably, when the mixed surface was run reductively without metallation, bipyridine was lost from that surface as well. Thus, the mechanism of loss of bipyridine from the surface was not necessarily metal-catalyzed but rather occurred independently of the presence of metal when the surface was cycled reductively. This reductive instability was in marked contrast to mixed methyl/vFc surfaces, which were stable to $-2\,\mathrm{V}$ vs. Fc/Fc$^+$ (see Figure 3.13), suggesting that the reduction of the bipy ligand itself may play some role in this instability.

4.3.4   Electrocatalysis of [Cp*Rh(bipy)Cl]Cl

Despite the apparent loss of electroactive Rh from our surfaces upon reductive cycling, catalytic reduction of protons to hydrogen could still occur. In solution, addition of p-toluenesulfonic acid (tosic acid) to a solution of [Cp*Rh(bipy)Cl]Cl results in loss of reversibility of the redox couple and an increase in the reductive current, corresponding to catalysis. This is shown in Figure 4.12.

Addition of tosic acid to our surface-attached [Cp*Rh(bipy)Cl]Cl should result in the same reductive current at $-1.0\,\mathrm{V}$ vs. Fc/Fc$^+$. In fact, we do see this catalytic current on a mixed methyl/vbpy surface metallated with Rh. This surface was previously cycled between -0.4 and $-1.5\,\mathrm{V}$ vs. Fc/Fc$^+$ several times, resulting in loss of the redox event. However, when tosic acid was added to the electrochemical cell, a reductive event starting at $-1.0\,\mathrm{V}$ vs. Fc/Fc$^+$ was observed. Figure 4.13 shows the reductive events on both a fresh mixed methyl/vbpy surface and a Rh-metallated mixed methyl/vbpy surface. The silicon wafer itself was catalytic for proton reduction at sufficiently negative potentials, as seen on the mixed methyl/vbpy surface. However, the onset of catalysis occurred at a less negative potential on the metallated surface, and the catalytic current was larger, suggesting that the Rh complex was doing above-background proton reduction catalysis on this surface. The
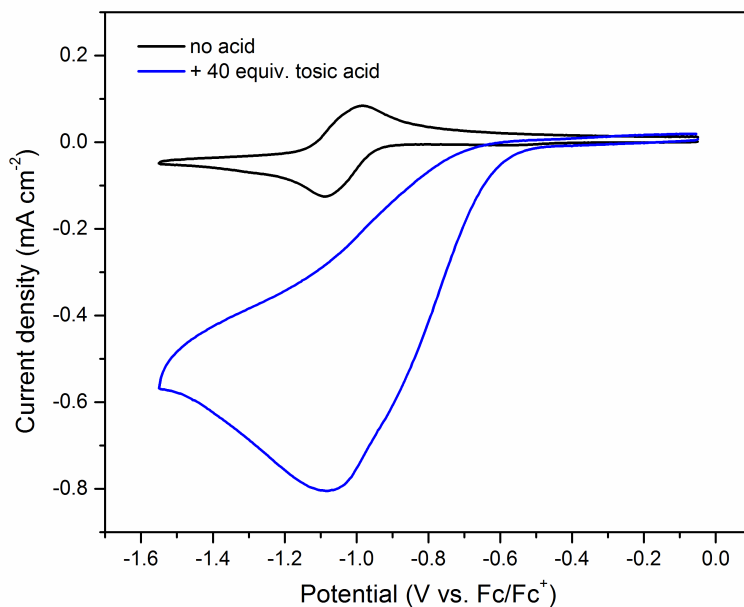
FIGURE 4.12: Electrocatalysis of solution-phase [Cp*Rh(bipy)Cl]Cl upon addition of tosic acid. [Rh] $= 10 \times 10^{-3}$ M. The electrolyte is 0.1 M $(NBu_4)PF_6$ in CH_3CN with basal-plane graphite working electrode, Pt counter electrode, and Ag/Ag+ pseudoreference electrode with ferrocene as external standard. Reproduced by permission of The Royal Society of Chemistry (RSC).[64]

onset of catalytic activity was more negative for the surface-attached complex than for the solution species (see Figures 4.12 and 4.13).
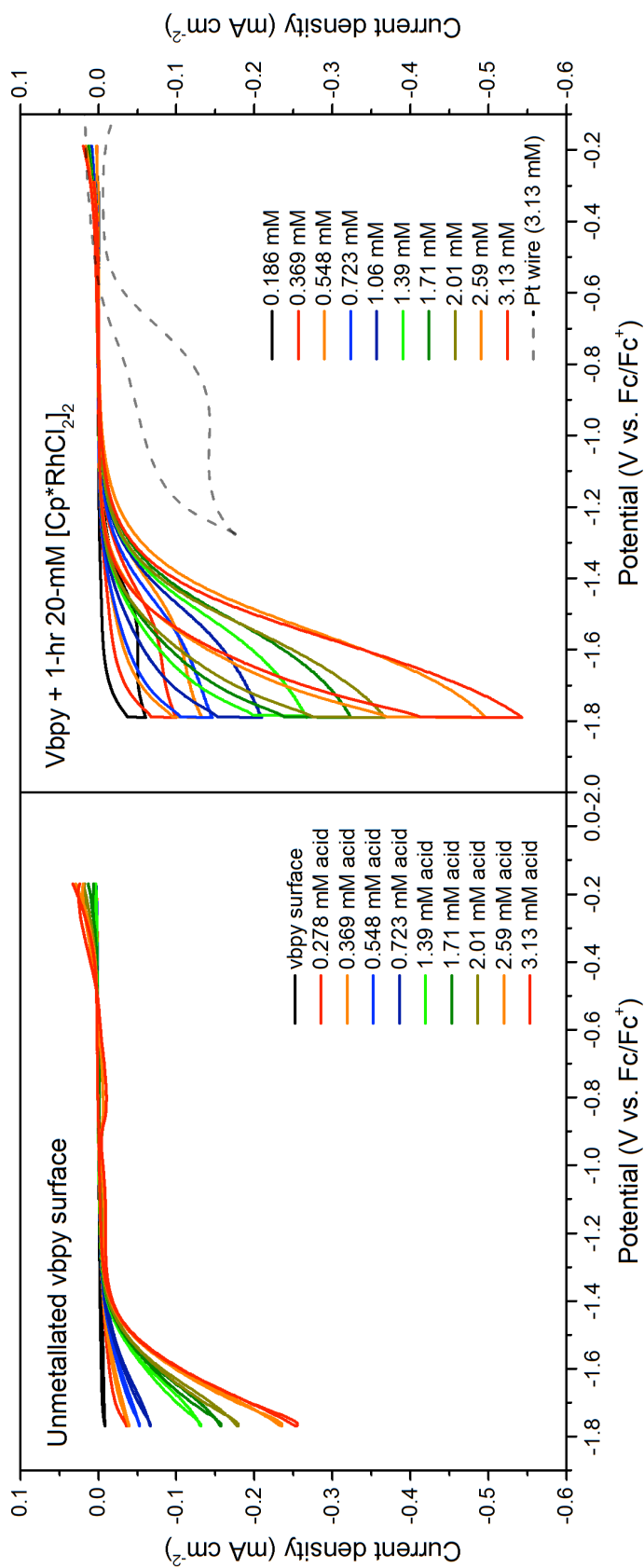
FIGURE 4.13: Electrocatalysis on surface-bound [Cp*Rh(vbpy)Cl]Cl upon addition of tosic acid. Left panel: Background electrocatalysis observed on a mixed methyl/vbpy surface in the presence of increasing tosic acid concentration. Right panel: Above-background electrocatalysis observed on a mixed methyl/vbpy surface metallated with [Cp*RhCl$_2$]$_2$ with increasing tosic acid concentration. Dotted line is hydrogen reduction catalysis with a Pt wire working electrode. The electrolyte is 0.1 M (NBu$_4$)PF$_6$ in CH$_3$CN with basal-plane graphite counter electrode, and Ag/Ag$^+$ pseudoreference electrode with ferrocene as external standard.

We tested whether the Rh complex responsible for the above background catalytic activity observed on the Rh-metallated mixed methyl/vbpy surface had fallen off the surface and into solution. This was done by removing the electrolyte from the electrochemical cell and rinsing the cell and working electrode with clean electrolyte solution, then refilling the cell with fresh electrolyte solution with $0.723\,\text{mM}$ tosic acid added. Figure 4.14 shows the electrocatalytic behavior observed on the Rh-metallated mixed methyl/vbpy surface before and after replacing the electrolyte solution. As can be seen clearly in the figure, the catalytic current was the same in both scans. This implied that the catalytic species was surface bound.

4.3.5 Metallation of Mixed Methyl/vbpy Surfaces with $[\text{Cp}^*\text{IrCl}_2]_2$

Mixed methyl/vbpy surfaces were metallated by submersion in $10\,\text{mM}$ $[\text{Cp}^*\text{IrCl}_2]_2$ in CH_2Cl_2 for 1 h at r.t. in air. They were then rinsed with CH_2Cl_2 to remove excess reagent and sonicated sequentially in CH_2Cl_2, CH_3OH, and water prior to characterization. $[\text{Cp}^*\text{IrCl}_2]_2$ was prepared following published methods by J. Blakemore.[71] These surfaces were characterized by XPS, with the results shown in Figures 4.15 and 4.16. The survey scan showed new peaks for Ir 4f at 65 eV, Ir 4d at 307 eV, and Ir 4p at 498 eV, in addition to the usual Si 2p, Si 2s, C 1s, O 1s, N 1s, and Cl 2p and 2s signals.

The Si 2p region had a small peak at 103 eV, indicating that the surface was not significantly oxidized during the metallation process. The surface oxide was quantified and increased from 0.13 ± 0.05 monolayers to 0.21 ± 0.05 monolayers upon metallation, an insignificant increase. The Ir 4f region consisted of a doublet of peaks at 62.9 and 65.9 eV, each fit to a single component, with an area ratio of 4:3, as expected for a 4f peak. This peak corresponded to 0.34 ± 0.05 monolayers of Ir. This matched well with the Ir 4f XP spectra obtained for the model compound $[\text{Cp}^*\text{Ir}(\text{bpy})\text{Cl}]\text{Cl}$ (synthesized according to literature procedures by J. Blakemore), which exhibited peaks at 62.9 and 65.9 eV.[73]

The N 1s region showed three contributions: a large peak at 400.8 eV, a smaller peak at 399.6 eV, and a small peak (visible as a minor shoulder) at 402.2 eV. For comparison, the model compound $[\text{Cp}^*\text{Ir}(\text{bipy})\text{Cl}]\text{Cl}$ showed a single N 1s peak at 400.7 eV, and so the dominant peak at 400.8 eV for the metallated surface corresponded to iridium-bound bipyridine on the surface, while the signal at 399.6 eV matched well with that for metal-free immobilized bipyridine. These peaks corresponded to 0.17 ± 0.05 monolayers of metallated
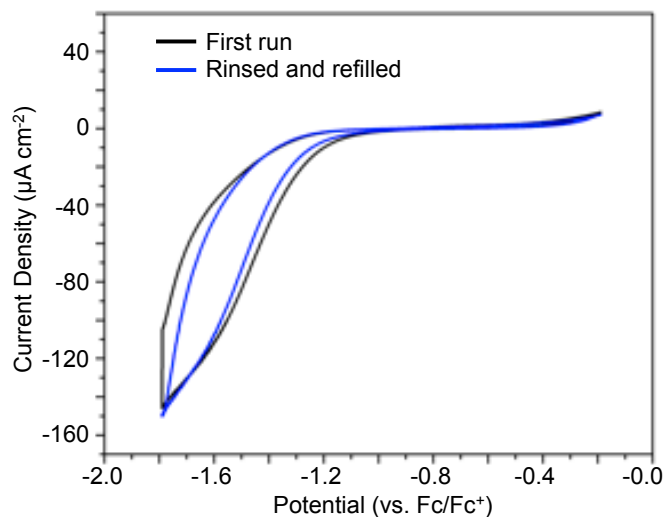
FIGURE 4.14: Electrocatalysis on surface-bound [Cp*Rh(vbpy)Cl]Cl upon addition of tosic acid after replacement of the electrolyte solution. Above-background electrocatalysis observed on a mixed methyl/vbpy surface metallated with [Cp*RhCl$_2$]Cl$_2$ with increasing tosic acid concentration (black line). Replacement of the electrolyte solution results in equivalent catalytic activity (blue line). The electrolyte is 0.1 M (NBu$_4$)PF$_6$ in CH$_3$CN with basal-plane graphite counter electrode, and Ag/Ag+ pseudoreference electrode with ferrocene as external standard.
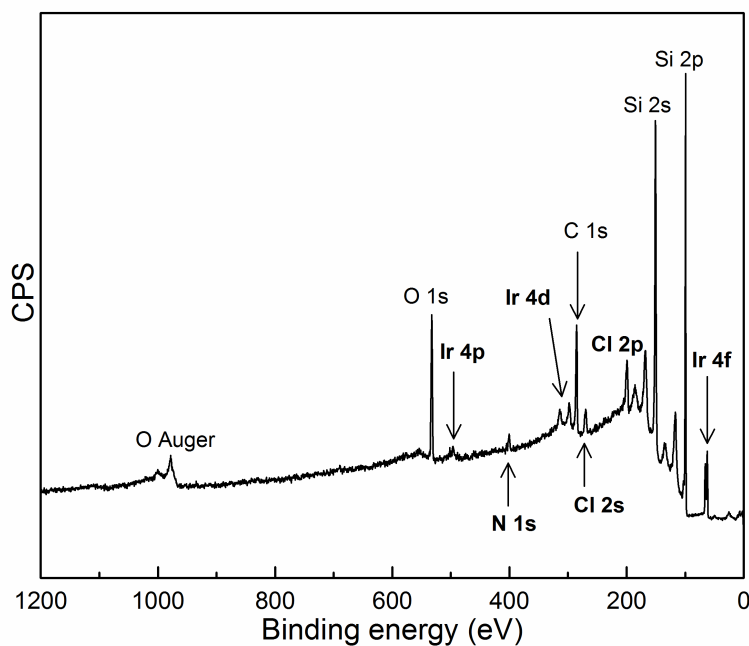
FIGURE 4.15: Survey XPS of a mixed methyl/vbpy surface metallated with [Cp*IrCl$_2$]$_2$. There were new peaks at 65, 307, and 498 eV for the Ir 4f, Ir 4d, and Ir 4p XPS signals, respectively. There was also an increase in the Cl 2s signal at 270 eV from the Cl$^-$ anions associated with the Ir complex. Reproduced by permission of The Royal Society of Chemistry (RSC).[64]
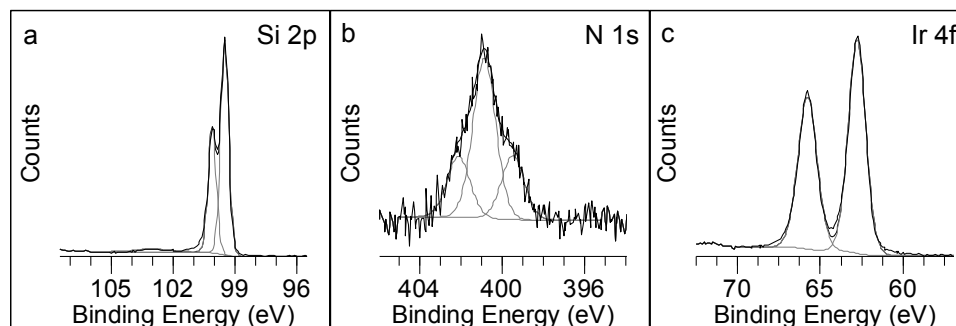
FIGURE 4.16: High res XPS of a mixed methyl/vbpy surface metallated with $[Cp^*IrCl_2]_2$. a) The Si 2p region showed a small surface oxide contribution at 103 eV, indicating that the surface was slightly oxidized by the metallation procedure. b) The N 1s region had a predominant peak at 400.8 eV, corresponding to metallated bipy. There was also a small shoulder at 399.6 eV, corresponding to free-base bipy, and an unassigned shoulder at 402.2 eV. c) The Ir 4f region had a doublet of peaks at 62.9 and 65.9 eV, each of which was fit to a single component. This indicates that there is a single Ir species on the surface.

bipy and 0.07 ± 0.05 monolayers of free-base bipy, respectively.

Ir L_{III}-edge X-ray absorption spectroscopy (XAS) provided further evidence for assembly of the desired complex on the surface. In Figure 4.17, the edge and post-edge data are shown for a powder of isolated $[Cp^*Ir(bipy)Cl]Cl$ (black line), while the data for analogous immobilized $[Cp^*Ir(vbpy)Cl]Cl$ are shown in blue circles. The iridium in both cases was characterized by a peak-top energy of 11 215 eV. These edge-energy values were consistent with iridium in the $+3$ oxidation state. In addition, the post-edge features were similar for $[Cp^*Ir(bipy)Cl]Cl$ and the silicon-immobilized analogue, suggesting a similar environment in the first coordination shell for the iridium centers in both cases. These spectra were collected with J. Blakemore at the Stanford Synchrotron Radiation Lightsource (SSRL) at the SLAC National Accelerator Laboratory in Menlo Park, CA with the generous assistance of S. Gul, R. Chatterjee, V. Yachandra, and J. Yano. Experimental details of the XAS experiments can be found in Appendix B.5.

4.3.6 Metallation of Mixed Methyl/vbpy Surfaces with $Ru(acac)_2(coe)_2$

The reductive instability displayed by the surface-attached $[Cp^*Rh(vbpy)Cl]Cl$ led us to study a less reductive couple on the surface. $[Ru(acac)_2(bipy)]PF_6$ (acac is acetylacetonate) was prepared and displayed a well-behaved, one-electron Ru(II)/Ru(III) couple at -0.5 V vs. Fc/Fc$^+$, where the mixed methyl/vbpy surface should be stable (see Figure 4.19).[74] Addition of 2,2′-bipyridyl to Ru(acac)2(coe)2 (coe is cis-cyclooctene) gives $Ru(acac)_2(bipy)$ at r.t.[75]
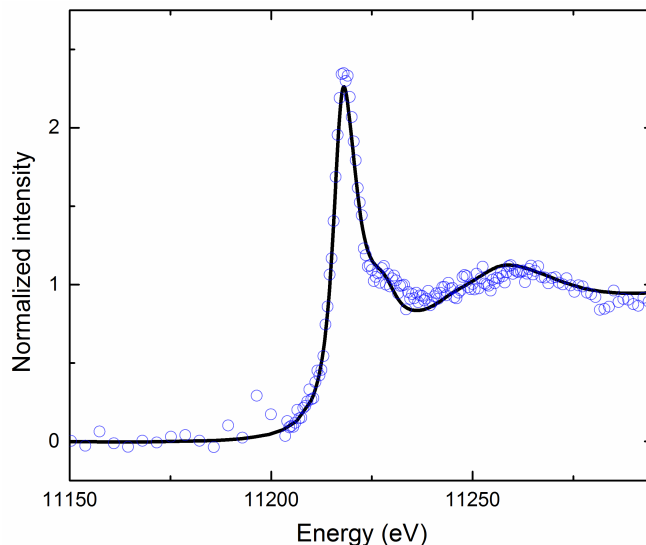
FIGURE 4.17: Comparison of Ir L_{III}-edge XAS results for the mixed methyl/vbpy surface exposed to $[Cp^*IrCl_2]_2$ (blue circles) and the $[Cp^*Ir(bipy)Cl]Cl$ model complex (black line). Reproduced by permission of The Royal Society of Chemistry (RSC).[64]

We wanted to form the oxidized version of this complex on the mixed methyl/vbpy surface. However, the Ru(III) species, $[Ru(acac)_2(bipy)]PF_6$, could only be prepared at elevated temperature in solution.[74,76] To prepare a Ru-metallated surface, a mixed methyl/bipyridyl-functionalized Si(111) sample was immersed in a ~6 mM solution of $Ru(acac)_2(coe)_2$ in THF under Ar gas and heated to 100 °C overnight in a sealed pressure vessel. This reaction was first attempted at r.t., but it did not proceed. Following the reaction, the pressure vessel was opened to room air after cooling, presumably resulting in oxidation of Ru(II) to Ru(III), and the samples were then sonicated for 10 min each in CH_2Cl_2, CH_3OH, and water prior to surface characterization.

High-resolution XPS of the surface after metallation with $Ru(acac)_2(coe)_2$ is shown in Figure 4.18. The Si 2p region showed a small oxide peak at 103 eV, corresponding to 0.6 ± 0.1 monolayers. The wafer was subjected to rather harsh conditions (refluxing overnight in THF), and so an increase in surface oxidation was not unexpected. The Ru 3p region showed a doublet of peaks at 463.2 and 485.4 eV, each fit to a single component. These peak positions corresponded to Ru(III), and agreed well with the Ru 3d peaks observed at 463.3 and 485.6 eV for $[Ru(acac)_2(bipy)]PF_6$. These peaks had an area ratio of 2:1, as expected for a 3p doublet in XPS. The Ru 3d peak corresponded to 0.21 ± 0.05 monolayers of Ru on the surface.

The N 1s region had a dominant signal at 400.5 eV and a smaller peak at 399.6 eV,
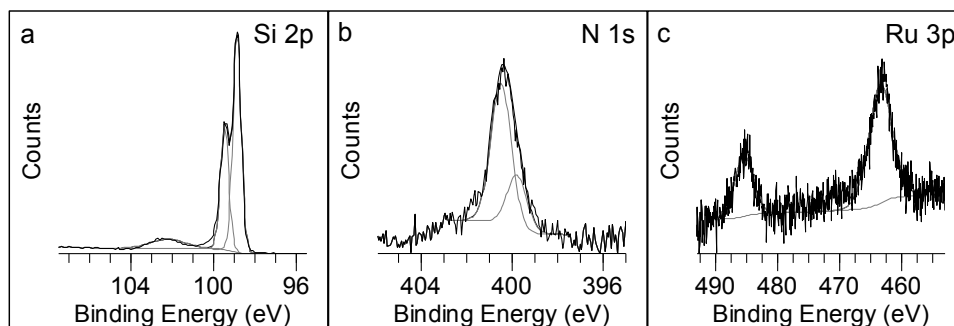
FIGURE 4.18: High-resolution XPS of the mixed methyl/vbpy surface exposed to $Ru(acac)_2(coe)_2$ by refluxing at $100\,°C$ overnight in THF. a) The Si 2p region had a small oxide peak at $103\,eV$. b) The N 1s region had a dominant peak at $400.5\,eV$ and a shoulder at $399.6\,eV$, corresponding to metallated and free-base bipy respectively. c) The Ru 3p region had a doublet of peaks at 363.2 and $485.4\,eV$, each fit to a single component, indicating that there was one Ru species on the surface.

corresponding to 0.26 ± 0.05 and 0.06 ± 0.02 monolayers, respectively. The model complex $[Ru(acac)_2(bipy)]PF_6$ had a N 1s signal at $400.5\,eV$, and so we assigned the peak at $400.5\,eV$ to metallated bipy and the peak at $399.6\,eV$ to free-base bipy. These coverages agreed well, indicating that the Ru complex was intact on the surface. The counter-ion that should be associated with this complex in the Ru(III) oxidation state is, however, unknown. While no explicit counter ions were added to the reaction mixture, the total amount of the Ru complex on the surface is quite low, and so trace anionic species in the reaction solution or rinsing solvents could have become associated with the complex to balance the charges.

4.3.7 Electrochemistry of Surface-Bound $[Ru(acac)_2(bipy)]^+$

The ruthenium complex $[Ru(acac)_2(bipy)]PF_6$ underwent a single one-electron transfer, cycling between the $+3$ and $+2$ oxidation states, at around $-0.48\,V$ vs. Fc/Fc$^+$ (Figure 4.19, upper panel) in a well-behaved, chemically reversible redox process. Similarly to $[Cp^*Rh(bipy)Cl]Cl$, this complex showed the expected square-root dependence of peak current on scan rate (see Figure 4.9). Redox cycling of surface-attached $[Ru(acac)_2(vbpy)]^+$ was performed using mixed methyl/vbpy surfaces metallated with $Ru(acac)_2(coe)_2$ (Figure 4.19, lower panel). We observed a redox couple on this surface with the half-wave potential centered at $-0.49\,V$ vs. Fc/Fc+, and with a peak-to-peak separation of $171\,mV$. Details of the electrochemical setup can be found in Appendix B.4. The peak-to-peak separation of model complex $[Ru(acac)_2(bpy)]PF_6$ in solution was $71\,mV$, suggesting slower electron
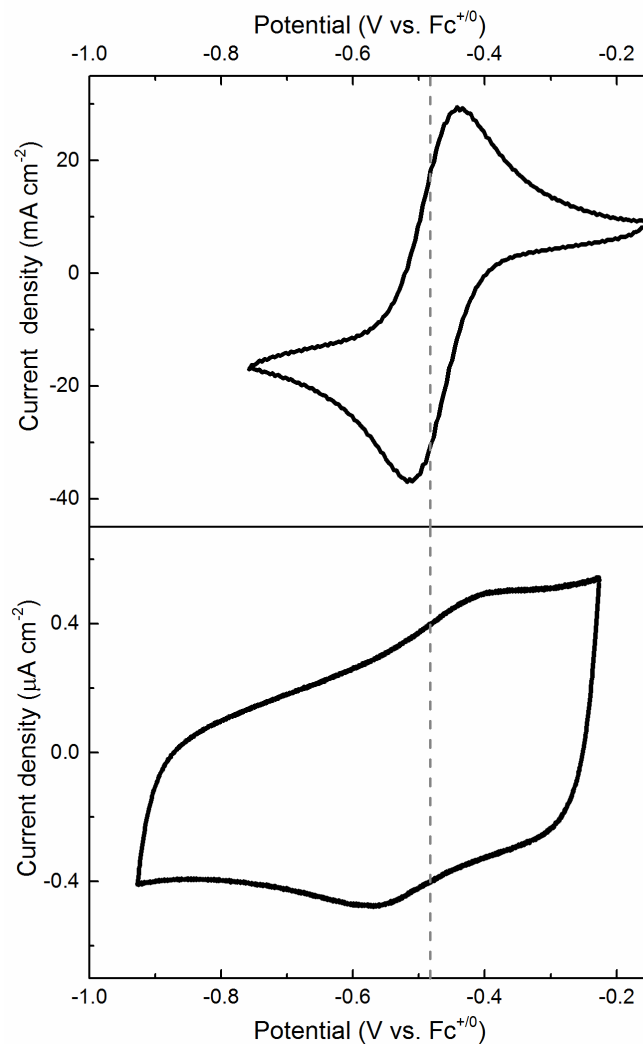
FIGURE 4.19: Comparison of the electrochemistry of $[Ru(acac)_2(bipy)]PF_6$ (upper panel) and the mixed methyl/vbpy surface metallated with $Ru(acac)_2(coe)_2$ (lower panel). These CVs were collected in $0.1\,M$ $(NBu_4)PF_6)$ in CH_3CN, with a Ag/Ag^+ pseudoreference electrode and a basal-plane graphite counter electrode. The electrochemistry of the solution-phase $[Ru(acac)_2(bipy)]PF_6$ was collected on a basal-plane graphite working electrode. The scan rate in both cases was $100\,mV\,s^{-1}$. Reproduced by permission of The Royal Society of Chemistry (RSC).[64]
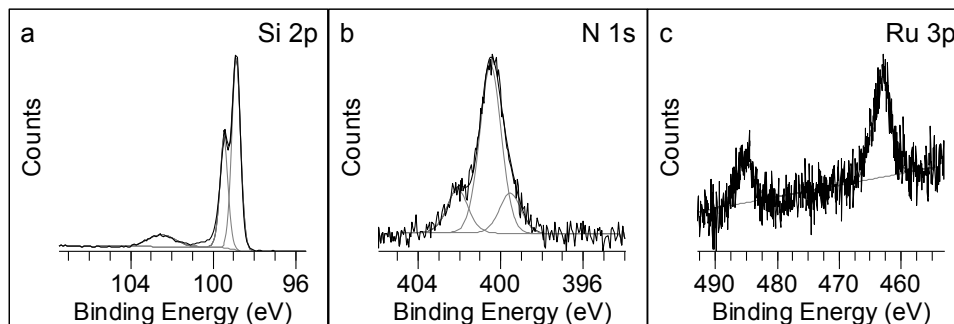
FIGURE 4.20: High-resolution XPS of the mixed methyl/vbpy surface exposed to $Ru(acac)_2(coe)_2$ following electrochemical cycling. a) The Si 2p region had an oxide peak at 103 eV. b) The N 1s region had a dominant peak at 400.5 eV and a shoulder at 399.6 eV, corresponding to metallated and free-base bipy, respectively. There was also a small peak at 402.2 eV that remains unassigned at this time. c) The Ru 3p region had a doublet of peaks at 363.2 and 485.4 eV, each fit to a single component, indicating that there was one Ru species on the surface. The amount of Ru on the surface decreased following electrochemical cycling, as is consistent with the loss of some electroactive material from the surface.

transfer to the immobilized complex than for the solution complex. While this redox couple persisted beyond ten complete cycles of voltammetry from -0.2 to -0.9 V, the redox couple was not sufficiently long-lived to allow more extensive characterization. Integration of the current-time data gave 0.002 ± 0.001 of a monolayer of electroactive ruthenium on the surface, similar to the case of the rhodium complex discussed above.

The XP spectra of the ruthenium-treated electrode collected following the electrochemical cycling indicated that some of the attached complex remained on the surface. This data is shown in Figure 4.20. Before electrochemical cycling, the surface coverage of ruthenium was 0.21 ± 0.05 monolayers, in good agreement with the estimated 0.26 ± 0.05 monolayers of metal-bound bipy based on the N 1s signal; the coverage of silicon oxide was 0.6 ± 0.1 monolayers, and the coverage by free-base bipy was estimated as 0.06 ± 0.02 monolayers. Following electrochemistry, the apparent coverage of silicon oxide increased slightly to 0.75 ± 0.10, while the free-base bipy coverage was essentially invariant at 0.05 ± 0.02. The metal-bound bipy coverage dropped slightly to 0.22 ± 0.05 monolayers, and the ruthenium coverage dropped to 0.11 ± 0.05. The decreases in metal-bound bipy and Ru coverages were thus consistent with the eventual loss of the electrochemical signal. However, the lack of electroactivity of the remaining material suggested nonideal interfacial electron transfer.

4.3.8 Discussion

Here, we investigated the attachment of bipyridine, a well-known ligand, to silicon, and subsequently assembled metal complexes on the surface. We demonstrated that the ligand was metallated readily via routes analogous to known solution chemistry. XPS was especially useful in characterizing the assembled complexes, since comparisons could be made between well-characterized molecular species and the immobilized material. From this work, we see that only ligation reactions that occur readily in solution can be expected to occur on the surface of an electrode with an immobilized ligand. This reduced reactivity was in part due to the small amount of ligand available on the surface; a metallation "yield" of less than 100 % will simply yield an electrode with very low activity. Furthermore, steric restrictions not present in solution could be present on the surface; for example if multiple bipyridine ligands were closely spaced or multilayers of bipyridine formed on the surface, incomplete metallation could result.

The challenge illustrated by this work was that assembled metal complexes are often unstable under electrochemical cycling conditions. Because our immobilized metal complexes were rapidly lost from the surface upon electrochemical reduction, limited studies of their catalytic activities were possible. However, in our bipyridine system, we observed a trend that stability improved when redox cycling could be performed at less reductive potentials. This trend correlates well with the stability of the mixed methyl/vinylferrocenyl surfaces investigated herein, which have no internal redox events below the Fe(III/II) couple and are stable even to $-2\,V$ vs. Fc/Fc^{+}.

A plausible mechanism for the loss of the assembled bipyridine-metal complexes from the surface involves the ligand-centered reduction of bipyridine. Reduction of the ligand results in increased reactivity of the vinyl moiety; this increased reactivity is exploited in the electropolymerization of vinyl bipyridine reagents.[77,78] In our system, the close connection between the silicon surface and the bipyridyl group could result in instability. The reduced Rh(I) form of $[Cp^{*}Rh(bpy)Cl]Cl$ is known to have bipyridine ligand-centered anion character, which would promote reactivity at the vinyl site. Consistent with this proposal, less instability was found when moving to the purely metal-centered Ru(II/III) couple in $[Ru(acac)_2(bipy)]PF_6$, because little bipyridine-centered reduction was involved. Reductive cycling of vinylferrocenyl-modified electrodes over the same potentials did not result in loss
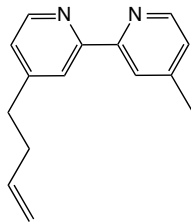
FIGURE 4.21: 4-(3-Butenyl),4′-methyl-2,2′-bipyridine.

of the redox couple from the surface, likely because the Cp ligand was not involved in any reduction events at reductive potentials. Future studies on surface immobilization could be benefitted by selection of partially insulating linkers between the immobilized ligand and the surface itself. Balancing the linker length and electron-transfer rate, however, may prove challenging.

4.4   Butenylbipyridyl-Modified Surfaces

The reductive instability of the mixed methyl/vbpy surfaces, as well as the apparent lack of electroactive metal centers on these surfaces, led us to explore other bipy-based ligands that could be attached to the surface. The hope was that by adding an ethylene bridge between the vinyl group and the bipy moiety, we would distance the bipy-based reduction from any connection with the vinyl group used for attachment, leading to greater reductive stability of the surface. We used butenylbipyridyl (butbipy), synthesized by M. Radlauer and graciously provided for our experiments, to test this hypothesis. This compound is shown in Figure 4.21.

H− and Cl−Si(111) were modified with butbipy by reaction in CH_2Cl_2 with trace BP under UV illumination for 1 h. Experimental details can be found in Appendix A.14. High-resolution XPS of these surfaces is shown in Figure 4.22. The Si 2p regions of these two surfaces were similar, with a small surface oxide peak at 103 eV. These peaks corresponded to 1.0 ± 0.1 and 1.4 ± 0.1 monolayers of surface oxide for the H- and Cl-terminated surfaces, respectively. There was more oxide on the Cl-terminated surface, suggesting that the reaction was less efficient on this surface, allowing more oxide to form.

The N 1s region showed strong signals on both the H- and Cl-terminal surfaces, suggesting that the reaction was successful on these surfaces. There were 0.34 ± 0.05 monolayers of bipy on the H-terminated surface and 0.17 ± 0.05 monolayers of bipy on the Cl-terminated surface,
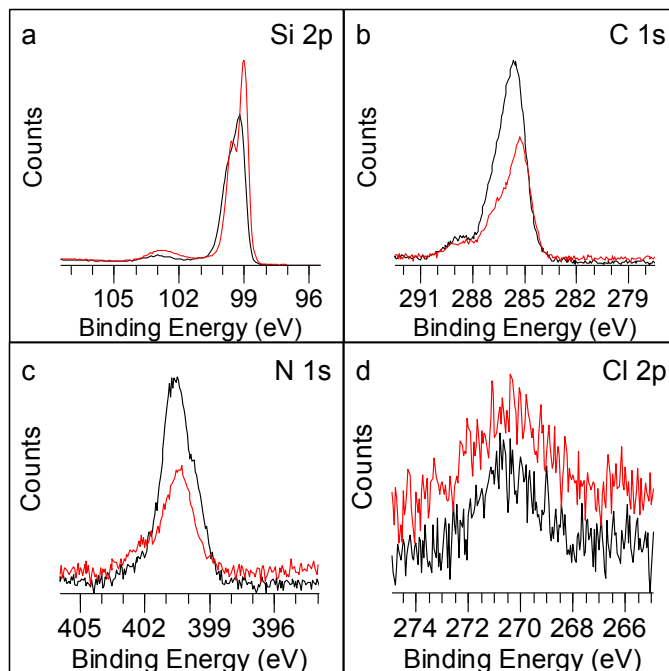
FIGURE 4.22: High-resolution XPS of H-terminated (black) and Cl-terminated (red) silicon modified with butbipy. a) The Si 2p region of both surfaces showed a surface oxide peak at 103 eV. b) The C 1s region of both surfaces had a large, broad peak around 286 eV. The H-terminated surface had a larger peak, suggesting that there was more butbipy attached to this surface. Neither surface had a Si-C peak at 284 eV. c) The N 1s region of both surfaces had a signal around 400 eV from the surface-attached butbipy group. There was a larger peak on the H-terminated surface, suggesting that there was more butbipy attached to this surface. d) The Cl 2s region showed a signal on both the H- and Cl-terminated surfaces.

suggesting that the reaction was less efficient on the Cl-terminated surfaces. The C 1s region showed multicomponent peaks around 285 eV on both surfaces, with about twice as much carbon signal on the H-terminated surface compared to the Cl-terminated surface. Both surfaces did not have a peak at 284 eV, which is usually associated with the Si-C bond.[13] However, the relatively low surface oxide and the large C 1s and N 1s signals indicate that the reaction did proceed on these surfaces. This peak at 284 eV was not observed on surfaces modified by vFc or vbpy either.

Interestingly, both the H- and Cl-terminated surfaces showed a signal in the Cl 2s region, despite the fact that the H-terminated surface was never chlorinated and so any Cl on the surface must be contamination. This contamination could be from the CH_2Cl_2 used as the reaction solvent, from cleaning solvents, or from the Cl-terminated surface through a radical exchange process. The H- and Cl-terminated surfaces were functionalized together in the same reaction vessel, making radical exchange a possibility, particularly if there was a long-lived solution radical species involved in the reaction mechanism.

4.4.1   Mixed Methyl/butbipy Surfaces

Mixed methyl/butbipy surfaces were also formed by reaction of Cl-terminated silicon with methyl Grignard, followed by reaction with butbipy in CH_2Cl_2 with trace BP under UV illumination for 1 h. High-resolution XPS of the mixed methyl/butbipy surface is shown in Figure 4.23. The mixed surface had a weak N 1s signal, suggesting that the reaction did not proceed efficiently on this surface. This surface also displayed significant surface oxidation, shown by the Si 2p region, which had a surface oxide peak at 103 eV, corresponding to 1.0 ± 0.1 monolayers. The N 1s region had a signal at 400.2 eV, corresponding to 0.09 ± 0.05 monolayers of bipy on the surface. The C 1s region had a peak at 285 eV from the bipy groups, but very little Si-C signal at 284 eV from the methyl groups. This is consistent with the surface oxidation, and suggests that coverage by methyl groups was lower on this surface than expected. There was no Cl 2s signal at 270 eV from residual chloride groups on the surface, however, and so it was unclear why the methylation was less efficient than usual.

4.4.2   Metallation of Butbipy-Modified Si Surfaces

The butbipy-modified surfaces were metallated with $[Cp^*RhCl_2]_2$, with the results shown in Figure 4.23 and 4.24. The Rh 3d region showed the expected peaks at 310.5 and 315.2 eV
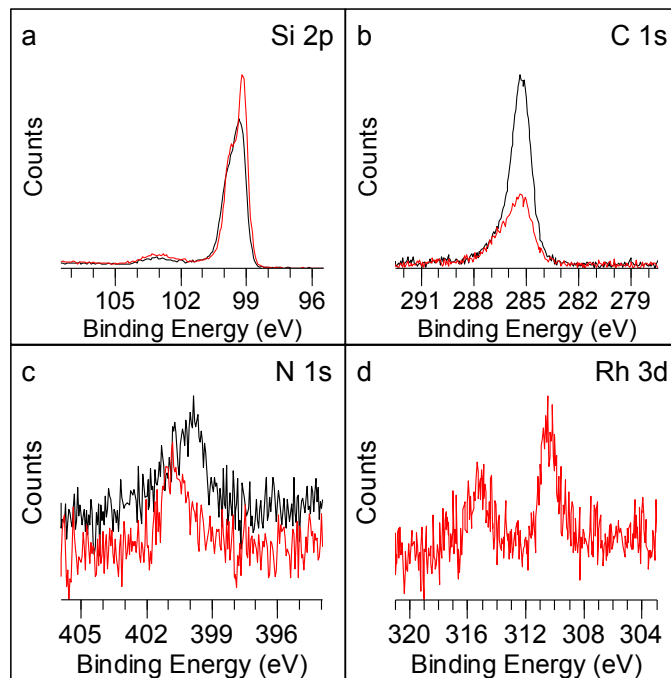
FIGURE 4.23: High-resolution XPS of a mixed methyl/butbipy suface (black) and a mixed methyl/butbipy surface metallated with $[Cp^*RhCl_2]_2$ (red). a) The Si 2p region of both surfaces showed a surface oxide peak at 103 eV. b) The C 1s region of both surfaces had a large, broad peak around 286 eV. The surface showed a significantly decreased carbon signal on the metallated surface. c) The N 1s region of the mixed methyl/butbipy surface had a signal around 400 eV from the surface-attached butbipy group. The peak shifted to 400.7 eV upon metallation by the Rh complex. d) The Rh 3d region of the metallated surface showed a doublet of peaks at 310.4 and 315.4 eV corresponding to Rh(III).
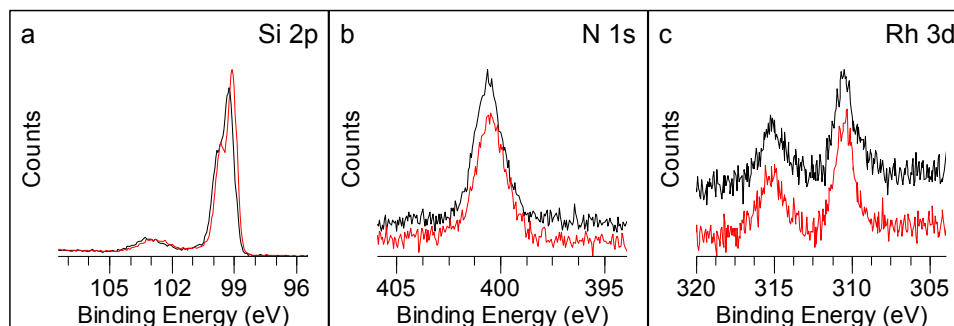
FIGURE 4.24: High-resolution XPS of Rh-metallated butbipy surfaces formed on H-terminated (black) and Cl-terminated (red) silicon. a) The Si 2p region showed some surface oxidation, with a silicon oxide peak on both surfaces at 103 eV. b) The N 1s region was similar on both surfaces, with a dominant peak around 400.6 eV and a shoulder at 399.6 eV, corresponding to metallated and free-base bipy, respectively. c) The Rh 3d region showed a doublet of peaks at 310.5 and 315.2 eV on both surfaces, corresponding to Rh(III).

for Rh(III), corresponding to 0.08 ± 0.02, 0.06 ± 0.02, and 0.04 ± 0.02 monolayers of Rh on the H-terminated, Cl-terminated, and mixed surfaces, respectively. The N 1s region of these surfaces had a dominant peak at 400.7 eV and a smaller shoulder at 399.7 eV, corresponding to metallated and free-base bipy, respectively. Surface coverage on the H-terminated surface was 0.32 ± 0.05 and 0.06 ± 0.02 monolayers of Ru-bound and free bipy, respectively. On the Cl-terminated surface, the coverage was 0.33 ± 0.05 and 0.30 ± 0.02 monolayers of Ru-bound and free bipy, respectively. The mixed surface had 0.06 ± 0.02 monolayers of Ru-bound bipy, and had no peak for free bipy. All the surfaces metallated with $[Cp^*RhCl_2]_2$ had a silicon oxide peak at 103 eV, but it remained unchanged before and after metallation. The C 1s region of the metallated mixed methyl/butbipy surface showed a significant decrease in intensity following metallation, which was unexpected. This suggested that the mixed methyl/butbipy surface, as prepared, had a significant amount of adventitious carbon on the surface which was removed during the metallation procedure.

Electrochemistry of the Rh-complex on these surfaces was performed, but no redox event was observed prior to the bipy-based reduction at -1.3 V vs. Fc/Fc$^+$. Some typical CVs of various surfaces modified with butbipy are shown in Figure 4.25. The mixed methyl/butbipy surface as prepared and after metallation with $[Cp^*RhCl_2]_2$ look very similar, with the same bipy-based reduction event around $-1/3$ V vs. Fc/Fc$^+$. There was no indication of any Rh-centered redox activity on the metallated mixed methy/butbipy surface, which should have appeared at -1.0 V vs. Fc/Fc$^+$. The metallated mixed methyl/butbipy surface
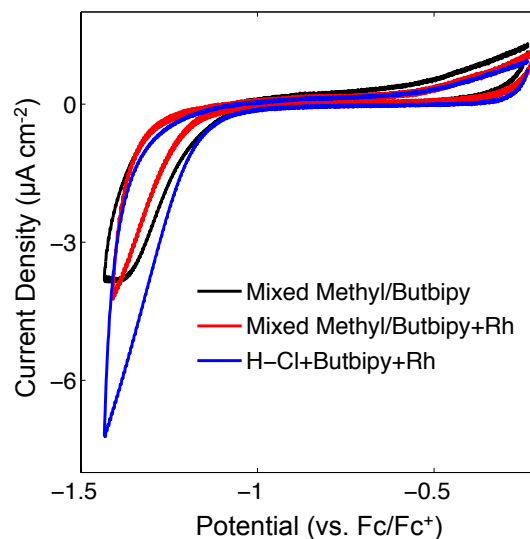
FIGURE 4.25: Electrochemistry on Rh-metallated butbipy surfaces. In black, the mixed methyl/butbipy surface as prepared. In red, the mixed methyl/butbipy surface after metallation with $[Cp^*RhCl_2]_2$. In blue, the H-terminated surface modified with butbipy and metallated with $[Cp^*RhCl_2]_2$. All CVs were collected at a scan rate of $100\,mV\,s^{-1}$ in 0.1 M $(NBu_4)PF_6$ in CH_3CN, using a basal-plane graphite counter electrode and a Ag/Ag^+ pseudoreference electrode. Fc/Fc^+ was added to the cell after each silicon surface was tested as an internal standard for the potential of the reference electrode.

had a slightly lower background current and more negative bipy-based reduction than the unmetallated mixed methyl/bipy surface. The H-terminated surface modified with butbipy and then metallated with $[Cp^*RhCl_2]_2$ also had no Rh-based redox event visible at $-1.0\,V$ vs. Fc/Fc^+. The bipy-based reduction at $-1.3\,V$ vs. Fc/Fc^+ is larger on this surface than the other two, which is consistent with the relative coverage of bipy quantified by XPS on this surface compared with the mixed methyl/bipy surface (0.38 ± 0.05 vs. 0.06 ± 0.02 monolayers of bipy). The absence of any Rh-based redox event on these surfaces suggests that either electron transfer to the surface-attached complex was impeded in some way, or the complex as formed on these surfaces was not electroactive. The spectroscopy of the Rh complex formed on these surfaces appeared identical to that on the vbpy-modified surfaces, however, and the bipy-based reduction did not appear affected. Thus we are unable to explain the lack of electrochemical signal on these surfaces at this time.

4.5 Conclusion

We have demonstrated a route to forming mixed methyl/bipyridyl monolayers on silicon(111) surfaces. The mixed monolayers are capable of binding metal ions via chelation of surface-immobilized bipyridine to the metal centers. We assembled analogues of [Cp*Rh(bpy)Cl]Cl, [Cp*Ir(bpy)Cl]Cl, and Ru(acac)$_2$(bpy) on silicon surfaces. Extensive XPS and XAS studies indicated that the metal complexes were intact on the surface. In the case of the Cp*Rh and Ru(acac)$_2$ systems, electrochemistry confirmed assembly of the molecular complexes on the surface, but stability of the assembled surfaces was sufficiently limited to preclude further study of their catalytic activity. This work illustrated that redox-active compounds could be assembled on silicon by attachment of the desired ligand(s) to the surface followed by metallation. However, more stable ligand architectures must be developed to enable catalytic monolayers assembled in this fashion to be used in photoelectrocatalytic devices. Portions of the preceding chapter have been adapted by permission of The Royal Society of Chemistry (RSC).[64]

Chapter 5

Discussion of the 'Chlorosilylation' Reaction Mechanism

5.1 Mechanism of the Hydrosilylation Reaction

Si(111) surfaces have been functionalized by 1-alkenes via hydrosilylation reactions for the past 20 years.[16] This reaction is thought to proceed through a radical mechanism, based on early work by Linford et al. that formed close-packed alkyl monolayers on Si(111) surfaces through the thermal decomposition of acyl peroxides.[15] A similar reaction, using acyl peroxide as a radical initiator, was used to form highly compact alkyl monolayers on H-terminated Si(111) surfaces with 1-alkenes.[16] The reaction mechanism proposed therein was that the acyl peroxide forms a radical in solution, which then abstracts a H-atom from the Si(111) surface, leaving a dangling bond. An olefin then adds to this dangling bond, resulting in a surface-bonded, secondary carbon radical. This radical can then abstract a H-atom from an olefin in solution or from a neighboring H−Si site on the surface. This generates a new radical on the surface or in solution that can propagate the reaction, ultimately resulting in functionalization of the silicon surface with an alkyl monolayer.

Some evidence for this surface chain reaction mechanism was found by Cicero et al. during STM studies of styrene attachment to H−Si(111) surfaces under ultra high vacuum (UHV) conditions.[79] In these studies, dangling bonds were created on a H-terminated Si(111) surface using an STM tip under UHV. Styrene was then introduced into the UHV chamber, where it reacted with the dangling bonds on the surface to form adsorbate islands of about 20 Å in diameter. These islands were centered on the sites of the dangling bonds and were self-limited in size, indicating that the reaction terminated when there were no adjacent
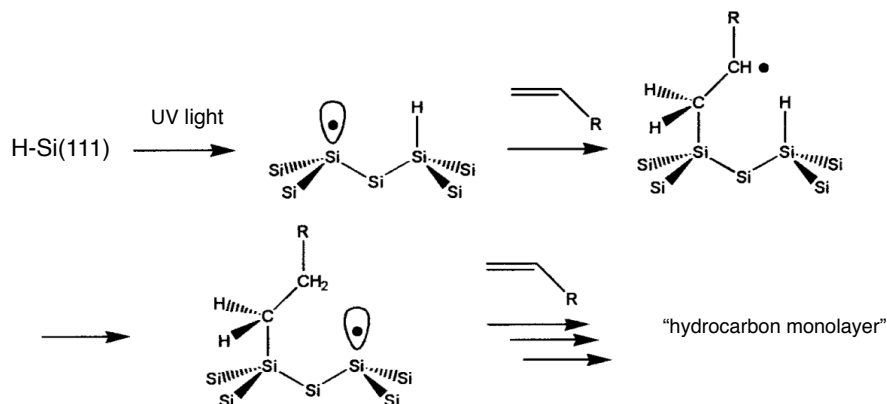
FIGURE 5.1: Proposed chain reaction mechanism for the addition of olefin bonds to H-terminated Si(111) surfaces. Silicon surface dangling bonds are formed by UV illumination. An olefin can then react with the dangling bond to form a secondary carbon radical, which can abstract another H-atom from the surface to create a new dangling bond and propagate the radical reaction. Adapted from Cicero et al.[79]

H-atoms on the surface to abstract. The presence of styrene islands only at the sites of dangling bonds indicated that the chain reaction was initiated by the radical on the surface.

Further investigations using light rather than a solution-based radical initiator to functionalize H-terminated silicon surfaces with terminal alkenes and alkynes showed that only wavelengths of less than 350 nm would initiate hydrosilylation on the surface.[18] They suggested that illumination of silicon with UV light formed dangling bonds at the surface. These surface-bound radicals could then add to unsaturated compounds to form covalently bound adsorbate radicals. These could then abstract the H-atom from a neighboring H−Si site to propagate the reaction. This proposed reaction scheme is shown in Figure 5.1.

Other terminal olefins, such as vinylferrocene, have been used to functionalize H-terminated silicon via thermal and UV-light initiated reactions.[47,48,80] These groups were predicted to react with the H-terminated silicon surface similarly to terminal alkenes, resulting in a saturated hydrocarbon linker to the silicon surface.[80] While alkenes formed self-limited monolayers on silicon surfaces via the hydrosilylation reaction, in keeping with the reaction scheme described in Figure 5.1,[18] vinylferrocene appeared able to form multilayers on the surface. This was based on the surface coverage of 58 % of a monolayer, where one monolayer is defined as one functional group per Si(111) atop site, measured on a surface formed via thermal immobilization of vinylferrocene on H−Si(111).[47] Previous calculations using the effective ferrocene diameter $(0.66\,\text{nm})$[51,52] and the silicon atop site spacing on a Si(111)

surface had shown that a closely-packed monolayer of ferrocene would occupy 34 % of the atop sites, and so a surface coverage of >34 % of a monolayer indicated multilayer formation of vinylferrocene.[47] Similar results were seen in this work where H-terminated surfaces modified by vinylferrocene via thermal and UV-light initiated reactions had surface coverages of up to 1 monolayer (see Figure 3.2). This suggested that the hydrosilylation reaction mechanism was somewhat more complicated for vinyl-appended species like vinylferrocene, possibly because of polymerization by the vinyl group.

5.1.1   The "Chlorosilylation" Reaction Mechanism

Our development of a new method for mixed monolayer formation hinged on our ability to perform a hydrosilylation-like reaction wherein a vinyl-appended functional group was reacted with a Cl-terminated silicon surface. This reaction is hereafter referred to as "chlorosilylation." We hypothesized that this reaction occurred through a similar radical mechanism to the hydrosilylation reaction based on the similarity of the resultant structures for H−Si and Cl−Si surfaces reacted thermally with vFc. This reaction appeared successful, using both thermal and UV-light initiated approaches, much like the hydrosilylation reaction.[14,17,18] The addition of a radical initiator, benzoyl peroxide, to the reaction solution dramatically increased the reaction rate, which supported our hypothesis of a radical mechanism for this reaction.

A similar radical chain reaction mechanism on the Cl−Si surface would require the abstraction of a neighboring Cl-atom, rather than a H-atom, by the surface-bonded secondary carbon radical. This would result in the addition of the chlorine to the β-carbon of the newly attached alkyl chain. There was frequently a chlorine signal by XPS on surfaces modified by the chlorosilylation reaction, but the Cl 2s peak was too broad to distinguish between residual Cl−Si and newly-formed Cl−C (see Figure 3.4). In addition, surfaces that were exposed to methyl Grignard following the chlorosilylation reaction did not generally have a Cl 2s XPS signal, presumably because any remaining Cl−Si sites would have reacted with the methyl Grignard. However, it is possible that a chlorine on the β-carbon of the alkyl group would also be reactive with methyl Grignard. It is also possible that having a chlorine group on the linker facilitated β-hydride elimination, resulting in a double bond and loss of a H−Cl group. We saw no evidence for a double bond on the surface, however. Thus we were unable to definitively characterize the linker between the silicon surface and the ferrocene or

bipyridine moiety, making it difficult to determine whether the chain reaction mechanism was the mechanism for the chlorosilylation reaction occurring on our surfaces.

The decreased efficiency of the UV-light induced reaction on the Cl−Si vs. the H−Si surfaces also presented a problem if these reactions were proceeding through similar mechanisms. The Si−H and Si−Cl bond energies are 70.4 and 85.7 kcal mol^{-1}, respectively, for non-hindered silanes.[81] These energies correspond to light of 406 and 333 nm, respectively, which are both much lower in energy than the 254 nm UV-light source used in the reaction. However, previous work using UV-light to initiate hydrosilylation on H-terminated silicon determined that the reaction did not proceed efficiently if light with wavelengths of ≥350 nm was used.[18] This implies that the energy required to form a dangling bond on the Si−H surface is actually higher than the non-hindered Si−H bond energy by at least 11.5 kcal mol^{-1}. There is a 15 kcal mol^{-1} difference in energy between the H−Si and Cl−Si bond energies, which corresponds to a difference of ∼70 nm. This energy difference could explain why illumination with 254 nm light initiates the hydrosilylation reaction, but is much less efficient for the chlorosilylation reaction. Using a higher-energy, shorter-wavelength UV-light source could increase the reactivity of the Cl−Si surface. Addition of the radical initiator, benzoyl peroxide, to the reaction solution alleviated this problem, resulting in efficient reaction of the Cl−Si surface with vinyl-appended reactants. However, it is unclear whether the radical initiator is increasing the reaction rate by creating dangling bonds on the surface, or by creating reactive vinyl radicals in solution.

5.1.2   Addition of 1-Alkenes to Cl−Si(111) Surfaces

Polymerization of the vinyl-appended reagents used to modify our Cl−Si surfaces often resulted in multilayer formation (see Table 4.1). Limiting the reaction time allowed us to control the surface coverage of the vinyl-appended moieties on the surface, but the surface characterization techniques available could not preclude the presence of some polymerized product on our surfaces. While the mixed methyl/bipyridyl surfaces formed using the chlorosilylation reaction displayed excellent photoelectrochemical properties, charge transfer to the attached species often did not proceed readily, and polymerization of the bipyridyl groups could be one explanation for that. Hydrosilylation of 1-alkenes does not result in polymerized product on the surface because there is no mechanism for the polymerization of these species in solution. We therefore decided to extend the chlorosilylation reaction to

include 1-alkenes and thus prevent polymerization of the reactant on the surface.

Figure 5.2 shows the high-resolution XPS of H−Si and Cl−Si surfaces reacted with 1-hexene under UV illumination for 1–2 h. Experimental details of this reaction can be found in Appendix A.15. The Si 2p region of both surfaces have the typical doublet around 99 and 100 eV, with an area ratio of 2:1. The Cl−Si surface had a small Si−O component at 103 eV that was absent on the H−Si surface. This suggested that the surface coverage of hexene was higher on the H−Si surface than on the Cl−Si surface. The C 1s region of the H−Si surface had a large peak at 285 eV, with smaller shoulders at 284, 286, and 287 eV. The signal at 284 eV was from the surface-bound carbon of the hexene group and corresponded to 0.28 ± 0.05 monolayers.[13,29] The total carbon coverage on this surface corresponded to 0.8 ± 0.1 monolayers of hexene, which indicated that there is some non-specific adsorption of the hexene onto the surface as well, or a large adventitious carbon contribution. The C 1s region of the Cl−Si surface had a peak at 285 eV, with smaller shoulders at 286 and 287 eV. There was no C−Si component at 284 eV on this surface, which indicated that there was little to no covalent attachment of the hexene under these reaction conditions. The total C 1s signal on this surface corresponded to 0.40 ± 0.05 monolayers of hexene, which could be from non-specific adsorption or from adventitious carbon. Both surfaces had a similar amount of non-covalently bound hexene, which suggested a similar mechanism for nonspecific adsorption of adventitious carbon. The Cl 2s region of the Cl−Si surface had a large peak at 270 eV, presumably from residual Cl−Si remaining on the surface, corresponding to 0.45 ± 0.05 monolayers. It was also possible that this Cl signal was from Cl-atoms that were transferred to the hexene chain during the radical chain reaction mechanism. However, the peak was too broad to distinguish multiple components or to detect any significant binding energy shift in the signal. The H−Si surface had a small chlorine signal at 271 eV, which was likely from residual solvent because this surface was not chlorinated.

These results indicated that 1-hexene reacted efficiently with the H−Si surface through a hydrosilylation reaction under UV illumination. The Cl−Si surface did not appear to react efficiently with 1-hexene under the same reaction conditions based on the absence of a C−Si peak in the C 1s region, which suggested that the chlorosilylation reaction did not proceed. However, the large adventitious contributions to the C 1s signal on both surfaces made an accurate assessment of the surface coverage of hexene complicated.
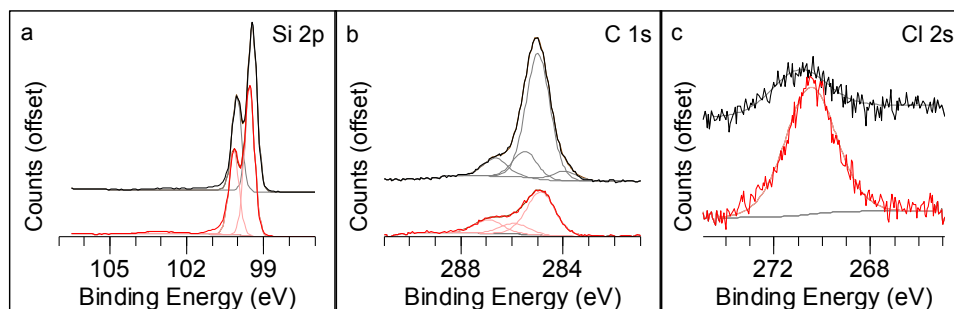
FIGURE 5.2: High-resolution XPS of 1-hexene-modified H−Si(111) (black) and Cl−Si(111) (red) surfaces. a) The Si 2p region was similar for these surfaces. The Cl−Si surface had a small Si−O contribution at 103 eV, while the H−Si surface did not. b) The C 1s region of the H−Si surface had a large carbon signal at 285 eV, with smaller shoulders at 284, 286, and 287 eV. The component at 284 eV was from the surface-bound carbon, and corresponded to 0.28 ± 0.05 monolayers. The Cl−Si surface had a much smaller C 1s signal, and there was no peak at 284 eV, which indicated that the reaction did not proceed efficiently on this surface. c) The Cl 2s region of the Cl−Si surface had a large peak at 270 eV, corresponding to 0.45 ± 0.05 monolayers of chlorine remaining on the surface. This is consistent with the lack of C 1s signal at 284 eV, and indicates that this surface was not reactive with the hexene under these conditions. The H−Si surface had a small Cl 2s signal at 271 eV corresponding to 0.15 ± 0.05 monolayers of chlorine.

5.1.3 Addition of Bromohexene to H− and Cl−Si(111)

To further investigate the reactivity of alkenes with the Cl−Si surface, we used 6-bromo-1-hexene to functionalize H− and Cl−Si surfaces. Experimental details for this reaction can be found in Appendix A.15. Bromohexene was used because it contains a bromine atom, which can serve as a spectroscopic tag in XPS to help us calculate surface coverage of the bromohexene, and it should have the same reactivity with H− and Cl−Si surfaces as 1-hexene. Figure 5.3 shows the high-resolution XPS of H− and Cl−Si(111) surfaces reacted with 6-bromohexene under UV illumination for 1–2 h. These surfaces were annealed in the UHV chamber of the XPS at 250 °C for 15 min prior to data collection to remove any adventitious carbon from the surface.

The Si 2p region of both surfaces had the typical doublet around 99 and 100 eV, with an area ratio of 2:1. The Cl−Si surface had a small Si−O component at 103 eV, while this peak was absent on the H−Si surface. The C 1s region of the H−Si surface had a main peak at 285 eV with smaller shoulders at 284 and 286.5 eV. The peak at 284 eV, from the carbon bound to the silicon surface, corresponded to 0.10 ± 0.05 monolayers. The total C 1s signal corresponded to 0.40 ± 0.05 monolayers of bromohexene, indicating that the C−Si peak at
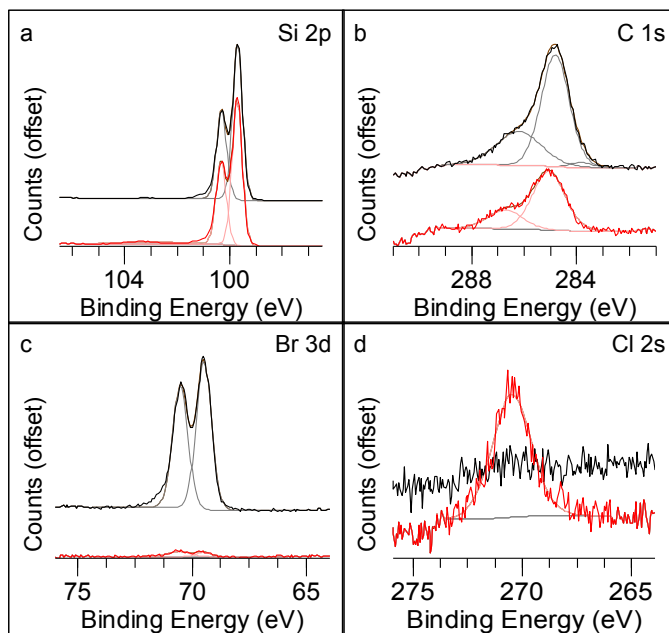
FIGURE 5.3: High-resolution XPS of 6-bromohexene-modified H−Si(111) (black) and Cl−Si(111) (red) surfaces after annealing at 250 °C. a) The Si 2p region was similar for these surfaces. The Cl−Si surface had a small Si−O contribution at 103 eV, while the H−Si surface did not. b) The C 1s region of the H−Si surface had a large carbon signal at 285 eV, with smaller shoulders at 284 and 286.5 eV. The component at 284 eV was from the surface-bound carbon, and corresponded to 0.10 ± 0.05 monolayers. The Cl−Si surface had a much smaller C 1s signal, and there was no peak at 284 eV, which indicated that the reaction did not proceed efficiently on this surface. c) The Br 3d region of the H−Si surface had a doublet of peaks at 69 and 70 eV, each fit to a single component, with an area ratio of 3:2, as expected for a 3d peak. This signal corresponded to 0.38 ± 0.05 monolayers of bromine on the surface. The Cl−Si surface had a very small doublet of peaks at the same position, which corresponded to 0.02 ± 0.01 monolayers of bromine on this surface. d) The Cl 2s region of the Cl−Si surface had a large peak at 270 eV, corresponding to 0.30 ± 0.05 monolayers of chlorine remaining on the surface. This is consistent with the lack of C 1s signal, and indicates that this surface was not reactive with the hexene under these conditions. The H−Si surface had no peak in the Cl 2s region from chlorine.

284 eV was smaller than expected. After annealing, most of the adventitious carbon on the surface should have been removed, leaving only contributions from the covalently bound bromohexene. The C 1s region of the Cl−Si surface had a smaller main peak at 285 eV and a shoulder at 286.5 eV. There was no peak at 284 eV on this surface. The total carbon signal on this surface corresponded to 0.20 ± 0.05 monolayers of bromohexene.

The Br 3d region of the H−Si surface had a doublet of peaks at 69 and 70 eV with an area ratio of 3:2, as expected for a 3d signal. These peaks were each fit to a single component that corresponded to 0.38 ± 0.05 monolayers of bromine on the surface. This agreed well with the surface coverage calculated from the total C 1s signal, but not to the surface coverage calculated from the C 1s component at 284 eV. That suggested that the peak at 284 eV was not an accurate measure of surface coverage on this surface. The Cl−Si surface had a small Br 3d doublet at 69 and 70 eV corresponding to 0.02 ± 0.01 monolayers of bromine on the surface. This was less bromine than expected based on the total C 1s signal, which suggested that the bromohexene could have decomposed during the attachment procedure, or that there was significant adventitious carbon remaining on this surface despite the annealing process. The Cl 2s region of the Cl−Si surface had a large peak at 270 eV corresponding to 0.30 ± 0.05 monolayers of chlorine remaining on the surface. The H−Si surface did not have any chlorine signal, as expected.

These results verified what we had seen previously during the attachment of 1-hexene and butbipy to Cl−Si(111) surfaces, which was that this surface did not react as efficiently with alkenes as the H−Si surface under UV illumination. The larger bond energy of the Cl−Si vs. the H−Si bond could be preventing the formation of surface radicals because the UV-light source was not of sufficiently high energy to excite the Cl−Si bond on the surface. The difference in reactivity observed for alkenes vs. vinyl-appended reactants can be explained by the ability of the vinyl-appended groups to self-polymerize under thermal and UV illumination conditions. The vinyl groups formed radicals independently of the silicon surface under the thermal and UV-light conditions explored in this work, particularly after the addition of the radical initiator, benzoyl peroxide, to the reaction solution. The alkenes, on the other hand, could not form radicals under UV illumination. This suggested that the reaction between the Cl−Si surface and vFc, for example, could have been initiated by a radical on the vinyl group of the vFc rather than by a dangling bond on the surface. This would explain why the Cl−Si surface seemed to react with vFc but not hexene. It would also

explain why multilayers formed on H−Si surfaces modified thermally with vinylferrocene,[47] for which the chain reaction mechanism is insufficient.[79]

5.2   Evidence for Surface Attachment

Direct proof of the Si-C bond on surfaces formed via hydrosilylation was generally difficult to find. Much of the evidence for the covalent attachment of alkenes to silicon surfaces was based on the robustness of the resultant structures.[16,82] Direct proof of covalent attachment was more straightforward for methyl-terminated silicon formed by the halogenation/alkylation method, where spectroscopic evidence of the Si-C bond can be obtained.[13,29,83] The C 1s XPS signal at $284\,\text{eV}$, attributed to carbon from the Si−CH$_3$ group, provided strong evidence for a covalent linkage between the methyl group and the surface. Further studies with other alkyl chains attached via the halogen/alkylation method also showed this signal at $284\,\text{eV}$, indicating that these longer chains were attached through a C−Si linkage.[32,37] This C−Si peak at $284\,\text{eV}$ was also seen on some alkylated silicon surfaces formed via hydrosilylation of terminal olefins, providing further evidence of the covalent attachment.[18,82]

However, surfaces modified by styrene and vinylferrocene via thermal immobilization did not have this peak at $284\,\text{eV}$ in the high-resolution C 1s XPS region.[47,84] The absence of this peak was given as evidence for a saturated hydrocarbon linkage between the ferrocene group and the silicon surface. This was consistent with results seen in this work on H- and Cl-terminated surfaces modified by vinylferrocene, vinylbipyridine, and 4-fluorostyrene via thermal and UV-light initiated reactions. These surfaces did not have peaks at $284\,\text{eV}$ in the high-resolution C 1s XPS region. It was unclear why silicon surfaces terminated by alkyl groups like methyl, allyl, or octyl would have this peak at $284\,\text{eV}$, ostensibly attributed to the C−Si carbon, but silicon surfaces terminated by styrene or vinylferrocene, which were also covalently attached to the surface through a C−Si group, did not.

One possible explanation was that the presence of an electron-withdrawing group, like the fluorophenyl ring of 4-fluorostyrene or the Cp* of vinylferrocene, could shift the binding energy of the carbon bound to silicon. The electronegativity of Si is less than that of C, and so the carbon bound to the Si surface was more negatively charged, or reduced, compared to the rest of the carbons in the alkyl chain, which decreased the binding energy of the surface attached carbon to $284\,\text{eV}$ from $285\,\text{eV}$. On the other hand, when an electron-withdrawing group
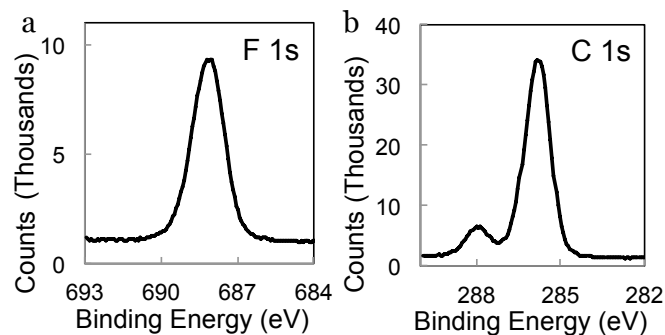
FIGURE 5.4: High-resolution F1s and C 1s XPS of silicon surfaces formed by thermal-immobilization of 4-fluorostyrene on Cl−Si(111). a) The F 1s region had a single peak at 688 eV from the fluorine group of the 4-fluorostyrene moiety. b) The C 1s region had a large peak at 286 eV from the carbon atoms of the styrene group. There was also a smaller component at 288 eV from the carbon bound to the fluorine. This peak was shifted to higher binding energy because the fluorine group is more electron-withdrawing than the carbon. Adapted with permission from Lattimer et al.[34] Copyright 2013 American Chemical Society.

was bound to carbon, the carbon becomes more positively charged, or oxidized, resulting in increased binding energy, as for the carbon bound to fluorine seen on 4-fluorostyrene-modified silicon surfaces (Figure 5.4). The experimental details for the formation of the 4-fluorostyrene-terminated silicon surface can be found in Appendix A.9. The binding energy of this carbon was shifted from 286 eV to 288 eV because of the fluorine group. When the surface-bound carbon is also bound to an electron-withdrawing group, like a hydroxide or fluorine group, these two effects could be offset, resulting in the absence of the expected C−Si peak at 284 eV. Some evidence for this theory was given by Yaffe et al. in their work on the reaction between 1-alcohols and H−Si(111).[85] They showed that the C 1s region of a surface formed via the UV-light initiated radical chain reaction between H−Si(111) and 1-decanol had no peak at 284 eV because the surface-bound carbon had bonds to both the silicon surface and to the alcohol group. These competing groups had opposite effects on the binding energy of the surface-bound carbon, resulting in an intermediate shift that was indistinguishable from the bulk C 1s signal. They performed DFT computations which supported this assertion, calculating that the C−Si binding energy shift was −1.1 eV, while the C−O binding energy shift was +1 eV. This agreed well with their experimental results, and with our observations on methyl-terminated surfaces. Fluorine is even more electronegative than oxygen, and so a larger shift in the C−F binding energy was not unexpected.

These competing shifts in the binding energy could explain why the C 1s peak at 284 eV
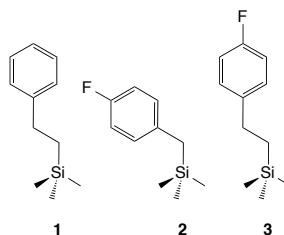
FIGURE 5.5: Structures of surface-bound phenylethyl (**1**), 4-fluorobenzyl (**2**), and 4-fluorostyrene (**3**).

was smaller than expected for the H−Si(111) surface modified with bromohexene. The bromine, despite being 5 methylene units from the surface-bound carbon atom, could have exerted an electron-withdrawing effect that shifted the binding energy of the alkyl chain more positive. Even a small shift in the binding energy could make the various components of the C 1s signal less easily distinguished and more difficult to deconvolute, making the fitting of each peak less accurate. However, the total C 1s signal still provided an accurate estimation of the total bromohexene surface coverage.

Spectroscopic evidence, aside from the C 1s XPS signal at 284 eV, for the C−Si bond has been seen for methyl-terminated surfaces formed using the halogenation/alkylation procedure using methyl Grignard.[22] High-resolution electron energy loss spectroscopy (HREELS) of the methylated surface showed a peak at $510\,\text{cm}^{-1}$, which was assigned to the C−Si bond. This was independent confirmation of the C−Si bond on surfaces formed via halogenation/alkylation using an alkyl Grignard reagent. Therefore, we used phenylethyl Grignard and 4-fluorobenzyl Grignard to modify Cl-terminated silicon, with the assumption that these reactions would definitely result in a C−Si bond on the surface. The experimental details for these reactions can be found in Appendix A.16. We could then look for the C−Si peak at 284 eV in the C 1s XPS region on these surfaces and assess whether it was affected by the phenyl ring. These reagents were chosen because the final products should be structurally similar to the surface-attached 4-fluorostyrene, which we had previously characterized. Figure 5.5 shows the presumed surface-bound structures of these three reagents for comparative purposes.

While neither of these two Grignard reagents were exact analogues of 4-fluorostyrene, each had a similar functional moiety. This should allow us to assess how these functional groups affect the binding energy of the surface-bound carbon. The high-resolution C 1s and F 1s XPS regions of the Cl−Si surfaces modified by phenylethyl Grignard and 4-fluorobenzyl
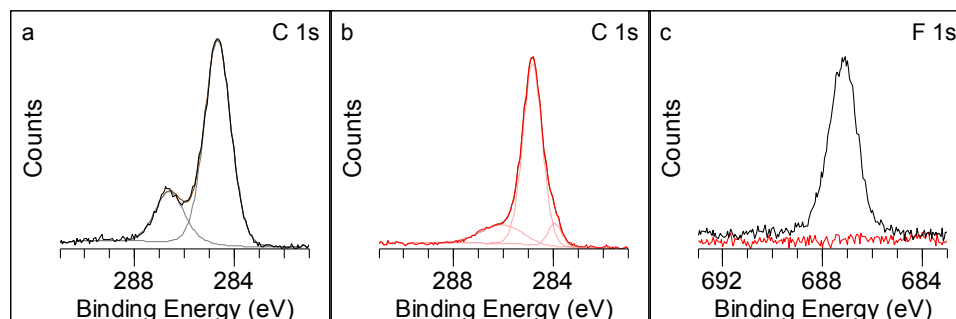
FIGURE 5.6: High-resolution C 1s and F 1s XPS of Cl−Si(111) surfaces after reaction with 4-fluorobenzyl Grignard (black) and phenylethyl Grignard (red). a) The C 1s region of the 4-fluorobenzyl-modified surface was fit to a broad peak at 285 eV and a smaller peak at 287 eV. The peak at 287 eV can be attributed to the carbon bound to the fluorine group, while the broad peak at 285 eV contains contributions from the benzene ring and the surface-attached carbon. There was no distinct C−Si peak at 284 eV in this spectrum. b) The C 1s region of the phenylethyl-modified surface was fit to a large peak at 285 eV, with two shoulders at 284 and 286 eV. The peak at 284 eV, corresponding to 0.30 ± 0.05 monolayers, was attributed to the surface-bound carbon. c) The F 1s region of the 4-fluorobenzyl-modified surface had a single peak at 687 eV, while the phenylethyl surface had no peak in the F 1s region.

Grignard are shown in Figure 5.6. The C 1s region of the 4-fluorobenzyl-modified surface appeared similar to the 4-fluorostyrene-modified surface shown in Figure 5.4. There was one large, broad peak at 285 eV and a smaller peak at 287 eV, which was attributed to the carbon bound to the fluorine group. This indicated that the fluorine group shifted the C−F binding energy by about 2 eV, as seen on the 4-fluorostyrene-modified surface. The total carbon signal corresponded to 0.45 ± 0.05 monolayers of 4-fluorobenzyl on the surface. The F 1s region of this surface had a single peak at 687 eV from the fluorine on the surface-bound 4-fluorobenzyl group, corresponding to 0.34 ± 0.05 monolayers. This indicated that the 4-fluorobenzyl was intact on the surface, and that there was some adventitious carbon. The Cl 2s region (not shown) had a signal corresponding to 0.28 ± 0.05 monolayers, indicating that there were still unreacted Cl−Si sites on the surface, which was not unexpected since the surface coverage of 4-fluorobenzyl was only ∼35 % of the Si atop sites.

The C 1s region of the phenylethyl-modified surface was fit to a large peak at 285 eV, with two shoulders at 284 and 286 eV. The peak at 284 eV, which corresponded to 0.30 ± 0.05 monolayers, was attributed to the surface-bound carbon of the phenylethyl group.[13,29] The total C 1s signal corresponded to 0.47 ± 0.05 monolayers, indicating that the phenylethyl group was intact on the surface and that there was some adventitious carbon. The phenylethyl-modified surface did not have any signal in the F 1s region, as expected.

These results indicated that the presence of the phenylethyl group did not significantly obscure the C 1s peak at $284\,\mathrm{eV}$ from the surface-attached carbon. This suggested that the phenyl group did not shift the binding energy of that surface-attached carbon. However, the fluorine group did seem to have some effect, obscuring the C 1s peak at $284\,\mathrm{eV}$ on surfaces modified by both 4-fluorobenzyl and 4-fluorostyrene. This suggested that the fluorine group, possibly in conjunction with the phenyl ring, exerted some effect on the binding energy of the surface-bound carbon, shifting it back toward $285\,\mathrm{eV}$ from $284\,\mathrm{eV}$. This gave some credence to the theory proposed by Yaffe et al. about the effects of electron-withdrawing groups on the binding energy of alkyl groups bound to silicon surfaces, and could explain why we often do not see a peak at $284\,\mathrm{eV}$ on surfaces with covalently-bound carbon groups.[85]

5.3 Conclusion

Determination of the reaction mechanism for the chlorosilylation reaction developed in this dissertation was ultimately inconclusive. We began with the hypothesis that the reaction occurred through a similar mechanism to that proposed for hydrosilylation of terminal alkenes onto silicon surfaces. We had some evidence for a radical mechanism, based on the increase in reaction rate observed upon the addition of radical initiators to the reaction solution. The presence of a chlorine signal in XPS on surfaces modified by chlorosilylation suggested that the radical chain reaction mechanism observed in hydrosilylation reactions could be occurring on our surfaces as well. However, the Cl 2s signal was too broad to distinguish between Cl−Si and Cl−C bonds, making it impossible to tell whether the chlorine on the surface is from residual, unreacted Cl−Si sites or from chlorine that was abstracted by a surface-bonded secondary carbon radical. The inability of our Cl−Si surfaces to react with hexene under UV-illumination suggested that our reaction did not proceed via a UV-light generated dangling-bond on the surface, unlike the hydrosilylation reaction. Rather, we only saw reactivity of the Cl−Si bond with vinyl-appended functional groups that were capable of self-polymerization. This suggested that the chlorosilylation reaction actually proceeded via a vinyl-radical on the reactant species in solution which could add to the Cl−Si bond on the surface. However, we currently have only circumstantial evidence that this is the case. Further experiments, possibly using a shorter-wavelength UV-light source or reacting model compounds in solution, could help to elucidate the reaction mechanism.

Appendix A

Materials and Methods

All chemicals were used as received, unless otherwise specified. Water with a resistivity $\geq 18.0\,\mathrm{M\Omega \cdot cm}$ was obtained from a Barnstead E-pure system. Electrochemical experiments were performed using single-side polished, degenerately B-doped p^+-Si(111) wafers with a resistivity of 0.01–$0.03\,\Omega \cdot \mathrm{cm}$. Charge-carrier lifetime measurements were performed using double-side polished monocrystalline, high-purity As-doped n-type Si(111) wafers of $350 \pm 25\,\mu\mathrm{m}$ thickness with resistivity of 4–$8\,\mathrm{k\Omega \cdot cm}$ (Topsil, Santa Clara, CA). FTIR and photoelectrochemical experiments were performed using double-side polished, float-zone grown, n-type Si(111) wafers (Silicon Quest International, Santa Clara, CA) with resistivity of 63–$77\,\Omega \cdot \mathrm{cm}$ and a thickness of $440 \pm 10\,\mathrm{mm}$. Addition photoelectrochemical experiments were performed using degenerately doped n^+-type silicon with resistivity of 0.004–$0.006\,\Omega \cdot \mathrm{cm}$, and n-type silicon with resistivities of 0.019–$0.023\,\Omega \cdot \mathrm{cm}$, 0.8–$1.5\,\Omega \cdot \mathrm{cm}$, 1–$10\,\Omega \cdot \mathrm{cm}$, and 23–$34\,\Omega \cdot \mathrm{cm}$ (Silicon Quest International, Santa Clara, CA). All wafers were modified using techniques described previously and characterized by XPS.[13,22,32,34,37,58]

A.1 Preparation of H-terminated and Cl-terminated Si(111) Wafers

Si(111) wafers were cut into $\sim 1\,\mathrm{cm}^2$ pieces which were immersed in boiling piranha solution (1:2 v/v 10.1 M hydrogen peroxide (H_2O_2, aq):18 M sulfuric acid (H_2SO_4)) for 10 min, followed by rinsing with H_2O. The wafers were then etched for 18 s in buffered HF (aq) (NH_4F/HF, Transene) and placed for 15 min, without rinsing, in a solution of 40 % NH_4F (aq) (Transene) that had been degassed with Ar(g) for at least 30 min. The resulting $H-Si(111)$ samples were rinsed with water and dried under a stream of N_2(g). After being transferred to a

N_2(g)-purged flush box, the H$-$Si(111) surfaces were placed in a saturated solution of PCl$_5$ (98 %, Alfa Aesar) in chlorobenzene (99.8 %, Sigma-Aldrich) with a few grains of benzoyl peroxide (reagent grade, 97 %, Sigma-Aldrich) added as a radical initiator. After 45–60 min at 90–100 °C, the resulting Cl$-$Si(111) samples were removed from the solution, allowed to cool, and rinsed with tetrahydrofuran (THF, $\geq$99.9 %, inhibitor free, Sigma-Aldrich).

A.2 Preparation of Methyl-Terminated Si(111) Surfaces

CH$_3$$-$Si(111) surfaces were produced in a N_2-purged flush box by immersing Cl$-$Si(111) surfaces in 1.0 M CH$_3$MgCl (diluted with THF from 3.0 M CH$_3$MgCl, Sigma-Aldrich) at 65 °C for 2–3 h. To remove and quench any unreacted Grignard reagent, the samples were rinsed with THF, then rinsed with CH$_3$OH (Sigma-Aldrich, 99.8 %), and removed from the flush box. All subsequent Grignard-modified surfaces were also cleaned in this manner before removal from the flush box. H$-$Si(111) surfaces were also reacted in the same manner with methyl Grignard as a control. After removal from the flush box, all surfaces were subjected to sonication sequentially in THF, CH$_3$OH, and water for 10 min each to clean the surfaces prior to characterization by surface-sensitive spectroscopy.

A.3 Preparation of Allyl- and Mixed Methyl/Allyl-Terminated Si(111) Surfaces

Allyl-Si(111) surfaces were produced in a N_2-purged flush box by immersing Cl$-$Si(111) surfaces in 1.0 M C$_3$H$_5$MgCl (diluted with THF from 2.0 M C$_3$H$_5$MgCl, Sigma-Aldrich) at 65 °C for 2–3 h. Mixed methyl/allyl-terminated surfaces were produced by forming solutions of 1.0 M Grignard with varying ratios of methyl:allyl components. For example, the 10 % allyl solution was produced by combining 0.25 mL 2.0 M C$_3$H$_5$MgCl, 1.5 mL 3.0 M CH$_3$MgCl, and 3.25 mL THF to form 5 mL of the 10 % allyl solution. Cl$-$Si(111) surfaces were then immersed in this solution at 65 °C for 2–3 h to produce the mixed surface. After functionalization with the Grignard solution, the surfaces were rinsed, removed from the flush box, and cleaned as described above.

A.4 Bromination of Functionalized Si(111) Surfaces

Bromination reactions were all carried out in a N_2-purged flush box. Surfaces were brominated by immersion in a 5 % Br_2 solution in CH_3OH. This solution was formed by dilution of 0.5 mL Br_2 (Sigma-Aldrich) with CH_3OH to a final volume of 10 mL. All reactions were carried out at RT. Immersion time was varied between 2 and 60 min, depending on the desired product. Surfaces were rinsed with CH_3OH before removal from the flush box, and then sonicated sequentially in CH_3OH and water for 10 min each prior to characterization.

A.5 Preparation of Butenyl- and Mixed Methyl/Butenyl-Terminated Si(111) Surfaces

Butenyl−Si(111) surfaces were produced by immersing Cl−Si(111) surfaces in a N_2-purged flush box in 0.5 M C_4H_7MgBr (Sigma-Aldrich) at 65 °C for 2–3 h. Mixed methyl/butenyl-terminated surfaces were produced in a one-step synthesis by forming solutions of 1.0 M Grignard with varying ratios of methyl:butenyl components. For example, the 15 % butenyl solution was produced by combining 1.5 mL 0.5 M C_4H_7MgBr, 1.4 mL 3.0 M CH_3MgCl, and 2.1 mL THF to form 5 mL of the 15 % butenyl solution. Cl−Si(111) surfaces were then immersed in this solution at 65 °C for 2–3 h to produce the mixed surface. Partial butenyl-terminated surfaces were produced by decreasing the reaction temperature to room temperature (r.t.) and decreasing the time in which the Cl−Si(111) surface was immersed in the 0.5 M C_4H_7MgBr solution to between 5 and 90 min. Mixed methyl/butenyl-terminated surfaces were produced in a two-step synthesis by first immersing Cl−Si(111) surfaces in 0.5 M C_4H_7MgBr at r.t. for a predetermined period of time between 5 and 90 min, followed by immersion in 1.0 M CH_3MgCl at 65 °C for 1–2 h. After functionalization all surfaces were rinsed, removed from the flush box, and cleaned by sonication as described above.

A.6 Cross-Coupling Reactions with 4-VinylPhenyl Acetamide, 4-VinylPhenyl Isocyanide, and Vinylferrocene

Cross-coupling reactions with the mixed butenyl/methyl surfaces were performed in a two-step process. All reaction steps were carried out under an Ar atmosphere in a dry glove box. First,

the mixed surface was immersed in 1.0 M Grubbs' catalyst, 2nd generation (Sigma-Aldrich) in CH_2Cl_2 in a 15 mL glass pressure vessel (Chemglass) with a Teflon screw-cap. The vessel was held at 50 °C in an oil bath for 6–10 h. After cooling, the surface was rinsed with CH_2Cl_2 and immersed in 1.0 M 4-vinylphenyl acetamide (4-VPA, synthesized by M. Rose), 4-vinylphenyl isocyanide (4-VPI, synthesized by M. Rose), or vinylferrocene (vFc, Alfa Aesar) in CH_2Cl_2 in a fresh 15 mL glass pressure vessel. This vessel was held at 50 °C in an oil bath for 12–18 h. After cooling, the surface was rinsed with CH_2Cl_2 and removed from the dry box. The surface was then sonicated sequentially in CH_2Cl_2, CH_3OH, and water for 10 min each prior to characterization.

A.7 Metallation of 4-VinylPhenyl Isocyanide with Codmg

The mixed butenyl/methyl surface with cross-coupled 4-VPI was placed in a solution of 10 mg $Co(dimethylglyoxime)_2(BF_2)_2$ (Codmg, synthesized by M. Rose) in 8 mL CH_3CN at r.t. for 2.5 h. The surface was then rinsed with CH_3CN to remove unreacted Codmg prior to characterization.

A.8 Thermally-Induced Formation of Vinylferrocenyl-Terminated Si(111) Surfaces

Vinylferrocene-terminated Si surfaces were produced in a N_2-purged flush box by immersing H− and Cl−Si(111) surfaces in neat vFc for 2–3 h at 140 °C in pressure vessels. As a separate control reaction, the H−Si(111) and Cl−Si(111) surfaces were also exposed to ferrocene (Fc, Sigma-Aldrich) for 2–3 h at 140 °C in a N_2(g)-purged glove box. Samples with a range of surficial vFc coverage were prepared from Cl−Si(111) surfaces by lowering the reaction temperature to 100 °C and by decreasing the immersion time in vFc to between 10 min and 1 h. To form mixed monolayers, these partially vFc-functionalized Si(111) samples were then rinsed with THF and placed in 1.0 M CH_3MgCl in THF at 65 °C for 2 h. As a control reaction, CH_3−Si(111) surfaces were immersed in vFc for 2–3 h at 140 °C in a N_2(g)-purged glove box. After functionalization, all these surfaces were rinsed with THF and CH_3OH, and removed from the flush box. All functionalized surfaces were then sonicated sequentially in THF, CH_3OH, and H_2O for at least 10 min each, prior to characterization by surface-sensitive

spectroscopy.

A.9 Preparation of 4-Fluorostyrene-Modified Surfaces

In a N_2-purged flush box, $Cl-Si(111)$ wafers were immersed in neat 4-fluorostyrene (Aldrich, 99 %, with *tert*-butylcatechol as an inhibitor) at 100 °C for 3 h. Mixed 4-fluorostyrene/methyl surfaces were prepared by immersion of $Cl-Si(111)$ surfaces in neat 4-fluorostyrene at 100 °C for 5 min. The samples were then rinsed with THF and immersed in 1.0 M CH_3MgCl in THF at 65 °C for 3 h. The resulting surfaces were rinsed with THF and CH_3OH, removed from the glove box, and then sonicated sequentially in THF, CH_3OH, and H_2O for at least 10 min each prior to surface characterization.

A.10 UV-light Induced Formation of Vinylferrocenyl-Terminated Si(111) Surfaces

In a N_2-purged flush box, $H-$ and $Cl-Si$ surfaces were placed polished-side down in a solution of $\sim$50–100 mg vinylferrocene in $\sim$3 mL THF in a glass dish with a quartz bottom. The wafers were illuminated from below with UV light (254 nm, 18.4 W, Mineralight, Upland, CA) for 1 h. The dish was covered with aluminum foil to minimize solvent evaporation. After functionalization the wafers were rinsed with THF. Mixed monolayers were formed by placing the vFc-modified wafer in 1 M CH_3MgCl in THF at 65 °C. This procedure was later modified by changing the solvent to dichloromethane (CH_2Cl_2, Sigma-Aldrich, anhydrous) or acetonitrile (CH_3CN, Sigma-Aldrich, anhydrous), adding a few grains of benzoyl peroxide (Aldrich reagent grade, 97 %, Sigma-Aldrich) as a radical initiator, decreasing the amount of vFc used in solution to $\sim$10 mg, and decreasing the illumination time to between 30 and 180 min to control surface coverage. After functionalization, all wafers were rinsed with THF and CH_3OH, then removed from the flush box and sonicated sequentially for 10 min each in THF, CH_3OH, and water prior to characterization.

A.11 Formation of Mixed Vinylbipyridyl/Methyl Surfaces

In a N_2-purged flush box, H$-$ and Cl$-$Si surfaces were immersed polished-side down in a solution of $\sim$10–20 mg vinylbipyridine (vbpy, synthesized by W. Sattler) in $\sim$3 mL CH_3CN with a few grains of BP in a glass dish with a quartz bottom, and exposed to UV light (254 nm, 18.4 W, Mineralight, Upland, CA) from below for 0.5 to 3 h. The dish was covered with aluminum foil to minimize solvent evaporation, with extra solvent added to the reaction solution as needed to maintain volume. The surfaces were then rinsed with CH_3CN and placed in 1 M CH_3MgCl in THF at 65 °C. The wafers were then rinsed with THF and CH_3OH and removed from the flush box, then cleaned by sonication as described above.

A.12 Attachment of $[Cp^*Rh(vbpy)CH_3CN](PF_6)_2$

In a N_2-purged flush box, Cl$-$Si surfaces were immersed polished-side down in a solution of $\sim$10–20 mg $[Cp^*Rh(vbpy)CH_3CN](PF_6)_2$ (synthesized by J. Blakemore) in $\sim$3 mL CH_3CN with a few grains of BP in a glass dish with a quartz bottom, and exposed to UV light (254 nm, 18.4 W, Mineralight, Upland, CA) from below for 2 h. The dish was covered with aluminum foil to minimize solvent evaporation. The surfaces were then rinsed with CH_3CN and CH_3OH and removed from the flush box, then cleaned by sequential sonication for 10 min each in CH_3CN, CH_3OH, and water.

A.13 Formation of Mixed Methyl/Vinylbipyridyl Surfaces

In a N_2-purged flush box, H$-$ and Cl$-$Si surfaces were immersed in a solution of 1 M CH_3MgCl in THF at r.t. for 5 min. These partially methylated surfaces were rinsed with THF and then immersed in a solution of $\sim$10–20 mg vinylbipyridine (vbpy, synthesized by W. Sattler) in $\sim$3 mL CH_2Cl_2 with a few grains of BP in a glass dish with a quartz bottom, and exposed to UV light (254 nm, 18.4 W, Mineralight, Upland, CA) from below for 1 to 2 h. The dish was covered with aluminum foil to minimize solvent evaporation, with extra solvent added as necessary to maintain the solution volume. The surfaces were then rinsed with CH_2Cl_2 and CH_3OH and removed from the flush box, then cleaned by sequential sonication for 10 min each in CH_2Cl_2, CH_3OH, and water.

A.14 Reaction of Butbipy with H− and Cl−Si(111) Surfaces

In a N_2-purged flush box, H- and Cl-terminated silicon wafers were placed polished-side down in a glass dish with a quartz bottom filled with a solution of 10 mg 4-(3-Butenyl),4′-methyl-2,2′-bipyridine (butbipy, synthesized by M. Radlauer) in ∼3 mL CH_2Cl_2 with trace BP added as a radical initiator. This vessel was illuminated with UV light (254 nm, 18.4 W, Mineralight, Upland, CA) from below for 1 h. The dish was covered with aluminum foil to minimize solvent evaporation. The surfaces were then removed from the dish and rinsed with CH_2Cl_2 and CH_3OH, and removed from the flush box. Mixed methyl/butbipy surfaces were formed by placing a Cl-terminated silicon surface in 1.0 M CH_3MgCl in THF at r.t. for 5 min. The wafer was then rinsed with THF and placed in a glass dish with a quartz bottom filled with a solution of 10 mg butbipy in CH_2Cl_2 with trace BP added as a radical initiator. This dish was illuminated with UV light (254 nm, 18.4 W, Mineralight, Upland, CA) from below for 1 h, and covered with aluminum foil to minimize solvent evaporation. The surface was then removed from the dish, rinsed with CH_2Cl_2 and CH_3OH, and removed from the flush box. All surfaces modified with butbipy were cleaned by sonication as described above prior to surface characterization.

A.15 Reaction of Hexene with H− and Cl−Si(111) Surfaces

In a N_2-purged flush box, H- and Cl-terminated silicon wafers were placed in an empty glass dish with a quartz bottom. Three drops of neat 1-hexene (≥99 %, Sigma-Aldrich) were placed on top of each of the wafers, ensuring an even coating of the hexene over the entire surface. The wafers were then illuminated with UV light (254 nm, 18.4 W, Mineralight, Upland, CA) from above for 1–2 h. The wafers were then removed from the vessel and rinsed with CH_2Cl_2 and CH_3OH to remove excess reactant, and removed from the flush box. H− and Cl−Si(111) surfaces were reacted independently with 1-hexene to prevent cross-contamination of any reactant between the wafers. 6-Bromo-1-hexene (95 %, Sigma-Aldrich) was also reacted with H− and Cl−Si(111) surfaces following this same procedure. All surfaces were sonicated sequentially for 10 min each in THF, CH_3OH, and water prior to characterization.

A.16 Formation of Phenylethyl- and 4-Fluorobenzyl-Modified Surfaces

In a N_2-purged flush box, phenylethyl-modified surfaces were prepared by immersing a Cl−Si(111) surface in a solution of 1.0 M phenylethylmagnesium chloride ($C_6H_5CH_2CH_2MgCl$, 1.0 M, Sigma-Aldrich) in THF at 65 °C for 3 h. The surface was then rinsed with THF and CH_3OH, then removed from the flush box. 4-Fluorobenzyl-modified surfaces were prepared in a similar manner, by placing a Cl-terminated silicon wafer in a solution of 0.25 M 4-fluorobenzylmagnesium chloride ($FC_6H_4CH_2MgCl$, 0.25 M, Sigma-Aldrich) in THF at 65 °C for 3 h. The surface was then rinsed with THF and CH_3OH and removed from the flush box. All surfaces were cleaned by sonication as described above prior to surface characterization.

Appendix B

Instrumentation

B.1 X-ray Photoelectron Spectroscopy

Two X-ray photoelectron spectrometers were used to collect data for this work. The first is a Surface Science Instruments M-Probe system that has been described previously.[24] The sample chamber was kept at $<5 \times 10^{-9}$ torr and ejected electrons were collected at an angle of 55° from the surface normal. Survey scans were performed to identify the elements on the surface of the silicon. Additionally, high-resolution spectra were collected for the Si 2p, C 1s, Fe 2p, Cl 2s, Br 3d, N 1s, F 1s, Co 2p, and Rh 3d XPS regions. The XPS data were analyzed using the Hawk Data Analysis Application (V7.03.04; Service Physics, Bend, OR). The remainder of the X-ray photoelectron spectroscopy (XPS) data were collected using a Kratos AXIS Ultra system, described previously.[62] The pressure in the sample chamber was kept at $<5 \times 10^{-9}$ torr, and ejected electrons were collected at an angle of 90° from the surface normal. Survey scans were performed to identify the elements on the surface of the silicon. Additionally, high-resolution spectra were collected for the Si 2p, C 1s, Fe 2p, Cl 2s, N 1s, Rh 3d, Ir 4f, Ru 3p, and Br 3d regions. The XPS data were analyzed using the program Computer Aided Surface Analysis for X-ray Photoelectron Spectroscopy, or CasaXPS. All XPS signals reported herein are binding energies and are reported in eV. For spectra that exhibited multiple XPS peaks arising from a single element, the peak was fit to multiple Voigt functions (80 % Gaussian and 20 % Lorentzian) when possible to quantitate the amount of each detectable species for that specific element.

B.1.1 Surface Coverage Quantification

The surface coverages of carbon, iron, chlorine, bromine, nitrogen, fluorine, cobalt, rhodium, iridium, ruthenium, and silicon oxide were calculated as described previously.[32] To account for any variation in the focus or power of the X-ray beam, the Si 2p bulk peak at 99–100 eV was used to normalize the XPS signals during quantification of surface coverages. Spectra were not used for quantification if the Si 2p signal showed any significant change in intensity due to organic overlayers. Hence, an elemental peak, when corrected by its relative sensitivity factor (RSF), which is a unique value for each elemental peak for each instrument, was normalized by the observed area of the Si 2p peak. When using the M-probe data for quantification, the RSF of the C 1s signal is defined as 1.0, while for the Kratos data the RSF of the F 1s signal is defined as 1.0.

The $CH_3-Si(111)$ surface was used as a reference to provide a standard signal area ratio, θ_{Me}, that corresponded to a complete monolayer wherein every Si atop site had been functionalized by a CH_3 group. Accordingly, on $CH_3-Si(111)$ surfaces, the area of the C 1s peak at 284 eV, ascribable to carbon directly attached to silicon, was normalized by the area of the Si 2p peak, and this ratio was used to determine the value of θ_{Me}.[25]

To calculate the fraction of a monolayer of $Si-CH_3$ groups, η_{Si-CH_3}, that were present on the mixed-monolayer surfaces, the ratio of the area of the lowest-energy C 1s peak (at 284 eV) to the Si 2p peak area on that surface was divided by the value of θ_{Me}, or $\eta_{Si-CH_3} = \theta_{Si-CH_3}/\theta_{Me}$. The total amount of C on a given surface was estimated by using the entire C 1s peak (i.e., adding the areas of all the C 1s components) normalized by the area of the Si 2p signal. A ratio of at least 12:1 C:Fe on the surface (10 carbons from the Cp groups, and 2 from the vinyl linker) was taken as confirmation of intact Fc groups on the surface for surfaces modified by vFc.

The amount of Fe on Si(111) surfaces, θ_{Fe}, was calculated by dividing the area of the Fe $2p_{3/2}$ peak at 708 eV, which corresponds to the Fe(II) signal,[86] by the relative sensitivity factor (RSF) of Fe and then by the area of the Si 2p signal on such surfaces. The ratio of θ_{Fe} to θ_{Me} gave the ratio of the number of Fe(II) atoms on the surface to the number of Si(111) atop sites, η_{Fe}, i.e., the fraction of the surface sites that were functionalized by vFc. A similar calculation was performed using the Fe $2p_{1/2}$ peak at 721 eV. The two methods in general gave values for the surface coverage of Fe that were within experimental error of each other.

The surface coverage of chlorine was calculated using the Cl 2s peak at $270\,\text{eV}$ to calculate θ_{Cl}, by taking the area of the Cl 2s peak, dividing by its RSF, and normalizing that area to the area of the Si 2p signal on that surface. The ratio of θ_{Cl} to θ_{Me} gave the surface coverage of chlorine as a fraction of Si atop sites, η_{Cl}. The fluorine coverage was quantified by taking the area of the F 1s peak at $\sim 688\,\text{eV}$, dividing by its RSF, and normalizing to the area of its Si 2p peak. This process yielded a value for θ_{F}, which was then divided by θ_{Me} to calculate the number of F atoms per Si atop site, η_{F}. For surfaces modified by 4-fluorostyrene or 4-fluorobenzyl Grignard, this number was taken to equal the surface coverage of 4-fluorostyrene or 4-fluorobenzyl. For surfaces modified by Codmg, that number was divided by 4 to give the total coverage of Codmg on the surface, as there were 4 F atoms per Codmg unit. For surfaces modified by $[\text{Cp}^*\text{Rh}(\text{vbpy})\text{CH}_3\text{CN}]\text{PF}_6$, that number was divided by 6 to give the total coverage of $[\text{Cp}^*\text{Rh}(\text{vbpy})\text{CH}_3\text{CN}]\text{PF}_6$ on the surface.

The surface coverage of bromine was calculated using the Br 3d doublet at 69 and $70\,\text{eV}$ to calculated θ_{Br}, by taking the area of the Br 3d peak, dividing by its RSF, and normalizing that area to the area of the Si 2p signal on that surface. The ratio of θ_{Br} to θ_{Me} gave the surface coverage of bromine as a fraction of Si atop sites, η_{Br}. For surfaces with multiple contributions in the Br 3d region, each set of doublets was analyzed separately to calculate η_{Br} for each type of bromine.

The surface coverage of nitrogen was calculated using the N 1s peak at $\sim 400\,\text{eV}$ to calculate θ_{N}, by taking the area of the N 1s peak, dividing by its RSF, and normalizing that area to the area of the Si 2p signal on that surface. The ratio of θ_{N} to θ_{Me} gave the surface coverage of chlorine as a fraction of Si atop sites, η_{N}. On surfaces modified by 4-VPA or 4-VPI, η_{N} was taken as the coverage of the group on the surface. For surfaces modified by Codmg, η_{N} was divided by 5 to get the coverage of Codmg on the surface]. For surfaces modified by bipy or butbipy, η_{N} was divided by 2 to give the total bipy coverage, as there were 2 N atoms per bpy unit. For surfaces with multiple contributions in the N 1s region, each component was analyzed separately to calculate η_{N} for each component.

The surface coverage of cobalt was calculated using the Co 2p doublet at 782 and $797\,\text{eV}$ to calculate θ_{Co}, by taking the area of the Co 2p peak, dividing by its RSF, and normalizing that area to the area of the Si 2p signal on that surface. The ratio of θ_{Co} to θ_{Me} gave the surface coverage of chlorine as a fraction of Si atop sites, η_{Co}. For surfaces modified by Codmg, η_{Co} is taken as the total coverage of the Codmg group on the surface.

The coverage of rhodium was calculated using the Rh 3d doublet at 310 and 315 eV, which corresponded to Rh(III), to calculate θ_{Rh} by taking the area of the Rh 3d peak, dividing by its RSF, and normalizing that area to the area of the Si 2p signal on that surface. The ratio of θ_{Rh} to θ_{Me} gave the ratio of the number of Rh(III) atoms on the surface to Si(111) atop sites, η_{Rh}, which was taken as the surface coverage of any of the Rh(III) complexes, which each contain one rhodium. A similar calculation was performed using the Rh(I) signal at 308 and 313 eV to calculate the surface coverage of any Rh(I) formed by reduction or decomposition of the Rh(III) complexes used in this work. The coverage of iridium was calculated similarly using the Ir 4f peak at 64 and 65 eV, which corresponded to Ir(III), to find η_{Ir}. This was taken as the surface coverage of the Cp*Ir complex, which contained one iridium. The Ru 3p peaks at 463 and 485 eV, which corresponded to Ru(III), were similarly used to calculate ruthenium coverage, η_{Ru}. This was taken as the surface coverage of the Ru(acac)$_2$ complex, which contained one ruthenium.

The amount of silicon oxide on the surface was calculated by taking the area of the broad Si 2p peak at 101–105 eV (corresponding to oxidized silicon),[13] dividing by its RSF, and normalizing to the area of the bulk Si 2p peak at 99–100 eV, to give θ_{Si-O}. This value was then divided by θ_{Me} to give the surface coverage of silicon oxide as a fraction of Si atop sites, η_{Si-O}.

B.2 Fourier-Transform Infrared Spectroscopy

Transmission infrared spectroscopy (FTIR) measurements were collected using a Thermo Scientific Nicolet 6700 Optical Spectrometer that was equipped with a deuterated triglycine sulfate (DTGS) detector and a purified air purge, described previously.[32] FTIR spectra were collected by mounting the samples at a fixed 74° angle, as measured between the incident light and the surface normal. The sample chamber was purged with N$_2$ for at least 1 h before collection of spectra. All of the FTIR spectra represent averages of greater than 2000 consecutive scans. Double-side polished, n-type Si(111) wafers with resistivity of 63–77 $\Omega \cdot$ cm and a thickness of $440 \pm 10\,\mu$m were used for all FTIR measurements. Samples were cut into 1 cm $\times$ 3 cm pieces and mounted horizontally. Wafers were prepared for FTIR by rinsing with water and drying under a stream of N$_2$.

B.3 Surface Recombination Velocity

Surface recombination velocity (S) measurements were made using a contactless microwave conductivity apparatus.[30,37] A 20-ns pulsed-diode laser with a wavelength of 905 nm (OSRAM laser diode with an ETX-10A-93 driver) was used to generate electron-hole pairs in high-purity, nearly intrinsically As-doped n-Si(111) wafers with resistivity of 4–8 k$\Omega \cdot$ cm, with both sides of the wafer polished and processed equivalently at all stages. The lifetime of the photogenerated charge carriers was monitored using a PIN diode that detected the microwave radiation reflected from the sample. Functionalized surfaces that had been prepared using nearly intrinsically doped Si(111) wafers were tested immediately after preparation, and for several days or weeks afterward. Between measurements, the samples were stored in the dark, in air.

Charge-carrier lifetimes were measured by fitting the excess charge-carrier density, $A = \Delta n + \Delta p$, where Δn and Δp are the photogenerated electron and hole concentrations, respectively, to a single-exponential decay:

$$A = y_0 + a\mathrm{e}^{-t/\tau}. \tag{B.1}$$

The extracted lifetime, τ, was converted to a surface recombination velocity, S, using:

$$\frac{1}{\tau} = \frac{1}{\tau_B} + \frac{2S}{d}, \tag{B.2}$$

where τ and τ_B are the measured and bulk lifetimes, respectively, and d is the wafer thickness.[32] For high-purity Si, the bulk-carrier lifetime is much larger than the measured τ ($\tau_B^{-1} \ll \tau^{-1}$) which allowed the simplification:

$$S = \frac{d}{2\tau}. \tag{B.3}$$

B.4 Electrochemistry

Nonaqueous electrochemistry of vinylferrocene-modified surfaces was performed in an argon-filled glove box with acetonitrile (CH$_3$CN, JT Baker, 99.8 %) as the solvent and 0.10 M tetraethylammonium perchlorate ((NEt$_4$)ClO$_4$, Alfa Aesar, 98 % dry wt, 10 % water) as

the supporting electrolyte. Prior to use, the $(NEt_4)ClO_4$ was recrystallized from CH_3OH and diethyl ether, and was stored under $Ar(g)$. All measurements were made in a three-electrode cell connected to a Gamry Instruments Reference 600 potentiostat controlled by Gamry Instruments Framework v.5.61 (2010) software. The counterelectrode was a Pt mesh and the reference electrode was $Ag/AgNO_3$ (Ag wire immersed in 0.01 M $AgNO_3$ in electrolyte), separated from the solution by a porous Teflon tip (CH Instruments). Ohmic contact to the p^+-Si(111), n^+-Si(111), and n-Si(111) samples, for electrochemistry and photoelectrochemistry, was made by scratching the back of the functionalized wafer with a Ga-In eutectic and placing the wafer on Cu foil on a stainless steel base. The wafers were then secured in a custom-made Teflon cell with an O-ring seal used to define the electrode area ($0.28\,cm^2$), as described previously.[34] A methyl-terminated Si(111) surface was used to confirm the absence of redox activity on the surface and in the electrolyte between $-1\,V$ and $+0.4\,V$ vs. $Ag/AgNO_3$. Photoelectrochemistry experiments were performed using an ELH-type W-halogen bulb with a dichroic rear reflector, adjusted to produce an effective light intensity of $\sim250\,mW \cdot cm^{-2}$ at the electrode surface. The light and dark scans were alternated to minimize heating of the materials by the lamp.

Electrochemistry of bipy-modified surfaces was performed in a nitrogen-filled glove box using alumina-dried acetonitrile as the solvent and 0.10 M tetrabutylammonium hexafluorophosphate $((NBu_4)PF_6$, Fluka electrochemical grade) as the supporting electrolyte. Measurements were made using a three-electrode configuration and a Princeton Applied Research Parstat 4000 potentiostat controlled by Princeton Applied Research VersaStudio v.2.2 (2012) software. The counter electrode was basal plane graphite (BPG) and the reference electrode was Ag/Ag+ (silver wire immersed in electrolyte, separated from the solution by a porous Vycor tip (Bioanalytical Systems, Inc.)). Ferrocene (99 %, Alfa Aesar) was added to the electrolyte solution at the conclusion of each experiment ([Fc] $\sim1\,mM$); the ferrocene/ferrocenium couple served as an internal standard for comparing potentials. Voltammetry on the functionalized surfaces was carried out by first scanning cathodically to sufficiently reducing potentials to examine redox events for the immobilized metal complexes. Generally, the sweep width was from 0 to $-1.5\,V$ vs. Fc/Fc^+ at a scan rate of $100\,mV\,s^{-1}$. Ohmic contact to the Si wafers was made as described above. Electrochemistry was performed in the Teflon cell described above.

B.4.1 Surface Coverage Quantification

A linear fit was used to subtract the background current from the voltammetric scans to remove capacitive current from our calculations. The anodic and cathodic waves were integrated independently to estimate the surface coverage of the electroactive groups. The area under the background-subtracted current-versus-time plot gave the total charge transferred to the redox couple, which was then divided by the projected electrode area ($0.28 \, \mathrm{cm^2}$) to yield the number of electroactive groups per $\mathrm{cm^2}$. The integrated areas of the anodic and cathodic peaks, respectively, were generally within 10% of each other. Multiple scan rates were used to ensure the reproducibility of the data. For vFc-modified surfaces, the total number of electrochemically active Fc groups per $\mathrm{cm^2}$ divided by the surface density of silicon atop atoms on a Si(111) surface, 7.8×10^{14} atoms per $\mathrm{cm^2}$,[25] yielded the fraction of the Si atop sites covered by electroactive Fc groups, η_{Fc}. 1.0 monolayers of coverage in this case refers to a situation in which the electrochemically detected coverage corresponded to 7.8×10^{14} electroactive Fc groups per $\mathrm{cm^2}$ of projected electrode area. Similar calculations were performed for bipy-modified surfaces metallated with rhodium and ruthenium complexes to get the electroactive surface coverage of the Rh or Ru complexes.

B.4.2 Electron Transfer Rate Calculation

Potential-step chronoamperometry was used to measure the electron transfer rate on Si surfaces modified with vFc. In these experiments, the potential was held at a potential below the ferrocene redox couple for 3 s, then stepped to a potential above the redox couple and held for 5 s, then stepped back to a potential below the redox couple. The current follows a simple exponential decay:

$$i(t) = kQ \exp(-kt), \tag{B.4}$$

where i is the current in amps as a function of time, k is the charge transfer rate in s^{-1}, and $Q = nFA\eta_{\mathrm{Fc}}$, where n is the number of electrons in the reaction (one for the $\mathrm{Fc/Fc^+}$ couple), F is Faraday's constant, A is the area of the electrode, and η_{Fc} is the surface coverage of electroactive centers. A plot of $\log(i)$ vs. t will be linear for the portion of the transient after double-layer charging, with a slope of $-k$ and an intercept of $\log(kQ)$. Because n, F, and A are all known, and η_{Fc} can be calculated as described in Appendix B.4.1, k can be found for both the oxidation and reduction of the surface-attached ferrocene redox couple in the dark

and in the light.

B.4.3   Aqueous Electrochemistry

Aqueous electrochemistry of vFc-modified surfaces was carried out under ambient conditions using 1.0 M potassium phosphate dibasic (KH_2PO_4, 99.95 %, Sigma-Aldrich) in $18\,M\Omega\cdot cm$ water, at pH 4.2, as the electrolyte. Measurements were made using a three-electrode configuration and a Princeton Applied Research Parstat 4000 potentiostat controlled by Princeton Applied Research VersaStudio v.2.2 (2012) software. The counter electrode was a platinum wire and the reference electrode was Ag/Ag+ (silver wire immersed in saturated KCl ($\geq$99.0 %, Sigma-Aldrich), separated from the solution by a porous Vycor tip (Bioanalytical Systems, Inc.)). The reference electrode was stored in 3.0 M NaCl when not in use and had a potential of 0.197 V vs. NHE. Potassium ferricyanide (($K_3Fe(CN)_6$, 99.98 %, Sigma-Aldrich) was added to the electrolyte solution at the conclusion of each experiment to serve as an internal standard for comparing potentials. Ohmic contact to the Si wafers was made as described above, and electrochemistry was performed in the Teflon cell described above (Appendix B.4).

B.5   X-ray Absorption Spectroscopy (XAS) Data Collection

Ir L_{III} XAS measurements were performed at the Stanford Synchrotron Radiation Laboratory (SSRL) on Beamline 7-3 at an electron energy of 3.0 GeV and an average current of 500 mA. The intensity of the incident X-ray beam was monitored using a N_2-filled ion chamber (I_0) in front of the sample. A Si(220) double-crystal monochromator was used to detune to 50 % of the maximum flux to attenuate higher harmonics. The data was collected as fluorescence excitation spectra with a Ge 30-element detector (Canberra). The monochromator energy was calibrated using Ir foil (a rising edge energy of 11 215.00 eV).

The powder sample was diluted with boron nitride (1 % w/w). The mixture was packed into 0.5 mm thick aluminum sample holders and sealed with Mylar tape. To ensure that no X-ray induced radiation damage occurred, the L_{III} edge position was closely monitored for any reduction.

Data reduction of the XANES spectra was performed using SamView (SixPACK software, Dr. Samuel M. Webb, SSRL). The pre-edge and post-edge backgrounds were subtracted

from the XAS spectra using Athena (IFEFFIT software), and the resulting spectra were normalized with respect to the edge height.

References

[1] Ibrahim, H.; Ilinca, A.; Perron, J. Energy storage systems—Characteristics and comparisons. *Renew. Sust. Energ. Rev.* **2008**, *12*, 1221–1250.

[2] Gray, H. B. Powering the planet with solar fuel. *Nat. Chem.* **2009**, *1*, 7–7.

[3] Tran, P. D.; Barber, J. Proton reduction to hydrogen in biological and chemical systems. *Phys. Chem. Chem. Phys.* **2012**, *14*, 13772–13784.

[4] Santori, E. A. Si microwire array photoanodes for artificial photosynthetic devices. Ph.D. thesis, California Institute of Technology, 2013.

[5] Tan, M. X.; Laibinis, P. E.; Nguyen, S. T.; Kesselman, J. M.; Stanton, C. E.; Lewis, N. S. Principles and Applications of Semiconductor Photoelectrochemistry. *Prog. Inorg. Chem.* **1994**, *41*, 21–144.

[6] Streetman, B. G.; Banerjee, S. *Solid state electronic devices*; Prentice Hall: Upper Saddle River, N.J., 2000.

[7] Grimes, C. A.; Varghese, O. K.; Ranjan, S. *Light, water, hydrogen*; The Solar Generation of Hydrogen by Water Photoelectrolysis; Springer: New York, NY, 2008.

[8] DeBenedetti, W.; Chabal, Y. J. Functionalization of oxide-free silicon surfaces. *J. Vac. Sci. Technol. A* **2013**,

[9] Pike, A. R.; Lie, L. H.; Eagling, R. A.; Ryder, L. C.; Patole, S. N.; Connolly, B. A.; Horrocks, B. R.; Houlton, A. DNA On Silicon Devices: On-Chip Synthesis, Hybridization, and Charge Transfer. *Angew. Chem. Int. Ed.* **2002**, *41*, 615–617.

[10] Strother, T.; Cai, W.; Zhao, X. S.; Hamers, R. J.; Smith, L. M. Synthesis and characterization of DNA-modified silicon (111) surfaces. *J. Am. Chem. Soc.* **2000**, *122*, 1205–1209.

[11] Bansal, A.; Lewis, N. S. Stabilization of Si photoanodes in aqueous electrolytes through surface alkylation. *J. Phys. Chem. B* **1998**, *102*, 4058–4060.

[12] Yablonovitch, E.; Allara, D.; Chang, C.; Gmitter, T.; Bright, T. Unusually low surface-recombination velocity on silicon and germanium surfaces. *Phys. Rev. Lett.* **1986**, *57*, 249–252.

[13] Nemanick, E. J.; Hurley, P. T.; Brunschwig, B. S.; Lewis, N. S. Chemical and electrical passivation of silicon (111) surfaces through functionalization with sterically hindered alkyl groups. *J. Phys. Chem. B* **2006**, *110*, 14800–14808.

[14] Sieval, AB,; Demirel, A. L.; Nissink, J.; Linford, M. R.; van der Maas, J. H.; de Jeu, W. H.; Zuilhof, H.; Sudholter, E. Highly stable Si-C linked functionalized monolayers on the silicon (100) surface. *Langmuir* **1998**, *14*, 1759–1768.

[15] Linford, M. R.; Chidsey, C. E. D. Alkyl monolayers covalently bonded to silicon surfaces. *J. Am. Chem. Soc.* **1993**, *115*, 12631–12632.

[16] Linford, M. R.; Fenter, P.; Eisenberger, P. M.; Chidsey, C. Alkyl Monolayers on Silicon Prepared From 1-Alkenes and Hydrogen-Terminated Silicon. *J. Am. Chem. Soc.* **1995**, *117*, 3145–3155.

[17] Terry, J.; Linford, M. R.; Wigren, C.; Cao, R. Y.; Pianetta, P.; Chidsey, C. Determination of the bonding of alkyl monolayers to the Si(111) surface using chemical-shift, scanned-energy photoelectron diffraction. *Appl. Phys. Lett.* **1997**, *71*, 1056–1058.

[18] Cicero, R. L.; Linford, M. R.; Chidsey, C. Photoreactivity of unsaturated compounds with hydrogen-terminated silicon(111). *Langmuir* **2000**, *16*, 5688–5695.

[19] Stewart, M. P.; Buriak, J. M. Photopatterned hydrosilylation on porous silicon. *Angew. Chem. Int. Ed.* **1998**, *37*, 3257–3260.

[20] Sun, Q. Y.; de Smet, L.; van Lagen, B.; Giesbers, M.; Thune, P. C.; van Engelenburg, J.; de Wolf, F. A.; Zuilhof, H.; Sudholter, E. Covalently attached monolayers on crystalline hydrogen-terminated silicon: Extremely mild attachment by visible light. *J. Am. Chem. Soc.* **2005**, *127*, 2514–2523.

[21] Lewis, L. N. On the Mechanism of Metal Colloid Catalyzed Hydrosilylation - Proposed Explanations for Electronic Effects and Oxygen Cocatalysis. *J. Am. Chem. Soc.* **1990**, *112*, 5998–6004.

[22] Bansal, A.; Li, X. L.; Lauermann, I.; Lewis, N. S.; Yi, S. I.; Weinberg, W. H. Alkylation of Si surfaces using a two-step halogenation Grignard route. *J. Am. Chem. Soc.* **1996**, *118*, 7225–7226.

[23] Bansal, A.; Lewis, N. S. Electrochemical properties of (111)-oriented n-Si surfaces derivatized with covalently-attached alkyl chains. *J. Phys. Chem. B* **1998**, *102*, 1067–1070.

[24] Bansal, A.; Li, X. L.; Yi, S. I.; Weinberg, W. H.; Lewis, N. S. Spectroscopic studies of the modification of crystalline Si(111) surfaces with covalently-attached alkyl chains using a chlorination/alkylation method. *J. Phys. Chem. B* **2001**, *105*, 10266–10277.

[25] Webb, L. J.; Lewis, N. S. Comparison of the electrical properties and chemical stability of crystalline silicon(111) surfaces alkylated using grignard reagents or olefins with Lewis acid catalysts. *J. Phys. Chem. B* **2003**, *107*, 5404–5412.

[26] Yu, H.; Webb, L. J.; Heath, J. R.; Lewis, N. S. Scanning tunneling spectroscopy of methyl- and ethyl-terminated Si(111) surfaces. *Appl. Phys. Lett.* **2006**, *88*.

[27] Nemanick, E. J.; Solares, S. D.; Goddard, W. A.; Lewis, N. S. Quantum mechanics calculations of the thermodynamically controlled coverage and structure of alkyl monolayers on Si(111) surfaces. *J. Phys. Chem. B* **2006**, *110*, 14842–14848.

[28] Yu, H. B.; Webb, L. J.; Ries, R. S.; Solares, S. D.; Goddard, W. A.; Heath, J. R.; Lewis, N. S. Low-temperature STM images of methyl-terminated Si(111) surfaces. *J. Phys. Chem. B* **2005**, *109*, 671–674.

[29] Hunger, R.; Fritsche, R.; Jaeckel, B.; Jaegermann, W.; Webb, L.; Lewis, N. Chemical and electronic characterization of methyl-terminated Si(111) surfaces by high-resolution synchrotron photoelectron spectroscopy. *Phys. Rev. B* **2005**, *72*, 045317.

[30] Royea, W. J.; Juang, A.; Lewis, N. S. Preparation of air-stable, low recombination velocity Si (111) surfaces through alkyl termination. *Appl. Phys. Lett.* **2000**,

[31] Grimm, R. L.; Bierman, M. J.; O'Leary, L. E. Comparison of the Photoelectrochemical Behavior of H-Terminated and Methyl-Terminated Si (111) Surfaces in Contact with a Series of One-Electron, Outer-Sphere .... *J. Phys. Chem. C* **2012**,

[32] O'Leary, L. E.; Johansson, E.; Brunschwig, B. S.; Lewis, N. S. Synthesis and characterization of mixed methyl/allyl monolayers on Si(111). *J. Phys. Chem. B* **2010**, *114*, 14298–14302.

[33] O'Leary, L. E.; Rose, M. J.; Ding, T. X.; Johansson, E.; Brunschwig, B. S.; Lewis, N. S. Heck Coupling of Olefins to Mixed Methyl/Thienyl Monolayers on Si(111) Surfaces. *J. Am. Chem. Soc.* **2013**, *135*, 10081–10090.

[34] Lattimer, J. R. C.; Brunschwig, B. S.; Lewis, N. S.; Gray, H. B. Redox Properties of Mixed Methyl/Vinylferrocenyl Monolayers on Si(111) Surfaces. *J. Phys. Chem. C* **2013**, *117*, 27012–27022.

[35] Schwab, P.; France, M. B.; Ziller, J. W.; Grubbs, R. H. A Series of Well-Defined Metathesis Catalysts - Synthesis of [Rucl2(=Chr')(Pr(3))(2)] and Its Reactions. *Angew. Chem. Int. Ed.* **1995**, *34*, 2039–2041.

[36] Schwab, P.; Grubbs, R. H.; Ziller, J. W. Synthesis and applications of RuCl2(=CHR')(PR(3))(2): The influence of the alkylidene moiety on metathesis activity. *J. Am. Chem. Soc.* **1996**, *118*, 100–110.

[37] Plass, K. E.; Liu, X.; Brunschwig, B. S.; Lewis, N. S. Passivation and secondary functionalization of allyl-terminated Si(111) surfaces. *Chem. Mater.* **2008**, *20*, 2228–2233.

[38] Juang, A.; Scherman, O. A.; Grubbs, R. H.; Lewis, N. S. Formation of covalently attached polymer overlayers on Si(111) surfaces using ring-opening metathesis polymerization methods. *Langmuir* **2001**, *17*, 1321–1323.

[39] Dutta, S.; Perring, M.; Barrett, S.; Mitchell, M.; Kenis, P. J. A.; Bowden, N. B. Cross metathesis on olefin-terminated monolayers on Si(111) using the Grubbs' catalyst. *Langmuir* **2006**, *22*, 2146–2155.

[40] Haber, J. A.; Lewis, N. S. Infrared and X-ray photoelectron spectroscopic studies of the reactions of hydrogen-terminated crystalline Si(111) and Si(100) surfaces with Br-2, I-2, and ferrocenium in alcohol solvents. *J. Phys. Chem. B* **2002**, *106*, 3639–3656.

[41] Webb, L. J.; Rivillon, S.; Michalak, D. J.; Chabal, Y. J.; Lewis, N. S. Transmission infrared spectroscopy of methyl- and ethyl-terminated silicon(111) surfaces. *J. Phys. Chem. B* **2006**, *110*, 7349–7356.

[42] Ohashi, M.; Nakato, Y.; Mashima, K. Surface modification of n-Si(111) electrodes with brominated and sulfonylated alkyl chains and their photoelectrochemical characteristics. *Chem. Lett.* **2006**, *35*, 1360–1361.

[43] Chretien, J. R.; Coudert, J. D. Solvation and steric effects on electrophilic reactivity of ethylenic compounds. 3. Stereo-, regio-, and chemoselectivity of alkene bromination in methanol. *J. Org. Chem.* **1993**,

[44] Connolly, P.; Espenson, J. H. Cobalt-Catalyzed Evolution of Molecular Hydrogen. *Inorg. Chem.* **1986**, *25*, 2684–2688.

[45] Baffert, C.; Artero, V.; Fontecave, M. Cobaloximes as functional models for hydrogenases. 2. Proton electroreduction catalyzed by difluoroborylbis(dimethylglyoximato)cobalt(II) complexes in organic media. *Inorg. Chem.* **2007**, *46*, 1817–1824.

[46] Strutz, J.; Diegruber, H.; Jaeger, N. I.; Moseler, R. X-Ray Photoelectron-Spectroscopy of Ni-Bis and Co-Bis (Dimethylglyoximato)-Complexes Within a Na-X Matrix. *Zeolites* **1983**, *3*, 102–105.

[47] Tajimi, N.; Sano, H.; Murase, K.; Lee, K.-H.; Sugimura, H. Thermal immobilization of ferrocene derivatives on (111) surface of n-type silicon: parallel between vinylferrocene and ferrocenecarboxaldehyde. *Langmuir* **2007**, *23*, 3193–3198.

[48] Dalchiele, E. A.; Aurora, A.; Bernardini, G.; Cattaruzza, F.; Flamini, A.; Pallavicini, P.; Zanoni, R.; Decker, F. XPS and electrochemical studies of ferrocene derivatives anchored on n- and p-Si(100) by Si-O or Si-C bonds. *J. Electroanal. Chem.* **2005**, *579*, 133–142.

[49] Bard, A. J.; Faulkner, L. R. *Electrochemical Methods*, 2nd ed.; fundamentals and applications; Wiley: New York, 2001.

[50] Langner, A.; Panarello, A.; Rivillon, S.; Vassylyev, O.; Khinast, J. G.; Chabal, Y. J. Controlled silicon surface functionalization by alkene hydrosilylation. *J. Am. Chem. Soc.* **2005**, *127*, 12798–12799.

[51] Chidsey, C.; Bertozzi, C. R.; Putvinski, T. M.; Mujsce, A. M. Coadsorption of Ferrocene-Terminated and Unsubstituted Alkanethiols on Gold - Electroactive Self-Assembled Monolayers. *J. Am. Chem. Soc.* **1990**, *112*, 4301–4306.

[52] Seiler, P.; Dunitz, J. D. A new interpretation of the disordered crystal structure of ferrocene. *Acta Crystallogr.* **1979**, *B 35*, 1068–1074.

[53] Buriak, J. M. Organometallic chemistry on silicon and germanium surfaces. *Chem. Rev.* **2002**, *102*, 1271–1308.

[54] Laviron, E. General expression of the linear potential sweep voltammogram in the case of diffusionless electrochemical systems. *J. Electroanal. Chem.* **1979**, *101*, 19–28.

[55] Li, L.; Kang, E.; Neoh, K. Preparation of well-defined polymer-silicon wafer hybrids via surface-initiated RAFT-mediated process. *Appl. Surf. Sci.* **2008**, *254*, 2600–2604.

[56] Krawicz, A.; Yang, J.; Anzenberg, E.; Yano, J.; Sharp, I. D.; Moore, G. F. Photofunctional construct that interfaces molecular cobalt-based catalysts for H2 production to a visible-light-absorbing semiconductor. *J. Am. Chem. Soc.* **2013**, *135*, 11861–11868.

[57] Santangelo, P. G.; Miskelly, G. M.; Lewis, N. S. Cyclic Voltammetry at Semiconductor Photoelectrodes .1. Ideal Surface-Attached Redox Couples with Ideal Semiconductor Behavior. *J. Phys. Chem.* **1988**, *92*, 6359–6367.

[58] Amy, S. R.; Michalak, D. J.; Chabal, Y. J.; Wielunski, L.; Hurley, P. T.; Lewis, N. S. Investigation of the reactions during alkylation of chlorine-terminated silicon (111) surfaces. *J. Phys. Chem. C* **2007**, *111*, 13053–13061.

[59] Walter, M. G.; Warren, E. L.; McKone, J. R.; Boettcher, S. W.; Mi, Q.; Santori, E. A.; Lewis, N. S. Solar Water Splitting Cells. *Chem. Rev.* **2010**, *110*, 6446–6473.

[60] McKone, J. R.; Warren, E. L.; Bierman, M. J.; Boettcher, S. W.; Brunschwig, B. S.; Lewis, N. S.; Gray, H. B. Evaluation of Pt, Ni, and Ni–Mo electrocatalysts for hydrogen evolution on crystalline Si electrodes. *Energy Environ. Sci.* **2011**, *4*, 3573–3583.

[61] Song, W.; Chen, Z.; Brennaman, M. K.; Concepcion, J. J.; Patrocinio, A. O. T.; Murakami Iha, N. Y.; Meyer, T. J. Making solar fuels by artificial photosynthesis. *Pure and Applied Chemistry 83*.

[62] Blakemore, J. D.; Gupta, A.; Warren, J. J.; Brunschwig, B. S.; Gray, H. B. Noncovalent immobilization of electrocatalysts on carbon electrodes for fuel production. *J. Am. Chem. Soc.* **2013**, *135*, 18288–18291.

[63] Schley, N. D.; Blakemore, J. D.; Subbaiyan, N. K.; Incarvito, C. D.; D'Souza, F.; Crabtree, R. H.; Brudvig, G. W. Distinguishing homogeneous from heterogeneous catalysis in electrode-driven water oxidation with molecular iridium complexes. *J. Am. Chem. Soc.* **2011**, *133*, 10473–10481.

[64] Lattimer, J. R. C.; Blakemore, J. D.; Sattler, W.; Gul, S.; Yachandra, V.; Yano, J.; Brunschwig, B. S.; Lewis, N. S.; Gray, H. B. Assembly, Characterization, and Electrochemical Properties of Immobilized Metal Bipyridyl Complexes on Silicon(111) Surfaces. *Dalton Trans.* **2014**, *submitted*.

[65] Kölle, U.; Grützel, M. Organometallic Rhodium(III) Complexes as Catalysts for the Photoreduction of Protons to Hydrogen on Colloidal TiO2. *Angew. Chem. Int. Ed.* **1987**, *26*, 567–570.

[66] Kölle, U.; Kang, B.-S.; Infelta, P.; Comte, P.; Grätzel, M. Elektrochemische und pulsradiolytische Reduktion von (Pentamethylcyclopentadienyl)(polypyridyl)rhodium-Komplexen. *Chem. Ber.* **1989**, *122*, 1869–1880.

[67] Cosnier, S.; Deronzier, A.; Vlachopoulos, N. Carbon/poly pyrrole-[(C5Me5)Rh III (bpy)Cl]+ modified electrodes; a molecularly-based material for hydrogen evolution (bpy = 2,2?-bipyridine). *J. Chem. Soc., Chem. Commun.* **1989**, 1259–1261.

[68] Mestroni, G.; Zassinovich, G.; Camus, A. Complexes of rhodium(I) and iridium(I) with 2,2´-bipyridine and similar ligands as hydrogenation catalysts. *Journal of Organometallic Chemistry* **1977**, *140*, 63–72.

[69] Steckhan, E.; Herrmann, S.; Ruppert, R.; Dietz, E.; Frede, M.; Spike, E. Analytical Study of a Series of Substituted (2,2'-Bipyridyl)(Pentamethylcyclopentadienyl)Rhodium and Iridium Complexes with Regard to Their Effectiveness as Redox Catalysts for the Indirect Electrochemical and Chemical-Reduction of Nad(P)+. *Organometallics* **1991**, *10*, 1568–1577.

[70] Lo, H. C.; Leiva, C.; Buriez, O.; Kerr, J. B.; Olmstead, M. M.; Fish, R. H. Bioorganometallic Chemistry. 13. Regioselective Reduction of NAD +Models, 1-Benzylnicotinamde Triflate and β-Nicotinamide Ribose-5'-methyl Phosphate, with in Situ Generated [Cp*Rh(Bpy)H] +: Structure—Activity Relationships, Kinetics, and Mechanistic Aspects in the Formation of the 1,4-NADH Derivatives †. *Inorg. Chem.* **2001**, *40*, 6705–6716.

[71] White, C.; Yates, A.; Maitlis, P. M.; Heinekey, D. M. *(η5-Pentamethylcyclopentadienyl)Rhodium and -Iridium Compounds*; Inorganic Syntheses; John Wiley & Sons, Inc.: Hoboken, NJ, USA, 2007; Vol. 29.

[72] Kaim, W.; Reinhardt, R.; Waldho r, E.; Fiedler, J. Electron transfer and chloride ligand dissociation in complexes [(C5Me5)ClM(bpy)]+/[(C5Me5)M(bpy)]n (M=Co, Rh, Ir;n = 2+, +, 0, −): A combined electrochemical and spectroscopic investigation. *Journal of Organometallic Chemistry* **1996**, *524*, 195–202.

[73] Ziessel, R. Efficient homogeneous photochemical water gas shift reaction catalysed under extremely mild conditions by novel iridium(III) complexes: [(η5-Me5C5)Ir(bpy)Cl]+, [(η5-Me5C5)Ir(bpy)H]+, and [(η5-Me5C5)Ir(phen)Cl]+(bpy = 2,2´-bipyridine; phen = 1,10-phenanthroline). *J. Chem. Soc., Chem. Commun.* **1988**, 16–17.

[74] El-Hendawy, A. M.; Alqaradawi, S. Y.; Al-Madfa, H. A. Ruthenium(III) mono (2,2´-bipyridine) complexes containing O,O-donor ligands and their oxidation properties for organic compounds. *Transition Metal Chemistry* **2000**, *25*, 572–578.

[75] Bennett, M. A.; Chung, G.; Hockless, D. C. R.; Neumann, H.; Willis, A. C. Bis(acetylacetonato)bis(cyclooctene)ruthenium(II), cis-[Ru(acac)2(η2-C8H14)2]: a synthetic precursor to trans- and cis-bis(acetylacetonato)ruthenium(II) complexes†. *Dalton Trans.* **1999**, 3451–3462.

[76] Wu, A.; Masland, J.; Swartz, R. D.; Kaminsky, W.; Mayer, J. M. Synthesis and Characterization of Ruthenium Bis(β-diketonato) Pyridine-Imidazole Complexes for Hydrogen Atom Transfer. *Inorg. Chem.* **2007**, *46*, 11190–11201.

[77] Harrison, D. P.; Lapides, A. M.; Binstead, R. A.; Concepcion, J. J.; Méndez, M. A.; Torelli, D. A.; Templeton, J. L.; Meyer, T. J. Coordination Chemistry of Single-Site Catalyst Precursors in Reductively Electropolymerized Vinylbipyridine Films. *Inorg. Chem.* **2013**, *52*, 4747–4749.

[78] Calvert, J. M.; Schmehl, R. H.; Sullivan, B. P.; Facci, J. S.; Meyer, T. J.; Murray, R. W. Synthetic and Mechanistic Investigations of the Reductive Electrochemical Polymerization of Vinyl-Containing Complexes of Iron(Ii), Ruthenium(Ii), and Osmium(Ii). *Inorg. Chem.* **1983**, *22*, 2151–2162.

[79] Cicero, R. L.; Chidsey, C. E. D.; Lopinski, G. P.; Wayner, D. D. M.; Wolkow, R. A. Olefin Additions on H−Si(111): Evidence for a Surface Chain Reaction Initiated at Isolated Dangling Bonds. *Langmuir* **2002**, *18*, 305–307.

[80] Decker, F.; Cattaruzza, F.; Coluzza, C.; Flamini, A.; Marrani, A. G.; Zanoni, R.; Dalchiele, E. A. Electrochemical reversibility of vinylferrocene monolayers covalently attached on H-terminated p-Si(100). *J. Phys. Chem. B* **2006**, *110*, 7374–7379.

[81] Pauling, L. *The nature of the chemical bond and the structure of molecules and crystals: an introduction to modern structural chemistry*; Cornell University Press: Ithaca, N.Y., 1960.

[82] Wallart, X.; Henry de Villeneuve, C.; Allongue, P. Truly Quantitative XPS Characterization of Organic Monolayers on Silicon: Study of Alkyl and Alkoxy Monolayers on H−Si(111). *J. Am. Chem. Soc.* **2005**, *127*, 7871–7878.

[83] Jaeckel, B.; Hunger, R.; Webb, L. J. High-resolution synchrotron photoemission studies of the electronic structure and thermal stability of CH3-and C2H5-functionalized Si (111) surfaces. *J. Phys. Chem. C* **2007**,

[84] Harada, Y.; Koitaya, T.; Mukai, K.; Yoshimoto, S.; Yoshinobu, J. Spectroscopic Characterization and Transport Properties of Aromatic Monolayers Covalently Attached to Si(111) Surfaces. *J. Phys. Chem. C* **2013**, *117*, 7497–7505.

[85] Yaffe, O.; Ely, T.; Har-Lavan, R.; Egger, D. A.; Johnston, S.; Cohen, H.; Kronik, L.; Vilan, A.; Cahen, D. Effect of Molecule-Surface Reaction Mechanism on the Electronic Characteristics and Photovoltaic Performance of Molecularly Modified Si. *J. Phys. Chem. C* **2013**, *117*, 22351–22361.

[86] Woodbridge, C. M.; Pugmire, D. L.; Johnson, R. C.; Boag, N. M.; Langell, M. A. HREELS and XPS studies of ferrocene on Ag(100). *J. Phys. Chem. B* **2000**, *104*, 3085–3093.